

# THE ROLE OF TOP IN HEAVY FLAVOR PHYSICS

JoAnne L. Hewett\*

Stanford Linear Accelerator Center  
Stanford University, Stanford, CA 94309

## ABSTRACT

The implications of the massive top quark on heavy flavor transitions are explored. We review the generation of quark masses and mixings and the determination techniques, and present the status of the elements of the weak mixing matrix. Purely leptonic decays of heavy mesons are briefly summarized. We present a general introduction to flavor changing neutral currents and an extensive summary of radiative and other rare decay modes. The physics of neutral meson mixing is reviewed and applied to each meson system. We describe the phenomenology of CP violation and how it may be measured in meson decays. Standard Model predictions are given in each case and the effects of physics beyond the Standard Model are also discussed. Throughout, we contrast these transitions in the  $K$  and  $B$  meson systems to those in the  $D$  meson and top-quark sectors.

---

\*Work supported by the Department of Energy, Contract DE-AC03-76SF00515.

©1995 by JoAnne L. Hewett.

# 1 Introduction

One of the outstanding problems in particle physics is the origin of the fermion mass and mixing spectrum. Despite the success of the Standard Model (SM) of particle physics, it does not provide any clues on the source of these parameters. In contrast to the case of electroweak symmetry breaking, we have no information about the relevant energy scale where these parameters originate; in fact, the relevant scale could lie anywhere from 1 TeV to the Planck scale. Other issues (besides quark mixing) related to the multifamilies of fermions are the suppression of FCNC effects and the CP-violation phases in fermion gauge couplings. Since the top quark has a mass at the electroweak symmetry breaking scale, it is believed that it may reveal some hints to these questions. In these lectures, we examine its role in heavy flavor transitions.

At present, the best approach in addressing these questions is to study the properties of all heavy fermions in detail. Detailed measurements of heavy quark systems are best realized at high precision, high luminosity machines, and several dedicated heavy flavor factories and experiments will be coming on line in the next decade. We will learn a wealth of new and precise information which will hopefully result in the development of a theory to explain the existence of families.

In these lectures, we review the generation of quark masses and mixings and the determination techniques, and present the status of the elements of the weak mixing matrix. Purely leptonic decays of heavy mesons are briefly summarized. We present a general introduction to flavor changing neutral currents and an extensive summary of radiative and other rare decay modes. The physics of neutral meson mixing is reviewed and applied to each meson system. We describe the phenomenology of CP violation and how it may be measured in meson decays. Standard Model predictions are given in each case and the effects of physics beyond the Standard Model are also discussed. Throughout, we contrast these transitions in the  $K$  and  $B$  meson systems to those in the  $D$  meson and top-quark sectors.

## 2 Quark Masses and Mixing

In the Standard Model (SM), a single complex scalar doublet is responsible for the spontaneous symmetry breaking  $SU(2)_L \times U(1)_Y \rightarrow U(1)_{em}$ . The fermions are massless before the symmetry breaking, with their masses being generated via

Yukawa couplings after the spontaneous symmetry breaking occurs. Denoting the gauge (or weak or flavor) quark eigenstates as  $q_L^0$  ( $q_R^0$ ) for the left-handed doublet (right-handed singlet) quark fields, one can form the most general renormalizable quark-Higgs interaction

$$\mathcal{L}_{mass} \sim \frac{v}{\sqrt{2}} \left[ \bar{u}_L^0 h_{ij}^u u_R^0 + \bar{d}_L^0 h_{ij}^d d_R^0 \right] + h.c., \quad (1)$$

with  $v$  being the vacuum expectation value of the Higgs field,  $i, j$  are generation indices, and  $h_{ij}^{u,d}$  are  $3 \times 3$  matrices of bare complex couplings which form the mass matrices for the up- and down-quarks

$$M_u = \frac{v}{\sqrt{2}} h^u, \quad M_d = \frac{v}{\sqrt{2}} h^d. \quad (2)$$

The mass matrices are completely arbitrary and contain 36 unknown parameters! These matrices can be diagonalized by a bi-unitary transformation,

$$M_u^{diag} = U_L^\dagger M_u U_R = \begin{pmatrix} m_u & 0 & 0 \\ 0 & m_c & 0 \\ 0 & 0 & m_t \end{pmatrix},$$

$$M_d^{diag} = D_L^\dagger M_d D_R = \begin{pmatrix} m_d & 0 & 0 \\ 0 & m_s & 0 \\ 0 & 0 & m_b \end{pmatrix}, \quad (3)$$

where we have performed distinct rotations of the left- and right-handed fields, and the  $m_i$  represent the quark masses. Hence, six of the above 36 parameters become quark masses. The interaction Lagrangian can now be written as (where the generation indices have now been dropped)

$$\mathcal{L}_{mass} \sim \bar{u}_L^0 U_L^\dagger M_u U_R^\dagger u_R^0 + \bar{d}_L^0 D_L^\dagger M_d D_R^\dagger d_R^0 + h.c., \quad (4)$$

which is just given by

$$\mathcal{L}_{mass} \sim \bar{u}_L M_u^{diag} u_R + \bar{d}_L M_d^{diag} d_R + h.c.,$$

$$\sim \sum_{i=1}^6 m_i \bar{q}_i q_i + h.c., \quad (5)$$

in the mass (or physical) eigenstate basis with  $u_L = U_L^\dagger u_L^0$ , etc., being the physical quark fields. Note that the Higgs-quark Yukawa couplings are manifestly diagonal

in the physical basis; this is a consequence of the fact that there is only one Higgs doublet in the SM. The SM charged current interaction in the weak basis,

$$\mathcal{L}_{cc} \sim \frac{g}{\sqrt{2}} \bar{u}_L^0 \gamma_\mu d_L^0 W^\mu + h.c., \quad (6)$$

then becomes

$$\mathcal{L}_{cc} \sim \frac{g}{\sqrt{2}} \bar{u}_L \gamma_\mu U_L^\dagger D_L d_L W^\mu \quad (7)$$

in terms of the physical fields. The product  $U_L^\dagger D_L$  is known as the Cabibbo-Maskawa-Kobayashi (CKM) weak mixing matrix  $V_{CKM}$ . Since there are no right-handed charged currents in the SM, there is no analogous right-handed weak mixing matrix. In extensions of the SM which enlarge the gauge group to  $SU(2)_R \times SU(2)_L \times U(1)$ , such as the left-right symmetric model,<sup>1</sup> the quantity  $V_{CKM}^R \equiv U_R^\dagger D_R$  is similarly defined.

The CKM matrix contains information on all quark flavor transitions and is the source of CP violation within the SM. Writing the charged current interaction explicitly in matrix form yields

$$\mathcal{L}_{cc} \sim \frac{g}{\sqrt{2}} [u_L \ c_L \ t_L] \gamma_\mu \begin{pmatrix} V_{ud} & V_{us} & V_{ub} \\ V_{cd} & V_{cs} & V_{cb} \\ V_{td} & V_{ts} & V_{tb} \end{pmatrix} \begin{pmatrix} d_L \\ s_L \\ b_L \end{pmatrix} W^\mu + h.c. \quad (8)$$

Note that by construction, the CKM matrix is unitary, *i.e.*,  $\sum_i V_{ij} V_{ik}^* = \delta_{jk}$ . Unitarity tests thus provide an excellent probe of the SM. In general, any unitary  $N \times N$  matrix can be expressed by  $N^2$  parameters,  $N(N-1)/2$  of which are rotation angles, and  $N(N+1)/2$  phase angles. Here, the phases are associated with the quark fields, and  $2N-1$  of them may be arbitrarily redefined, leaving  $(N-1)(N-2)/2$  independent phases. For three generations of quarks, this leaves three rotation angles and one independent phase. Extrapolation to four generations would then require six rotation angles and three phases. A common parameterization of the three generation CKM matrix,

$$V_{CKM} = \begin{pmatrix} c_1 & -s_1 c_3 & -s_1 s_3 \\ s_1 c_2 & c_1 c_2 c_3 - s_2 s_3 e^{i\delta} & c_1 c_2 s_3 + s_2 c_3 e^{i\delta} \\ s_1 s_2 & c_1 s_2 c_3 + c_2 s_3 e^{i\delta} & c_1 s_2 s_3 - c_2 c_3 e^{i\delta} \end{pmatrix}, \quad (9)$$

is based on three Euler angles for the flavor rotations and was first given by Kobayashi and Maskawa<sup>2</sup> in 1973. Note that this was postulated *before* the discovery of the third generation (as well as charm), in order to introduce a potential

source of CP violation. Here,  $c_i = \cos \theta_i$ ,  $s_i = \sin \theta_i$  with  $0 \leq \theta_i \leq \pi/2$  and  $-\pi \leq \delta \leq \pi$ . An instructive parameterization, which is based on an expansion of the elements in powers of  $V_{us} \equiv \lambda$ , is given by Wolfenstein<sup>3</sup>

$$V_{CKM} = \begin{pmatrix} 1 - \frac{\lambda^2}{2} & \lambda & A\lambda^3(\rho - i\eta + i\eta\lambda^2/2) \\ -\lambda & 1 - \frac{\lambda^2}{2} - i\eta A^2 \lambda^4 & A\lambda^2(1 + i\eta\lambda^2) \\ A\lambda^3(1 - \rho - i\eta) & A\lambda^2 & 1 \end{pmatrix} \quad (10)$$

to  $\mathcal{O}(\lambda^3)$  in the Real terms and  $\mathcal{O}(\lambda^5)$  in the Imaginary terms. This parameterization illustrates the approximate diagonal nature of the CKM matrix, and exhibits which elements (and hence measurements thereof) are most sensitive to the various parameters  $\lambda$ ,  $A$ ,  $\rho$ , and  $\eta$ .

We now review the status of the experimental determinations of the CKM matrix elements.<sup>4,5</sup> We stress that the values of the CKM elements are fundamental input parameters within the SM and precise knowledge of these parameters may provide some insight into their origin.

- $V_{ud}$ : This element is determined from super-allowed  $0^+ - 0^+$  nuclear  $\beta$  decays. These transitions have large radiative corrections as well as some nuclear  $Z$  dependence. Recent analyses<sup>6</sup> of the nuclear structure dependent radiative corrections are inconsistent with each other within the level of the estimated uncertainties. Taking an average value of these results yields the PDG value<sup>4</sup>  $|V_{ud}| = 0.9736 \pm 0.0023$ , where the error is dominated by the theoretical uncertainties. Neutron  $\beta$  decay is less dependent on these nuclear uncertainties; however, the present determination<sup>5</sup> of  $|V_{ud}|$  from this process is larger than the above value by several sigma. Pion  $\beta$  decay,  $\pi^+ \rightarrow \pi^0 e^+ \nu_e$ , would in principle yield the cleanest measurement of  $V_{ud}$ , but the branching fraction is of order  $10^{-8}$ , making a precision determination difficult.

- $V_{us}$ : This element is cleanly determined from the  $K_{e3}$  decays  $K^+ \rightarrow \pi^0 e^+ \nu_e$  and  $K_L^0 \rightarrow \pi^\pm e^\mp \nu_e$ , giving  $|V_{us}| = 0.2196 \pm 0.0023$  (Ref. 7). Hyperon decays yield<sup>7</sup> a slightly larger value of  $|V_{us}| = 0.222 \pm 0.003$ , but are plagued with uncertainties from SU(3) breaking effects. The average of these two measurements result in the PDG value<sup>4</sup>  $|V_{us}| = 0.2205 \pm 0.0018$ .

- $V_{ub}$ : The explanation of CP violation within the SM, *i.e.*, the phase in the CKM matrix, requires a nonvanishing value of  $V_{ub}$ . It can be measured at the  $\Upsilon(4S)$  by examining the endpoint region of the lepton momentum spectrum in inclusive

$B \rightarrow X\ell\nu_\ell$  decays and counting the excess of leptons beyond the kinematic limit for  $B \rightarrow X_c\ell\nu_\ell$ . While data has established that  $V_{ub}$  is nonzero, converting the measured rate into a value of  $V_{ub}$  introduces substantial errors. This conversion is highly model dependent due to the small phase space available at the endpoint, and to details in the hadronization from the large uncertainties in the calculation of the rates for the resonant modes, and the relative size of the contributions of resonant and nonresonant modes in this region. The subtraction of background from the small data sample injects an additional large source of error. The present experimental error on the ratio  $|V_{ub}|/|V_{cb}|$  is comparable to the theoretical uncertainty, yielding<sup>4,8</sup>  $|V_{ub}|/|V_{cb}| = 0.08 \pm 0.02$ , and thus new, less model-dependent techniques in extracting this CKM element are necessary.

Exclusive semileptonic decays,  $B \rightarrow X_u\ell\nu_\ell$  where  $X_u = \pi, \rho$ , or  $\omega$ , have recently been observed by CLEO.<sup>9</sup> Interpretation of these results in terms of  $V_{ub}$  relies on the evaluation of the shape of the contributing form factors, as well as uncertainties in the size of the contributions from nonresonant decays such as  $B \rightarrow \pi\pi\ell\nu_\ell$ . A fit to the data and averaging over the form factor models yields<sup>9</sup>  $|V_{ub}| = (3.3 \pm 0.2^{+0.3}_{-0.4} \pm 0.7) \times 10^{-3}$ , where the errors are due to statistics, systematics, and estimated model dependence. Reductions in the theoretical errors can be obtained via direct measurements of the form factor  $q^2$  distributions in  $c \rightarrow d$  transitions such as  $D \rightarrow \pi\ell\nu_\ell$ .

An alternative method<sup>10</sup> of extracting  $V_{ub}$  from semileptonic  $B$  decays is to measure the invariant mass spectrum of the final state hadrons below the charm hadron threshold, i.e.,  $m_X < m_D$ . More than 90% of the  $B \rightarrow X_u\ell\nu_\ell$  decays lie within this region, yielding almost an order of magnitude increase in data sample over the endpoint region. The theoretical uncertainties associated with the determination of the total semileptonic spectrum are significantly smaller within this kinematic region, and are less than those associated with exclusive semileptonic decays which rely on form factor calculations. In addition, the  $B \rightarrow X_u\ell\nu_\ell$  transitions are largely nonresonant and multiple jetlike final states dominate, making the inclusive decay theoretically well-understood throughout this kinematic region.

- $V_{cd}$ : This element is evaluated by examining charm production in neutrino and antineutrino scattering off valence d-quarks and folding in the semileptonic branching fraction of charm weighted by the ratio of  $D^0/D^+$  production in neutrino scattering. Averaging the experimental results and including the scale de-

pendence from the NLO QCD corrections leads to the PDG value<sup>4,11</sup>  $|V_{cd}| = 0.224 \pm 0.016$ .

- $V_{cs}$ : In principle, this element can also be determined in neutrino induced charm production. Here, the scattering of interest clearly takes place off of strange quarks and the results are quite dependent on the s-quark parton density distributions. The most conservative assumptions about the parton densities set<sup>4</sup> the constraint  $|V_{cs}| > 0.59$ , which is not very restrictive. A better determination can be obtained from  $D_{e3}$  decay,  $D \rightarrow \bar{K}e^+\nu_e$ , although this process is form factor dependent and hence contains theoretical uncertainties. Combining various form factor calculations with the measured decay rate gives the PDG value<sup>4</sup>  $|V_{cs}| = 1.01 \pm 0.18$ , which is still not very well-determined. Employing the three generation unitarity constraint on the CKM matrix results in the most precise evaluation of this element.

- $V_{cb}$ : Considerable theoretical and experimental progress has been made recently on the extraction of  $V_{cb}$  from exclusive and inclusive decays. Exclusive semileptonic decays offer a reliable model-independent determination of  $V_{cb}$  within the framework of heavy quark effective theory as the heavy quark symmetry normalizes the  $q^2$ -dependent hadronic form factors with good precision at zero recoil for the charm hadron system. This technique is best suited for the process  $B \rightarrow D^*\ell\nu_\ell$  as the leading corrections to the HQET result arise only at higher order,  $1/m_Q^2$ .

The inclusive semileptonic branching fraction  $B_{SL}$  can be determined from (i) measurement of the inclusive lepton momentum spectrum. This technique yields significant data samples, but the procedure used to fit the observed spectrum to the expected shape for primary and secondary leptons from  $B$  and charm decay, respectively, introduces a large model dependence. (ii) Charge and angular correlations in dilepton events. This offers less model dependence as the measured correlations can be used to separate the primary and secondary lepton spectra, instead of relying on theory. (iii) Separate measurement of  $B_{SL}$  for charged and neutral  $B$  meson decay. Here, one  $B$  in the event must be reconstructed in order to tag the charge of the other. Determination of  $V_{cb}$  from  $B_{SL}$  via technique (i) at CLEO and LEP is already saturated by the theoretical error, while methods (ii) and (iii) still offer room for improvement experimentally.

Combining the results<sup>4,12</sup> on the exclusive and inclusive semileptonic decays gives  $|V_{cb}| = 0.040 \pm 0.003$ .

- $V_{td}, V_{ts}$ : These elements can be determined from flavor changing neutral current processes which contain one-loop top-quark contributions. The value of  $|V_{td}|$  can be deduced from  $B_d^0 - \bar{B}_d^0$  mixing and from the decay  $K \rightarrow \pi\nu\bar{\nu}$ , with  $K \rightarrow \pi\nu\bar{\nu}$  ultimately offering the theoretically cleanest technique. The ratio  $|V_{td}/V_{ts}|$  can be found from the ratio of  $B_d$  to  $B_s$  mass differences, as well as from the ratio of exclusive rates  $B(B \rightarrow \rho\gamma)/B(B \rightarrow K^*\gamma)$ , if the long-distance physics can be cleanly separated out. Each of these processes will be thoroughly discussed below; however, we note here they all depend on the assumption that there are no large contributions from new physics. At present, three-generation CKM unitarity constraints offer the best restrictions on these elements within the SM.

- $V_{tb}$ : The b-tagged events observed in top-quark decays at the Tevatron<sup>13</sup> have afforded the first direct measurement of  $V_{tb}$ . CDF and DØ measure the ratio of events with zero, one, and two b-tags to extract the ratio  $B(t \rightarrow Wb)/B(t \rightarrow WX)$ , which has the advantage of being independent of the  $t\bar{t}$  production cross section and the  $W$  boson branching fractions. Within the three-generation SM, this procedure yields  $|V_{tb}| = 0.97 \pm 0.15 \pm 0.13$ . The most precise determination of this element is obtained from employing unitarity together with the direct measurements of  $V_{ub}$  and  $V_{cb}$ .

Combining the above data with the constraint of three-generation unitarity, results in the 90% C.L. bounds on the full  $3 \times 3$  CKM matrix<sup>4</sup>

$$V_{CKM} = \begin{pmatrix} 0.9745 - 0.9757 & 0.219 - 0.224 & 0.002 - 0.005 \\ 0.218 - 0.224 & 0.9736 - 0.9750 & 0.036 - 0.046 \\ 0.004 - 0.014 & 0.034 - 0.046 & 0.9989 - 0.9993 \end{pmatrix}. \quad (11)$$

These ranges differ slightly from those itemized above due to the inclusion of the unitarity constraint. However, it is important to note that the data does not preclude the existence of more generations.

### 3 Leptonic Decays

Pseudoscalar mesons can decay to a purely leptonic final state,  $P^\pm(Q\bar{q}) \rightarrow \ell^\pm\bar{\nu}_\ell$ , through the annihilation diagram. The matrix element for this process can be written as (for  $m_P^2 \ll M_W^2$ )

$$\begin{aligned} \mathcal{M} &= \langle \bar{\nu}_\ell \ell^- | \mathcal{L}_{eff} | P^- \rangle, \\ &= \frac{G_F}{\sqrt{2}} V_{Qq} \bar{u}(p_\ell) \gamma^\mu (1 - \gamma_5) v(p_{\bar{\nu}_\ell}) \langle 0 | \bar{v}(p_Q) \gamma_\mu (1 - \gamma_5) u(p_{\bar{q}}) | P^- \rangle. \end{aligned} \quad (12)$$

The hadronic matrix element must be of the form

$$\langle 0 | \bar{Q} \gamma_\mu \gamma_5 q | P^-(p) \rangle = i f_P p_\mu^P, \quad (13)$$

since  $p_\mu^P$  is the only four-vector associated with the initial state. The factor  $f_P$  is known as the pseudoscalar meson decay constant. Assuming massless neutrinos, the transition rate is then calculated to be

$$\Gamma(P^- \rightarrow \ell^- \bar{\nu}_\ell) = \frac{G_F^2 |V_{Qq}|^2}{8\pi} f_P^2 m_P m_\ell^2 \left(1 - \frac{m_\ell^2}{m_P^2}\right)^2, \quad (14)$$

and is helicity suppressed due to the overall  $m_\ell^2$  factor. In the case of pion decay, the inclusion of the radiative corrections and a comparison with the experimental value for  $\pi^- \rightarrow \mu^- \bar{\nu}_\mu + \mu^- \bar{\nu}_\mu \gamma$  yields the well-known value for the pion decay constant of  $f_\pi = 131$  MeV. Similarly, the kaon decay constant is measured to be  $f_K = 160$  MeV with a roughly 1% error due to the uncertainties associated with the value of  $V_{us}$ .

The leptonic decays of  $D$  and  $B$  mesons have not yet been observed (except for the case  $D_s^- \rightarrow \mu^- \bar{\nu}_\mu$ ), and will be discussed further below. Assuming that the relevant CKM matrix elements for these heavier quark systems are well-known, these decays would provide important information on the value of their associated pseudoscalar decay constants, which in turn are essential for the study of  $D^0 - \bar{D}^0$  and  $B^0 - \bar{B}^0$  mixing, CP violation in the charm and bottom sector, and in non-leptonic decays.

#### 3.1 Leptonic Decays of Charm Mesons

The SM transition rate for the purely leptonic decay of a pseudoscalar charm meson is given by Eq. (14) with the substitutions  $P \rightarrow D_q$  and  $Q \rightarrow c$ . The resulting branching fractions are small due to the helicity suppression and are listed in Table 1 using the central values of the CKM parameters given in Ref. 4 and assuming  $f_D = 200$  MeV and  $f_{D_s} = 230$  MeV. The existing upper limit for  $f_D$  is  $f_D < 290$  MeV, and is derived from the 90% C.L. bound<sup>14</sup>  $B(D^+ \rightarrow$

Meson	$\mu^- \bar{\nu}_\mu$	$\tau^- \bar{\nu}_\tau$
$D^-$	$3.52 \times 10^{-4}$	$9.34 \times 10^{-4}$
$D_s^-$	$4.21 \times 10^{-3}$	$4.11 \times 10^{-2}$

Table 1: SM branching fractions for the leptonic decay modes, assuming  $f_D = 200$  MeV and  $f_{D_s} = 230$  MeV.

$\mu^+ \nu_\mu$ )  $< 7.2 \times 10^{-4}$  from MARK III. One  $D \rightarrow \mu \bar{\nu}_\mu$  event has been observed<sup>15</sup> by the BES Collaboration, leading to  $f_D = 300^{+180}_{-150} {}^{+80}_{-40}$  MeV. This is consistent with the MARK III upper bound. Several measurements of  $f_{D_s}$  have now been performed, and they are all consistent within the present level of accuracy. CLEO has observed<sup>16</sup> the process  $D_s^{*+} \rightarrow D_s^+ \gamma \rightarrow \mu \nu \gamma$  by examining the mass difference  $\delta M \equiv M_{\mu \nu \gamma} - M_{\mu \nu}$  and have obtained

$$\frac{\Gamma(D_s^{*+} \rightarrow \mu^+ \nu)}{\Gamma(D_s^{*+} \rightarrow \phi \pi^+)} = 0.245 \pm 0.052 \pm 0.074. \quad (15)$$

Using  $\Gamma(D_s^+ \rightarrow \phi \pi^+) = 3.7 \pm 0.9\%$ , they find  $f_{D_s} = 344 \pm 37 \pm 52 \pm 42$  MeV where the last error reflects the uncertainty in the  $\phi \pi^+$  branching fraction. Two emulsion experiments have measured<sup>17</sup>  $f_{D_s} = 232 \pm 45 \pm 20 \pm 48$  MeV and  $f_{D_s} = 194 \pm 35 \pm 20 \pm 14$  MeV, respectively. And, the BES Collaboration has reported<sup>18</sup> the observation of candidate events in  $e^+ e^- \rightarrow D_s^+ D_s^-$  with the subsequent decay  $D_s^- \rightarrow \mu \bar{\nu}_\mu$  yielding  $f_{D_s} = 430^{+150}_{-130} \pm 40$  MeV. Here, the errors are expected to improve once more statistics are obtained. The current world average<sup>19</sup> value for the branching fraction is  $B(D_s^- \rightarrow \mu^- \bar{\nu}_\mu) = (4.6 \pm 0.8 \pm 1.2) \times 10^{-3}$ , corresponding to  $f_{D_s} = (241 \pm 21 \pm 30)$  MeV.

L3 has recently reported<sup>20</sup> the observation of  $D_s^- \rightarrow \tau^- \bar{\nu}_\tau$  with a branching fraction of  $(7.4 \pm 2.8 \pm 1.6 \pm 1.8)\%$ , allowing the determination  $f_{D_s} = 309 \pm 58 \pm 33 \pm 38$  MeV. Folding this determination with the world average  $f_{D_s}$  obtained from the  $\mu \bar{\nu}_\mu$  channel gives<sup>19</sup>  $f_{D_s} = (255 \pm 20 \pm 31)$  MeV.

A variety of theoretical techniques have been employed to estimate the value of  $f_D$  and  $f_{D_s}$ . Lattice QCD studies<sup>21</sup> calculate these quantities in the quenched approximation through a procedure that interpolates between the Wilson fermion scheme and the static approximation. The nonrelativistic quark model is used to relate the decay constant to the meson wave function at the origin,  $f_M = \sqrt{12/M_M} |\psi(0)|$ , which is then inferred from isospin mass splitting of heavy mesons.<sup>22</sup> Other approaches employ the relativistic quark model<sup>23</sup> or QCD sum rules.<sup>24</sup> For

Decay Constant	Lattice	Quark Model Nonrelativistic	Quark Model Relativistic	Sum Rule
$f_D$	$205 \pm 15$	$207 \pm 60$	$240 \pm 20$	$170 - 235$
$f_{D_s}$	$235 \pm 15$	$259 \pm 74$	$290 \pm 20$	$204 - 270$
$f_{D_s}/f_D$	$1.15 \pm 0.05$	$1.25$		$1.21 \pm 0.06$

Table 2: Theoretical estimates of the weak decay constants in units of MeV (taking  $m_c = 1.3$  GeV in the sum rule approach).

each of these calculational methods, the resulting ranges for the values of the pseudoscalar decay constants are presented in Table 2. A more complete collection of results is given in Ref. 23. Given the large errors, it is clear that these approaches are consistent. We also see that the theoretical predictions tend to be lower on average than the present experimental determinations. Once the experimental precision improves, discrimination between the various theoretical models should be possible, allowing for a better extrapolation to the  $B$  system. The theoretical uncertainties associated with the ratio  $f_{D_s}/f_D$  are much smaller, as this ratio should deviate from unity only in the presence of broken SU(3) flavor symmetry.

Non-SM contributions may affect the purely leptonic decays. Signatures for new physics include the measurement of non-SM values for the absolute branching ratios, or a deviation from the SM prediction

$$\frac{B(D_{(s)}^- \rightarrow \mu^- \bar{\nu}_\mu)}{B(D_{(s)}^- \rightarrow \tau^- \bar{\nu}_\tau)} = \frac{m_\mu^2 (1 - m_\mu^2/m_{D_{(s)}}^2)^2}{m_\tau^2 (1 - m_\tau^2/m_{D_{(s)}}^2)^2}. \quad (16)$$

This ratio is sensitive to violations of  $\mu - \tau$  universality.

As an example, we consider the case where the SM Higgs sector is enlarged by an additional Higgs doublet. As we will see below, these models generate important contributions<sup>25</sup> to the decay  $B^- \rightarrow \tau^- \bar{\nu}_\tau$ , and it is instructive to examine their effects in the charm sector. Two such models, which naturally avoid tree-level flavor changing neutral currents, are Model I; where one doublet ( $\phi_2$ ) generates masses for all fermions and the second ( $\phi_1$ ) decouples from the fermion sector, and Model II, where  $\phi_2$  gives mass to the up-type quarks, while the down-type quarks and charged leptons receive their mass from  $\phi_1$ . Each doublet receives a vacuum expectation value  $v_i$ , subject to the constraint that  $v_1^2 + v_2^2 = v_{\text{SM}}^2$ . The charged Higgs boson present in these models will mediate the leptonic decay through an

effective four-Fermi interaction, similar to that of the SM  $W$  boson. The  $H^\pm$  interactions with the fermion sector are governed by the Lagrangian

$$\mathcal{L} = \frac{g}{2\sqrt{2}M_W} H^\pm [V_{ij} m_u A_u \bar{u}_i (1 - \gamma_5) d_j + V_{ij} m_d A_d \bar{u}_i (1 + \gamma_5) d_j + m_\ell A_\ell \bar{\nu}_\ell (1 + \gamma_5) \ell] + h.c., \quad (17)$$

with  $A_u = \cot \beta$  in both models and  $A_d = A_\ell = -\cot \beta (\tan \beta)$  in Model I(II), where  $\tan \beta \equiv v_2/v_1$ . In Models I and II, we obtain the result

$$B(D^- \rightarrow \ell^- \bar{\nu}_\ell) = B_{SM} \left( 1 + \frac{m_D^2}{m_{H^\pm}^2} \right)^2, \quad (18)$$

where  $B_{SM}$  is the SM value of the leptonic branching fraction. In Model II, the  $D_s^-$  decay receives an additional modification

$$B(D_s^- \rightarrow \ell^- \bar{\nu}_\ell) = B_{SM} \left[ 1 + \frac{m_{D_s}^2}{m_{H^\pm}^2} \left( 1 - \tan^2 \beta \frac{m_s}{m_c} \right) \right]^2. \quad (19)$$

We see that the effect of the  $H^\pm$  exchange is independent of the leptonic final state and the above prediction for the ratio in Eq. 16 is unchanged. This is because the  $H^\pm$  contribution is proportional to the charged lepton mass, which is then a common factor with the SM helicity suppressed term. However, the absolute branching fractions can be modified; this effect is negligible in the decay  $D^- \rightarrow \ell^- \bar{\nu}_\ell$ , but could be of an order of a few percent in  $D_s^-$  decay if  $\tan \beta$  is very large.

### 3.2 Leptonic Decays of $B$ Mesons

The SM transition rate for the purely leptonic decays  $B^- \rightarrow \ell^- \bar{\nu}_\ell$  is again given by Eq. (14), with appropriate substitutions. Here, the resulting SM branching fractions, shown in Table 3, are even smaller than in the case of charm mesons due to the value of  $V_{ub}$ . These SM predictions are somewhat imprecise due to the uncertainty in  $f_B$  and  $V_{ub}$ , and hence can vary over the range

$$B_{SM} \left( \frac{f_B}{180 \text{ MeV}} \right)^2 \left( \frac{V_{ub}}{0.0035} \right)^2, \quad (20)$$

where  $B_{SM}$  is the result listed in the table. We see from the table that the 90% C.L. experimental bounds<sup>20,26</sup> are roughly one to two orders of magnitude above the SM predictions for the cases of  $B^- \rightarrow \mu^- \bar{\nu}_\mu, \tau^- \bar{\nu}_\tau$ . The B factories presently

Mode	SM Prediction	Experimental Bound
$e^- \bar{\nu}_e$	$6.9 \times 10^{-12}$	$< 1.5 \times 10^{-5}$ (CLEO)
$\mu^- \bar{\nu}_\mu$	$2.9 \times 10^{-7}$	$< 2.1 \times 10^{-5}$ (CLEO)
$\tau^- \bar{\nu}_\tau$	$6.6 \times 10^{-5}$	$< 5.7 \times 10^{-4}$ (L3)

Table 3: SM branching fractions for the  $B^-$  leptonic decay modes, assuming  $f_B = 180$  MeV and taking the central value<sup>4</sup> of the CKM matrix element  $V_{ub}$ . The results of experimental searches<sup>19,25</sup> are also shown.

Decay Constant	Lattice	Quark Model Nonrelativistic	Quark Model Relativistic	Sum Rule
$f_{B_d}$	$175 \pm 25$	$140 \pm 40$	$155 \pm 15$	$155 - 185$
$f_{B_s}$	$200 \pm 25$	$175 \pm 50$	$210 \pm 20$	$195 - 220$
$f_{B_s}/f_{B_d}$	$1.15 \pm 0.05$	1.25		$1.22 \pm 0.02$

Table 4: Theoretical estimates of the weak decay constants in units of MeV (taking  $m_b = 4.67$  GeV in the sum rule approach).

under construction at SLAC and KEK should be able to observe  $B \rightarrow \tau \nu_\tau$  (and potentially the  $\mu \bar{\nu}_\mu \gamma$  mode as well). This measurement will require the full (or partial) reconstruction of the other  $B$ 's in the event as well as a large statistical sample. Theoretical estimates for  $f_{B_{d,s}}$  are tabulated in Table 4 using the same approaches as in the cases discussed above in charm decays. See Ref. 23 for a more complete compilation.

Observation of these decays would, of course, provide a classic measurement of the decay constant  $f_B$  (assuming  $V_{ub}$  is known from other sources), but only if no new physics contributes to the decay. For example, in two-Higgs-doublet models (2HDM), tree-level charged Higgs exchange can again mediate this transition. In the 2HDM of Type II, the branching fraction is now modified by

$$B(B^- \rightarrow \ell^- \bar{\nu}_\ell) = B_{SM} \left( 1 - \tan^2 \beta \frac{m_B^2}{m_{H^\pm}^2} \right)^2. \quad (21)$$

Taking the SM and L3 bound on  $B^- \rightarrow \tau^- \bar{\nu}_\tau$  listed in Table 3 implies  $\tan \beta/m_{H^\pm} < 0.38 \text{ GeV}^{-1}$ , assuming  $f_B = 190$  MeV and  $|V_{ub}| = 0.0033 \pm 0.0008$ . Once this decay is detected, tests for this type of scalar exchange can be performed by measuring the helicity of the final state  $\tau$ . The measured branching fraction from

LEP for the decay  $B \rightarrow X\tau\nu$  yields<sup>25,26</sup> a similar constraint of  $\tan\beta/m_{H^\pm} < 0.52 \text{ GeV}^{-1}$ , which is independent of the uncertainties in  $f_B$  and  $V_{ub}$ .

## 4 Flavor Changing Neutral Current Decays

Flavor changing neutral current (FCNC) decays only occur at the loop level in the SM. Tree-level neutral currents are flavor diagonal due to the fact that all fermions with the same charge and helicity have identical transformation properties under the  $SU(2)_L \times U(1)_Y$  gauge group,<sup>27</sup> so that the flavor to mass eigenstate rotation matrices commute with the neutral current operator. In fact, this property provided the original motivation for Glashow, Iliopoulos, and Maiani<sup>28</sup> (GIM) to introduce the charm quark in order to suppress phenomenologically unacceptable large values of FCNC processes in the kaon system. This allowed for the strange quark to have the same electroweak quantum number assignments as the down quark; hence eradicating the tree-level strangeness changing neutral current. The GIM mechanism thus achieves this tree-level cancellation without any artificial adjustments to the parameters of the theory and also provides additional suppression for FCNC that are induced at the loop level.

The one-loop processes which mediate FCNC's can generally be classified as electromagnetic, weak, or gluon penguin diagrams and box diagrams. Samples of these classes of diagrams are displayed in Fig. 1. The generic amplitude for a diagram of this type can be written as

$$A \sim \sum_{i=1}^3 V_{iQ} V_{iQ}^* F(m_i^2/M_W^2), \quad (22)$$

where the sum extends over the three generations of quarks of mass  $m_i$  contributing internally to the diagram, the  $V_{ij}$  are the relevant CKM elements appearing at the vertices, and the function  $F$  represents the result of the loop integrals for the diagrams. Using the unitarity property of the three-generation CKM matrix,  $\sum_i V_{iQ} V_{iQ}^* = 0$ , allows one to rewrite the amplitude as

$$A \sim V_{2Q} V_{2Q}^* [F(m_2^2/M_W^2) - F(m_1^2/M_W^2)] + V_{3Q} V_{3Q}^* [F(m_3^2/M_W^2) - F(m_1^2/M_W^2)]. \quad (23)$$

This clearly demonstrates that the amplitude would vanish if all the contributing internal quarks were degenerate! Hence, the magnitude of FCNC transitions is related to the size of the internal quark mass splittings. This point is illustrated in

Meson/Quark	Branching Fraction
K	$10^{-10} - 10^{-8}$
D	$10^{-18} - 10^{-10}$
B	$10^{-8} - 10^{-4}$
t	$10^{-12} - 10^{-9}$

Table 5: Typical values of FCNC branching fractions in the SM.

Table 5 which displays the typical SM range of FCNC branching fractions for each meson/quark system. As we would expect, the  $B$  meson system has the largest FCNC rates due to the large degree of mass splitting in the up-quark sector and due to the diagonal structure of the CKM matrix, whereas the charm mesons and top-quark rates are very suppressed by the efficiency of the GIM mechanism.

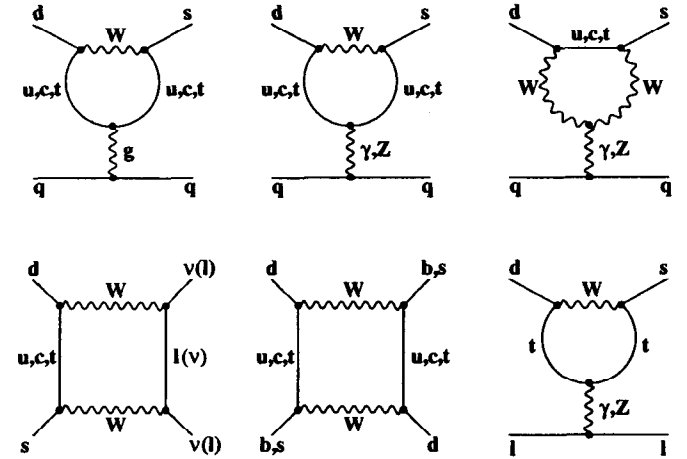


Figure 1: Feynman diagrams.

QCD corrections to these rare processes can be quite important. They are computed<sup>29</sup> via the Operator Product Expansion combined with renormalization group evolution. This procedure allows for an efficient separation of short-distance physics (corresponding to scales higher than  $\mu$ ) and long-distance contributions (scales lower than  $\mu$ ). Within this framework, the exclusive transition  $M \rightarrow F$

can be expressed as

$$\mathcal{A}(M \rightarrow F) = \frac{G_F}{\sqrt{2}} V_{CKM} \sum_i C_i(\mu) \langle F | \mathcal{O}_i(\mu) | M \rangle, \quad (24)$$

where  $\mathcal{O}_i$  represents the complete set of effective operators which govern the transition, the  $C_i$  are the Wilson coefficients which are related to the Inami-Lim functions at the scale  $\mu = M_W$ , and  $\mu$  corresponds to the scale at which the transition takes place. The  $\mu$  dependence of the Wilson coefficients is given by the renormalization group equations (RGE) and must be cancelled by the  $\mu$  dependence contained in  $\langle \mathcal{O}_i \rangle$ . The use of the RGE allows for the summation of the large logarithms  $\log(M_W/\mu)$  at a given order in perturbation theory. The long-distance, or nonperturbative, contributions are contained in the evaluation of the matrix elements of the operators.

#### 4.1 Radiative Decays

We start our discussion of FCNC transitions with the study of radiative decays,  $Q \rightarrow q'\gamma$ . The most general Lorentz decomposition of the radiative amplitude is

$$\begin{aligned} \mathcal{A}(Q \rightarrow q'\gamma) &= \epsilon^\lambda(q) \langle q' | J_\lambda^{em} | Q \rangle, \\ &= \epsilon^\lambda(q) \bar{u}_{q'}(p-q) [iq^\nu \sigma_{\lambda\nu} (A + B\gamma_5) + \gamma_\lambda (C + D\gamma_5) \\ &\quad + q_\lambda (E + F\gamma_5)] u_Q(p), \end{aligned} \quad (25)$$

where  $\epsilon^\lambda$  is the photon polarization,  $q$  represents the outgoing photon's momentum, and  $A-F$  are the invariant amplitudes for each case. Electromagnetic gauge invariance, which dictates  $\partial^\lambda J_\lambda^{em} = 0$ , yields the condition

$$-m_{q'}(C + D\gamma_5) + m_Q(C - D\gamma_5) + q^2(E + F\gamma_5) = 0. \quad (26)$$

For an on-shell photon ( $q^2 = 0$ ), this gives  $C = D = 0$ . Folding in the property  $\epsilon^\lambda \cdot q_\lambda = 0$ , we are left with the magnetic dipole transition amplitude

$$\mathcal{A}(Q \rightarrow q'\gamma) = \epsilon^\lambda(q) \bar{u}_{q'}(p-q) [iq^\nu \sigma_{\lambda\nu} (A + B\gamma_5)] u_Q(p). \quad (27)$$

This amplitude is represented by a gauge invariant set of loop diagrams (in this case, electromagnetic penguin diagrams) which sum to a finite result as there are

Quark	$F_2$	$ V_{ci}^* V_{ui}  F_2$	$ V_{ib} V_{is}  F_2$
d	$1.57 \times 10^{-9}$	$3.36 \times 10^{-10}$	
s	$2.92 \times 10^{-7}$	$6.26 \times 10^{-8}$	
b	$3.31 \times 10^{-4}$	$3.17 \times 10^{-8}$	
u	$2.27 \times 10^{-9}$		$1.29 \times 10^{-12}$
c	$2.03 \times 10^{-4}$		$7.34 \times 10^{-6}$
t	0.39		$1.56 \times 10^{-2}$

Table 6: Contributions to  $c \rightarrow u\gamma$  and  $b \rightarrow s\gamma$ .

no counterterms to absorb the infinities. The perturbative calculation of these diagrams yield the familiar result (neglecting the mass of the final state quark)

$$\begin{aligned} \Gamma(Q \rightarrow q'\gamma) &= \frac{G_F^2 \alpha_{em}^5}{128\pi^4} \left| V_{2Q} V_{2q}^* \left[ F_2(m_2^2/M_W^2) - F_2(m_1^2/M_W^2) \right] \right. \\ &\quad \left. + V_{3Q} V_{3q}^* \left[ F_2(m_3^2/M_W^2) - F_2(m_1^2/M_W^2) \right] \right|^2, \end{aligned} \quad (28)$$

where the function  $F_2$  is given in Inami and Lim.<sup>30</sup> It is instructive to compare the magnitude of these functions for the decays  $c \rightarrow u\gamma$  and  $b \rightarrow s\gamma$ , for the various internal quark states; this is presented in Table 6. Dominance of the t-quark intermediate state in  $b \rightarrow s\gamma$  is evident, even upon including the CKM factors. Its effect is so large that the other intermediate states are numerically negligible and hence are typically omitted. The amplitudes for  $c \rightarrow u\gamma$  differ from that of  $b \rightarrow s\gamma$  in two important respects: (i) there is no single intermediate state which dominates, and (ii) the overall magnitude is much smaller. The effectiveness of the GIM mechanism is clearly demonstrated.

##### 4.1.1 Radiative B Decays

Radiative  $B$  decays have become the benchmark FCNC process and provide one of the best testing grounds of the SM. The CLEO Collaboration has reported<sup>31</sup> the observation of the inclusive decay  $B \rightarrow X_s \gamma$  with a branching fraction of  $(2.32 \pm 0.57 \pm 0.35) \times 10^{-4}$  and 95% C.L. bounds of  $1 \times 10^{-4} < B(B \rightarrow X_s \gamma) < 4.2 \times 10^{-4}$ , as well as an updated measurement<sup>32</sup> for the related exclusive process  $B(B \rightarrow K^* \gamma) = (4.2 \pm 0.8 \pm 0.6) \times 10^{-5}$ . This yields a value of  $0.181 \pm 0.068$  for the ratio of exclusive to inclusive rates. On the theoretical side, the reliability of the calculation of the quark-level process  $B \rightarrow X_s \gamma$  has improved with the

completion of the next-to-leading logarithmic QCD corrections. It has thus provided strong restrictions on the parameters of several theories beyond the SM.<sup>33</sup> This constitutes the first direct observation of a penguin mediated process(!) and demonstrates the fertile ground ahead for the detailed exploration of the SM in rare  $B$  transitions.

In the SM, the quark-level transition  $B \rightarrow X_s \gamma$  is mediated by  $W$ -boson and  $t$ -quark exchange in an electromagnetic penguin diagram, as discussed above. To obtain the branching fraction, the inclusive rate is scaled to that of the semi-leptonic decay  $B \rightarrow X \ell \bar{\nu}_\ell$ . This procedure removes uncertainties from the overall factor of  $m_b^5$  and reduces the ambiguities involved with the imprecisely determined CKM factors. The result is then rescaled by the experimental value for the semi-leptonic branching fraction,

$$B(B \rightarrow X_s \gamma) = \frac{\Gamma(B \rightarrow X_s \gamma)}{\Gamma(B \rightarrow X \ell \bar{\nu}_\ell)} B(B \rightarrow X \ell \bar{\nu}_\ell). \quad (29)$$

The QCD corrections are calculated<sup>34</sup> via an operator product expansion based on the effective Hamiltonian

$$\mathcal{H}_{eff} = \frac{-4G_F}{\sqrt{2}} V_{tb} V_{ts}^* \sum_{i=1}^8 C_i(\mu) \mathcal{O}_i(\mu), \quad (30)$$

which is then evolved from the electroweak scale down to  $\mu \sim m_b$  by the Renormalization Group Equations (RGE). The  $\mathcal{O}_i$  are a complete set of renormalized operators of dimension six or less which mediate  $b \rightarrow s$  transitions. They consist of the two current-current operators  $\mathcal{O}_{1,2}$ , the four strong penguin operators  $\mathcal{O}_{3-6}$ , and the electro- and chromo-magnetic dipole operators  $\mathcal{O}_7$  and  $\mathcal{O}_8$ , respectively, and can be written as

$$\begin{aligned} \mathcal{O}_1 &= (\bar{c}_\alpha \gamma_\mu P_L b_\beta) (\bar{s}_\beta \gamma^\mu P_L c_\alpha), \\ \mathcal{O}_2 &= (\bar{c}_\alpha \gamma_\mu P_L b_\alpha) (\bar{s}_\beta \gamma^\mu P_L c_\beta), \\ \mathcal{O}_3 &= (\bar{s}_\alpha \gamma_\mu P_L b_\alpha) \sum_q (\bar{q}_\beta \gamma^\mu P_L q_\beta), \\ \mathcal{O}_4 &= (\bar{s}_\alpha \gamma_\mu P_L b_\beta) \sum_q (\bar{q}_\beta \gamma^\mu P_L q_\alpha), \\ \mathcal{O}_5 &= (\bar{s}_\alpha \gamma_\mu P_L b_\alpha) \sum_q (\bar{q}_\beta \gamma^\mu P_R q_\beta), \\ \mathcal{O}_6 &= (\bar{s}_\alpha \gamma_\mu P_L b_\beta) \sum_q (\bar{q}_\beta \gamma^\mu P_R q_\alpha), \end{aligned} \quad (31)$$

$$\begin{aligned} \mathcal{O}_7 &= \frac{e}{16\pi^2} m_b (\bar{s}_\alpha \sigma_{\mu\nu} P_R b_\alpha) F^{\mu\nu}, \\ \mathcal{O}_8 &= \frac{g_s}{16\pi^2} m_b (\bar{s}_\alpha \sigma_{\mu\nu} T_{\alpha\beta}^a P_R b_\beta) G^{a\mu\nu}, \end{aligned}$$

where the terms proportional to  $m_s$  in  $\mathcal{O}_{7,8}$  have been neglected. We note that the magnetic and chromomagnetic dipole operators,  $\mathcal{O}_{7,8}$ , contain explicit mass factors which must also be renormalized as shown below.

The  $C_i$  represent the corresponding Wilson coefficients which are evaluated perturbatively at the electroweak scale, where the matching conditions are imposed and then evolved down to the renormalization scale  $\mu$ . The expressions for the coefficients at the  $W$  scale are

$$\begin{aligned} C_{1,3-6}(M_W) &= 0, \quad C_2(M_W) = 1, \\ C_7(M_W) &= -\frac{1}{2} F_2(x_t), \quad C_8(M_W) = -\frac{1}{2} D(x_t), \end{aligned} \quad (32)$$

with  $x \equiv m_t^2/M_W^2$  and

$$\begin{aligned} F_2(x) &= Q \left[ \frac{x^3 - 5x^2 - 2x}{4(x-1)^3} + \frac{3x^2 \ln x}{2(x-1)^4} \right] + \frac{2x^3 + 5x^2 - x}{4(x-1)^3} - \frac{3x^3 \ln x}{2(x-1)^4}, \\ D(x) &= \frac{x^3 - 5x^2 - 2x}{4(x-1)^3} + \frac{3x^2 \ln x}{2(x-1)^4}, \end{aligned} \quad (33)$$

where  $Q$  represents the charge of the internal quark.

The leading logarithmic QCD corrections to the decay width have been completely resummed, but lead to a sizable  $\mu$  dependence of the branching fraction, and hence, it is essential to include the next-to-leading order corrections to reduce the theoretical uncertainty. In this case, the calculation of the perturbative QCD corrections involves several steps, requiring corrections to both the Wilson coefficients and the matrix elements of the operators in Eq. (30) in order to ensure a scheme-independent result. For the matrix elements, this includes the QCD bremsstrahlung corrections<sup>35</sup>  $b \rightarrow s \gamma + g$ , and the NLO virtual corrections which have recently been completed in both the naive dimensional regularization (NDR) and 't Hooft-Veltman schemes.<sup>36</sup> Summing these contributions to the matrix elements and expanding them around  $\mu = m_b$ , one arrives at the decay amplitude

$$\mathcal{M}(b \rightarrow s \gamma) = -\frac{4G_F V_{tb} V_{ts}^*}{\sqrt{2}} D \langle s \gamma | \mathcal{O}_7(m_b) | b \rangle_{tree}, \quad (34)$$

with

$$D = C_7^{eff}(\mu) + \frac{\alpha_s(m_b)}{4\pi} \left( C_i^{(0)eff}(\mu) \gamma_{ii}^{(0)eff} \log \frac{m_b}{\mu} + C_i^{(0)eff} r_i \right). \quad (35)$$

Here, the quantities  $\gamma_{i7}^{(0)eff}$  are the entries of the effective leading order anomalous dimension matrix, and the  $r_i$  are computed in Greub *et al.*,<sup>36</sup> for  $i = 2, 7, 8$ . The first term in Eq. (35),  $C_7^{eff}(\mu)$ , must be computed at NLO precision, while it is consistent to use the leading order values of the other coefficients. The explicit logarithms  $\alpha_s(m_b) \log(m_b/\mu)$  in the equation are cancelled by the  $\mu$  dependence of  $C_7^{(0)eff}(\mu)$ . This feature significantly reduces the scale dependence of the resulting branching fraction. The contribution to the inclusive width including these virtual corrections is then

$$\Gamma_{NLO}^{virt}(B \rightarrow X_s \gamma) = \frac{m_{b,pole}^5 G_F^2 \alpha_{em} |V_{ts} V_{tb}^*|^2}{32\pi^4} F |D|^2, \quad (36)$$

where the factor  $F = m_b^2(m_b)/m_{b,pole}^2 = 1 - 8\alpha_s(m_b)/3\pi$  arises from the mass factor present in the magnetic dipole operator. This should be compared to the familiar leading order result (which omits the virtual corrections to  $\langle \mathcal{O}_7 \rangle$ )

$$\Gamma(B \rightarrow X_s \gamma) = \frac{m_{b,pole}^5 G_F^2 \alpha_{em} |V_{ts} V_{tb}^*|^2 |C_7^{eff}(\mu)|^2}{32\pi^4}. \quad (37)$$

For the Wilson coefficients, the NLO result entails the computation of the  $\mathcal{O}(\alpha_s)$  terms in the matching conditions, and the renormalization group evolution of the  $C_i(\mu)$  must be computed using the  $\mathcal{O}(\alpha_s^2)$  anomalous dimension matrix. The former step has been computed in Ref. 37. The latter step is quite difficult, since some entries in the matrix have to be extracted from three-loop diagrams, and has recently been completed,<sup>38</sup> with the conclusion being that in the NDR scheme the NLO correction to  $C_7^{eff}(\mu)$  is small.

The total inclusive width is then given by the sum of the virtual and bremsstrahlung corrections,  $\Gamma(B \rightarrow X_s \gamma) = \Gamma^{virt} + \Gamma^{brems}$ , where  $\Gamma^{brems}$  is given in Greub *et al.*,<sup>35,36</sup> and the branching fraction is calculated by scaling to the semileptonic decay rate. The leading order power corrections in the heavy quark expansion are identical for  $B \rightarrow X_s \gamma$  and  $B \rightarrow X \ell \bar{\nu}_\ell$ , and hence cancel in the ratio.<sup>39</sup> This allows us to approximate  $\Gamma(B \rightarrow X_s \gamma)$  with the perturbatively calculable free quark decay rate. For  $m_t^{phys} = 175 \pm 6$  GeV (Ref. 13),  $m_b/2 \leq \mu \leq 2m_b$ ,  $\alpha_s = 0.118 \pm 0.003$  (Refs. 4, 40),  $B_{sl} = (10.23 \pm 0.39)\%$  (Ref. 41), and  $m_c/m_b = 0.29 \pm 0.02$ , we find the branching fraction

$$B(B \rightarrow X_s \gamma) = (3.25 \pm 0.30 \pm 0.40) \times 10^{-4}, \quad (38)$$

where the first error corresponds to the combined uncertainty associated with the value of  $m_t$  and  $\mu$ , and the second error represents the uncertainty from the

other parameters. This is well within the range observed by CLEO. In Fig. 2, the inclusive branching fraction is displayed as a function of the top mass from Ref. 42. The dashed lines indicate the error in the branching ratio if we fix  $\mu = m_b$  and vary all the other parameters over their allowed ranges given above. The solid lines indicate the error for  $m_b/2 < \mu < 2m_b$  with all other parameters fixed to their central values. This visually demonstrates that the error in the theoretical calculation of  $B \rightarrow X_s \gamma$  is not overwhelmed by the scale uncertainty; other uncertainties are now comparable. Within the SM (and assuming  $V_{tb} = 1$ ), comparison with the experimental result gives  $|V_{ts}/V_{cb}| = 0.85 \pm 0.12(exp) \pm 0.10(th)$ , which is consistent with unity.<sup>43</sup>

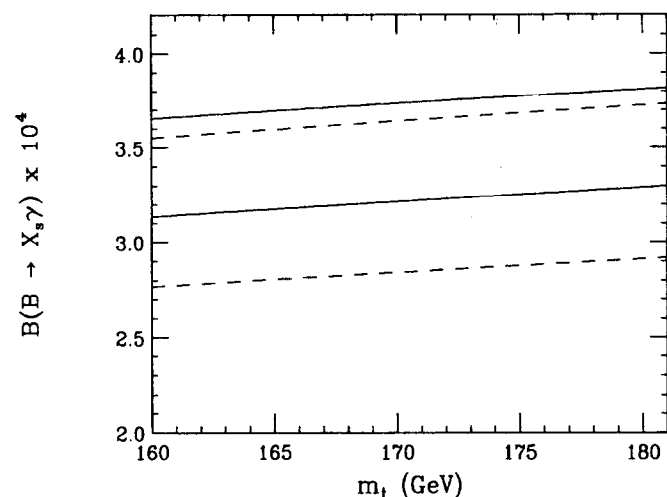


Figure 2: The branching ratio of  $B \rightarrow X_s \gamma$  vs  $m_t$ . The dashed lines indicate the error in the branching ratio if we fix  $\mu = m_b$  and vary all the other parameters over their allowed ranges:  $\alpha_s(M_Z) = 0.118 \pm 0.003$ ,  $B_{sl} = 10.23 \pm 0.39\%$ , and  $m_c/m_b = 0.29 \pm 0.02$ . The solid lines indicate the error for  $m_b/2 < \mu < 2m_b$  and all other parameters fixed to their central values.

Before discussing explicit models of new physics, we first investigate the constraints placed directly on the Wilson coefficients of the magnetic moment operators from the CLEO measurement of  $B \rightarrow X_s \gamma$ . Writing the coefficients at the matching scale in the form  $C_i(M_W) = C_i^{SM}(M_W) + C_i^{new}(M_W)$ , where  $C_i^{new}(M_W)$

represents the contributions from new interactions. Due to operator mixing, the CLEO measurement of  $B \rightarrow X_s \gamma$  then limits the possible values for  $C_i^{\text{new}}(M_W)$  for  $i = 7, 8$ . These bounds are summarized in Fig. 3, where the allowed regions lie inside the diagonal bands.<sup>42</sup> We note that two bands occur due to the overall sign ambiguity in the determination of the coefficients. Here, the solid bands correspond to the constraints obtained from the current CLEO measurement, taking into account the variation of the renormalization scale  $m_b/2 \leq \mu \leq 2m_b$ , as well as the allowed ranges of the other input parameters. The dashed bands represent the constraints when the scale is fixed to  $\mu = m_b$ . We note that large values of  $C_8^{\text{new}}(M_W)$  are allowed even in the region where  $C_7^{\text{new}}(M_W) \simeq 0$ . Experimental bounds on the decay  $b \rightarrow sg$  are needed to constrain  $C_8$ .

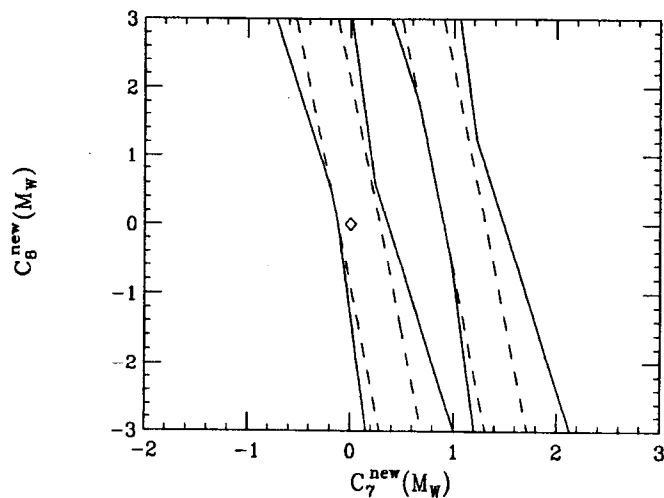


Figure 3: Bounds on the contributions from new physics to  $C_{7,8}$ . The region allowed by the CLEO data corresponds to the area inside the solid diagonal bands. The dashed bands represent the constraints when the renormalization scale is set to  $\mu = m_b$ . The diamond at the position (0,0) represents the Standard Model.

#### • Fourth Generation

In the case of four families, there is an additional contribution to  $B \rightarrow X_s \gamma$  from the virtual exchange of the fourth generation up-quark  $t'$  (Ref. 44). The

Wilson coefficients of the dipole operators are then modified by

$$C_{7,8}(M_W) = C_{7,8}^{\text{SM}}(m_t^2/M_W^2) + \frac{V_{t'b}V_{t's}^*}{V_{tb}V_{ts}^*} C_{7,8}^{\text{SM}}(m_{t'}^2/M_W^2). \quad (39)$$

$V_{ij}$  represents the  $4 \times 4$  CKM matrix which now contains nine parameters; six angles and three phases. The values of the elements of the  $4 \times 4$  CKM matrix are much less restricted than their three-generation counterparts, as one can no longer apply the three-generation unitarity constraints.<sup>4</sup> Hence, even the overall CKM factor in the  $B \rightarrow X_s \gamma$  branching ratio,  $|V_{ub}V_{cb}^*/V_{cb}|$ , can take on different values. Figure 4(a) displays the resulting branching fraction as a function of  $m_{t'}$  for  $m_t = 180$  GeV; here the vertical lines represent the range of possible values as the CKM elements are varied. These ranges were determined by generating  $10^8$  sets of the nine parameters in the  $4 \times 4$  CKM matrix and demanding consistency with (i) four-generation unitarity and the extraction of the CKM elements from charged current measurements, (ii) the value of the ratio  $|V_{ub}/V_{cb}|$ , (iii)  $\epsilon$ , and (iv)  $B^0 - \bar{B}^0$  mixing. We see that there is little or no sensitivity to the  $t'$ -quark mass, and that the CLEO measurement places additional constraints on the  $4 \times 4$  CKM matrix. In fact, we find that consistency with CLEO demands  $0.20 \leq |V_{ub}V_{cb}| \leq 1.5 \times 10^{-2}$  and  $0.23 \leq |V_{t'b}V_{t's}| \leq 1.1 \times 10^{-3}$ .

#### • Two-Higgs-Doublet Models

In 2HDM, the  $H^\pm$  contributes to  $B \rightarrow X_s \gamma$  via virtual exchange together with the top quark. At the  $W$  scale, the coefficients of the dipole operators take the form (in Model II described above)

$$C_i(M_W) = C_i^{\text{SM}}(m_t^2/M_W^2) + A_{1,i}^{H^\pm}(m_t^2/m_{H^\pm}^2) + \frac{1}{\tan^2 \beta} A_{2,i}^{H^\pm}(m_t^2/m_{H^\pm}^2), \quad (40)$$

where  $i = 7, 8$ . The analytic form of the functions  $A_{1,i}, A_{2,i}$  can be found in Refs. 45 and 46. In Model II, large enhancements appear for small values of  $\tan \beta$ , but more importantly, we see that  $B(B \rightarrow X_s \gamma)$  is always larger than that of the SM, independent of the value of  $\tan \beta$  due to the presence of the  $A_{1,i}^{H^\pm}$  term. This leads to the familiar bound<sup>31</sup>  $m_{H^\pm} > 260$  GeV obtained from the measurement of  $B(B \rightarrow X_s \gamma)$  by CLEO. However, this constraint does not make use of the recent NLO calculation. We remind the reader that a full NLO calculation would also require the higher order matching conditions for the  $H^\pm$  contributions. Nevertheless, we recall that the results on the NLO corrections to  $C_7^{\text{eff}}(\mu)$  indicate they are small,<sup>38</sup> and a good approximation is obtained by employing the uncorrected  $H^\pm$

matching conditions. Since the NLO corrections to the matrix element drastically reduces the  $\mu$  dependence of the branching fraction, we would expect the resulting  $H^\pm$  constraints to improve. Indeed, we find that<sup>42</sup> the CLEO bound excludes the region to the left and beneath the curves in Fig. 4(b). For  $m_t^{\text{phys}} = 169$  GeV, we see that  $m_{H^\pm} > 300$  GeV. This is calculated by using the same procedure that produced the previous charged Higgs mass bound by CLEO, *i.e.*, all the input parameters (*e.g.*,  $\alpha_s$ ,  $\mu$ ,  $m_c/m_b$ , and  $B(B \rightarrow X \ell \bar{\nu}_\ell)$ ) are varied over their allowed ranges in order to ascertain the most conservative limit. This bound holds in the general two-Higgs-doublet-model II, and in supersymmetry if the superpartners are all significantly massive.

### • Supersymmetry

There are several new classes of contributions to  $B \rightarrow X_s \gamma$  in supersymmetry. The large  $H^\pm$  contributions from Model II discussed above are present; however, the limits obtained in supersymmetric theories also depend on the size of the other super-particle contributions and are generally much more complex. In particular, it has been shown<sup>47,48</sup> that large contributions can arise from stop-squark and chargino exchange (due to the possibly large stop-squark mass splitting), as well as from the gluino and down-type squark loops (due to left-right mixing in the sbottom sector). The additional neutralino-down-squark contributions are expected to be small. Some regions of the parameter space can thus cancel the  $H^\pm$  contributions resulting in predictions for the branching fraction at (or even below) the SM value, while other regions always enhance the amplitude. In minimal supergravity models with radiative breaking, the sign of the sparticle loop contributions is found to be correlated with the sign of the higgsino mass parameter  $\mu$  (Refs. 48, 49). A scatter plot in the  $R_7 - R_8$  plane is presented<sup>42</sup> in Fig. 4(c), where  $R_i \equiv \frac{C_i^{\text{NSM}}(M_W)}{C_i^{\text{SM}}(M_W)} - 1 \equiv \frac{C_i^{\text{NSM}}(M_W)}{C_i^{\text{SM}}(M_W)}$ . Each point in the scatter plot is derived from the minimal supergravity model with different initial conditions, and is consistent with all collider bounds and is out of reach of LEP II. The first thing to note from the figure is that large values of  $R_7$  and  $R_8$  are generated, and the  $R_7$  and  $R_8$  values are very strongly correlated. The diagonal bands represent the bounds on the Wilson coefficients from the observation of  $B \rightarrow X_s \gamma$  as determined previously. We see that the current CLEO data already places significant restrictions on the supersymmetric parameter space. Further constraints will be obtainable once a 10% measurement of  $B(B \rightarrow X_s \gamma)$  is made, and the sign of

$C_7$  is determined from a global fit described below. In this case, if no deviations from the SM are observed, the supersymmetric contributions will be restricted to lie in the dashed band. It is clear that these processes can explore vast regions of the supersymmetric parameter space. In fact, it is possible that spectacularly large deviations in rare  $B$  decays could be manifest at  $B$  factories, while collider experiments would not detect a hint of new physics.

### • Anomalous Top-Quark Couplings

If the top quark has anomalous couplings to on-shell photons or gluons, the rate for  $B \rightarrow X_s \gamma$  would be modified. The effect of an anomalous magnetic and/or electric dipole moment in the Lagrangian

$$\mathcal{L} = e\bar{t} \left[ Q_t \gamma_\mu + \frac{1}{2m_t} \sigma_{\mu\nu} (\kappa_\gamma + i\tilde{\kappa}_\gamma \gamma_5) q^\nu \right] t A^\mu, \quad (41)$$

on the Wilson coefficients is

$$C_{7,8}(M_W) = C_{7,8}^{\text{SM}}(m_t^2/M_W^2) + \kappa_{\gamma,g} F_{1,8}(m_t^2/M_W^2) + \tilde{\kappa}_{\gamma,g} F_{2,8}(m_t^2/M_W^2). \quad (42)$$

The functions  $F_{1,2}$  can be found in Ref. 50. The effects of anomalous chromo-dipole moments arise from operator mixing. When the resulting branching fraction and the CLEO data are combined, the constraints (at leading order) in Fig. 4(d) are obtained<sup>51</sup> for  $m_t = 180$  GeV. In this figure, the allowed region is given by the area inside the solid (dashed) semicircle when  $\kappa_g, \tilde{\kappa}_g = 0$  ( $= \kappa_\gamma, \tilde{\kappa}_\gamma$ ). These bounds are considerably weaker than those obtainable from direct top-quark production at colliders.<sup>52</sup>

One of the goals of a high-luminosity  $B$  physics program is to extract the ratio of CKM elements  $|V_{td}|/|V_{ts}|$  from a measurement of

$$\frac{B(B^- \rightarrow \rho^- \gamma)}{B(B^- \rightarrow K^{*-} \gamma)} = \frac{B(B^0 \rightarrow \rho^0 \gamma) + B(B^0 \rightarrow \omega \gamma)}{B(B^0 \rightarrow K^{*0} \gamma)} = \left| \frac{V_{td}}{V_{ts}} \right|^2 \xi \Omega, \quad (43)$$

where  $\xi$  accounts for SU(3) symmetry breaking and  $\Omega$  represents the phase space ratio. CLEO has recently placed<sup>32</sup> the bounds on the exclusive branching fractions,  $B(B^0 \rightarrow \rho^0 \gamma) < 3.9 \times 10^{-5}$ ,  $B(B^- \rightarrow \rho^- \gamma) < 1.1 \times 10^{-5}$ , and  $B(B^0 \rightarrow \omega^0 \gamma) < 1.3 \times 10^{-5}$ . Combining this with their measurement of  $B \rightarrow K^* \gamma$  and theoretical estimates<sup>53</sup> of the SU(3) breaking factor places the 90% C.L. constraint  $|V_{td}|/|V_{ts}| < 0.45 - 0.56$ . However, this technique of determining this ratio of

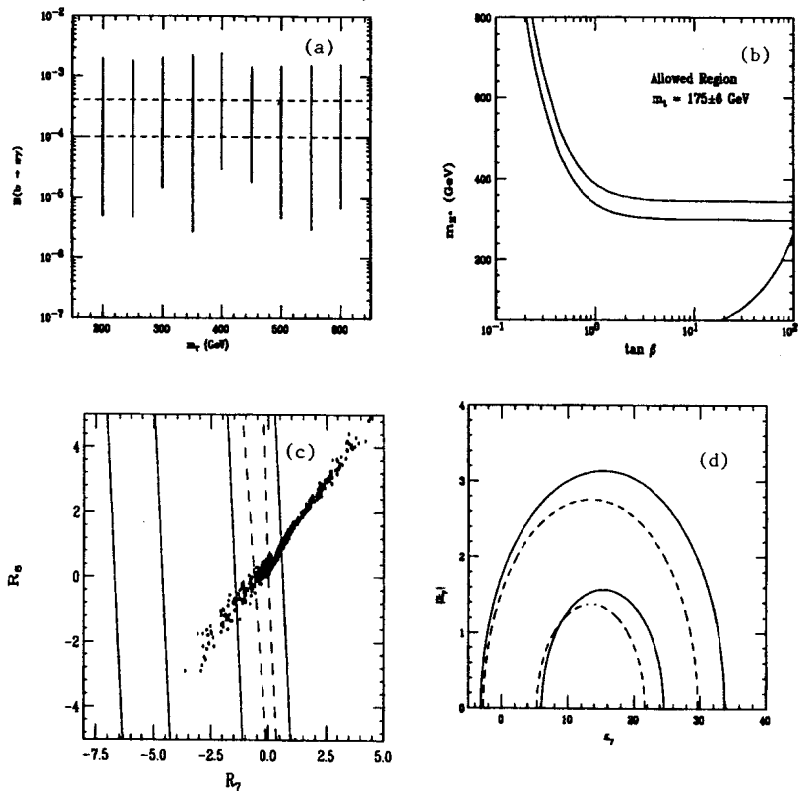


Figure 4: (a) The range of values for  $B(B \rightarrow X_s \gamma)$  in the four-generation SM as a function of  $m_\nu$ . (b) Constraints in the charged Higgs mass -  $\tan\beta$  plane from the CLEO bound on  $B(B \rightarrow X_s \gamma)$ . The excluded region is that to the left and below the curves. The top line is for  $m_t^{phys} = 181$  GeV and the bottom line is for  $m_t^{phys} = 169$  GeV. We also display the restriction  $\tan\beta/m_{H^\pm} > 0.52$  GeV $^{-1}$  which arises from measurements of  $B \rightarrow X \tau \nu$  as discussed in Ref. 25. (c) Parameter space scatter plot of  $R_7$  vs  $R_8$  in minimal supergravity model. The allowed region from CLEO data, as previously obtained, lies inside the two sets of solid diagonal bands. The dashed band represents the constraints from a potential 10% measurement of  $B \rightarrow X_s \gamma$ . (d) Bounds on anomalous top-quark photon couplings from  $B \rightarrow X_s \gamma$ . The solid and dashed curves correspond to the cases described in the text. In each case, the allowed regions lie inside the semicircles.

CKM elements depends critically on the assumption that these exclusive decay modes are dominated by short-distance penguin transitions. If this assumption is false, and the long-distance contributions to these decays were found to be large, this method would be invalidated. In fact, it has been pointed out by numerous authors<sup>54</sup> that long-distance contributions to  $B \rightarrow X_d \gamma$  may be significant, and hence, these decays may not yield a good determination of the CKM element  $V_{td}$ . These long-distance effects originate from annihilation diagrams and from the inclusion of the light-quark intermediate states in the penguin amplitudes. However, separate measurements of charged and neutral  $B$  decays into  $\rho\gamma$  and  $\omega\gamma$  may be useful in sorting out the magnitude of the long-distance contributions. In contrast, long-distance effects in exclusive  $B \rightarrow X_s \gamma$  decays are estimated to be small.<sup>55</sup>

#### 4.1.2 Radiative Charm Decays

It is instructive to compare radiative decays in the charm system,  $D \rightarrow X_u + \gamma$ , with those of  $B$  mesons. While separation of the long- from the short-distance contributions is somewhat difficult in the  $B$  sector, radiative charm decays provide an excellent laboratory for the determination of the long-distance effects and would hence test the calculational models. In the charm case, it should be possible to directly determine the rate of the long-distance reactions which are expected to dominate. For example, the inclusive  $c \rightarrow u\gamma$  penguin transitions do not contribute to  $D^0 \rightarrow \bar{K}^{*0}\gamma$ , and this mode would be a direct measurement of the nonperturbative effects. Before QCD corrections are applied, the short-distance inclusive rate is extremely small with  $B(c \rightarrow u\gamma) \approx 1 \times 10^{-17}$ ; however, the QCD corrections *greatly* enhance this rate.<sup>56</sup> These corrections are calculated via an operator product expansion, where the effective Hamiltonian is evolved at leading logarithmic order from the electroweak scale down to the charm quark scale by the Renormalization Group Equations. This procedure mirrors that used for  $b \rightarrow s\gamma$ , except that two effective Hamiltonians must be introduced in order to correctly account for the evolution above and below the scale  $\mu = m_b$ . We thus have

$$\mathcal{H}_{eff}(M_W > \mu > m_B) = -\frac{4G_F}{\sqrt{2}} \sum_{q=d,s,b} V_{cq}^* V_{uq} [C_1(\mu)\mathcal{O}_1^q + C_2(\mu)\mathcal{O}_2^q], \quad (44)$$

$$\mathcal{H}_{eff}(m_b > \mu > m_c) = -\frac{4G_F}{\sqrt{2}} \sum_{q=d,s,b} V_{cq}^* V_{uq} [C_1(\mu)\mathcal{O}_1^q + C_2(\mu)\mathcal{O}_2^q + \sum_{i=3}^8 C_i(\mu)\mathcal{O}_i],$$

where the operators are as defined in Eq. (32) with the appropriate substitutions. This procedure results<sup>57</sup> in the inclusive branching fraction  $B(D \rightarrow X_u \gamma) \simeq (2 - 5) \times 10^{-8}$ , with the range corresponding to the difference between neutral and charged  $D$  decay. (We note that these radiative branching fractions have also been scaled to semileptonic charm decay in order to reduce the CKM and  $m_c$  uncertainties.) We see that in this case, the rate is given entirely by operator mixing! The penguin contributions to the exclusive channels would then be typically of order  $10^{-9}$ , which is still significantly smaller than the long-distance estimates presented in the following text in Table 8. We note that for radiative charm decays, the predicted values of the exclusive branching fractions from long-distance effects are within reach of  $B$  factories.

## 4.2 Other Rare $B$ Decays

As discussed above, FCNC processes in the  $B$  sector are not as suppressed as in the other meson systems and can occur at reasonable rates in the SM. This is due to a sizable loop-level contribution from the top quark, which results from the combination of the large top mass (giving a big GIM splitting) and the diagonal nature of the CKM matrix. Long-distance effects are expected to play less of a role due to the heavy  $B$  mass, and hence rare processes are essentially short-distance dominated. Many classes of new models can also give significant and testable contributions to rare  $B$  transitions.

Other FCNC decays of  $B$  mesons include  $B_{d,s}^0 \rightarrow \ell^+ \ell^-, \gamma\gamma$ ,  $B \rightarrow X_{s,d} + \ell^+ \ell^-, X_{s,d} \nu \bar{\nu}$ , with  $\ell = e\mu\tau$ . In the SM, they are mediated by appropriate combinations of electromagnetic and weak penguins as well as box diagrams, and generally have larger rates, as discussed above, due to the heavy top quark and the diagonal nature of the CKM matrix. The SM predictions and current experimental situation<sup>4,58,59</sup> for these decays are summarized in Table 7, taking  $m_t = 180$  GeV. The purely leptonic decays,  $B^0 \rightarrow \ell^+ \ell^-$ , can be enhanced by contributions from new physics at both the loop-level (for example, in Extended Technicolor models<sup>60</sup>

Decay Mode	Experimental Limit	$B_{SM}$
$B_d^0 \rightarrow e^+ e^-$	$< 5.9 \times 10^{-6}$ (CLEO)	$2.6 \times 10^{-15}$
$B_d^0 \rightarrow \mu^+ \mu^-$	$< 1.6 \times 10^{-6}$ (CDF)	$1.1 \times 10^{-10}$
$B_d^0 \rightarrow \tau^+ \tau^-$	—	$2.1 \times 10^{-8}$
$B_s^0 \rightarrow e^+ e^-$	—	$5.3 \times 10^{-14}$
$B_s^0 \rightarrow \mu^+ \mu^-$	$< 8.4 \times 10^{-6}$ (CDF)	$(3.6 \pm 1.8) \times 10^{-9}$
$B_s^0 \rightarrow \tau^+ \tau^-$	—	$5.1 \times 10^{-7}$
$B^0 \rightarrow \mu^+ \mu^-$	$< 8.0 \times 10^{-6}$ (DØ)	
$B^0 \rightarrow e^\pm \mu^\mp$	$< 5.9 \times 10^{-6}$ (CLEO)	0
$B^0 \rightarrow e^\pm \tau^\mp$	$< 5.3 \times 10^{-4}$ (CLEO)	0
$B^0 \rightarrow \mu^\pm \tau^\mp$	$< 8.3 \times 10^{-4}$ (CLEO)	0
$B_d^0 \rightarrow \gamma\gamma$	$< 3.9 \times 10^{-5}$ (L3)	$1.0 \times 10^{-8}$
$B_s^0 \rightarrow \gamma\gamma$	$< 1.5 \times 10^{-4}$ (L3)	$3 \times 10^{-7}$
$B \rightarrow X_s + \gamma$	$(2.32 \pm 0.57 \pm 0.35) \times 10^{-4}$ (CLEO)	$(3.25 \pm 0.30 \pm 0.40) \times 10^{-4}$
$B \rightarrow K^* \gamma$	$(4.2 \pm 0.8 \pm 0.6) \times 10^{-5}$ (CLEO)	$(4.0 \pm 2.0) \times 10^{-5}$
$B^0 \rightarrow \rho^0 \gamma$	$< 3.9 \times 10^{-5}$ (CLEO)	$(0.85 \pm 0.65) \times 10^{-6}$
$B^0 \rightarrow \omega^0 \gamma$	$< 1.3 \times 10^{-5}$ (CLEO)	$(0.85 \pm 0.65) \times 10^{-6}$
$B^- \rightarrow \rho^- \gamma$	$1.1 \times 10^{-5}$ (CLEO)	$(1.9 \pm 1.6) \times 10^{-6}$
$B \rightarrow X_s + e^+ e^-$	—	$(6.25_{-0.93}^{+1.04}) \times 10^{-6}$
$B \rightarrow X_s + \mu^+ \mu^-$	$< 3.6 \times 10^{-5}$ (DØ)	$(5.73_{-0.78}^{+0.75}) \times 10^{-6}$
$B \rightarrow X_s + \tau^+ \tau^-$	—	$(3.24_{-0.54}^{+0.44}) \times 10^{-7}$
$B^0 \rightarrow K^0 ee/\mu\mu$	$< 1.5/2.6 \times 10^{-4}$ (CLEO)	$(5.0 \pm 3.0)/(3.0 \pm 1.8) \times 10^{-7}$
$B^- \rightarrow K^- ee/\mu\mu$	$< 1.2/0.9 \times 10^{-5}$ (CLEO)	$(5.0 \pm 3.0)/(3.0 \pm 1.8) \times 10^{-7}$
$\bar{B}^0 \rightarrow \bar{K}^{*0} ee/\mu\mu$	$< 1.6/2.5 \times 10^{-5}$ (CLEO/CDF)	$(2.0 \pm 1.0)/(1.25 \pm 0.62) \times 10^{-6}$
$\bar{B}^- \rightarrow \bar{K}^{*-} ee/\mu\mu$	$< 6.9/11 \times 10^{-4}$ (CLEO)	$(2.0 \pm 1.0)/(1.25 \pm 0.62) \times 10^{-6}$
$B^+ \rightarrow K^+ e^\pm \mu^\mp$	$< 1.2 \times 10^{-5}$ (CLEO)	0
$\bar{B}^0 \rightarrow \bar{K}^{*0} e^\pm \mu^\mp$	$< 2.7 \times 10^{-5}$ (CLEO)	0
$B \rightarrow X_s + \nu \bar{\nu}$	$< 7.7 \times 10^{-4}$ (ALEPH)	$(3.8 \pm 0.8) \times 10^{-5}$

Table 7: Standard Model predictions for the branching fractions for various rare  $B$  meson decays with  $f_{B_i} = 180$  MeV. Also shown are the current experimental limits.<sup>4,57,58</sup>

or by virtual  $H^\pm$  exchange<sup>61</sup> in 2HDM), and at tree-level, *e.g.*, with leptoquark exchange.<sup>62</sup> However, as can be seen from the table, the experimental probes of these purely leptonic decays, are orders of magnitude above the expected rates, and hence only potentially large tree-level contributions can currently be tested. Indeed, the most stringent constraints on tree-level leptoquark contributions in  $B$  decays are obtained from the exclusive reaction  $B \rightarrow Ke\mu$  (Ref. 62). However, in this case, there exist large uncertainties associated with the hadronic matrix elements, yielding some sloppiness in the resulting bounds.

The transition  $b \rightarrow s\ell^+\ell^-$  merits further attention as it offers an excellent opportunity to search for new physics. For example, it has been found<sup>63</sup> that Extended Technicolor models with a GIM mechanism already violate(!) the experimental upper bound on  $B \rightarrow X_s\mu\mu$ , but more traditional ETC models yield a rate which is close to the SM prediction. The decay proceeds via electromagnetic and  $Z$  penguin as well as by  $W$  box diagrams, and hence can probe different coupling structures than the pure electromagnetic process  $b \rightarrow s\gamma$ . For  $B \rightarrow X_s\ell^+\ell^-$  the Hamiltonian of the effective field theory [see Eq. (30)] is expanded to include two additional operators,  $\mathcal{O}_{9,10}$ . This formalism leads to the physical decay amplitude (neglecting the strange quark mass)

$$\begin{aligned} \mathcal{M}(B \rightarrow X_s\ell^+\ell^-) &= \frac{\sqrt{2}G_F\alpha}{\pi} V_{tb}V_{ts}^* \left[ C_9^{eff} \bar{s}_L\gamma_\mu b_L \bar{\ell}\gamma^\mu \ell + C_{10} \bar{s}_L\gamma_\mu b_L \bar{\ell}\gamma^\mu \gamma_5 \ell \right. \\ &\quad \left. - 2C_7^{eff} m_b \bar{s}_L i\sigma_{\mu\nu} \frac{q^\nu}{q^2} b_R \bar{\ell}\gamma^\mu \ell \right], \end{aligned} \quad (45)$$

where  $q^2$  represents the momentum transferred to the lepton pair. The expressions for  $C_i(M_W)$  are given by the Inami-Lim functions.<sup>30</sup> A NLO analysis for this decay has recently been performed,<sup>64</sup> where it is stressed that a scheme-independent result can only be obtained by including the leading and next-to-leading logarithmic corrections to  $C_9(\mu)$  while retaining only the leading logarithms in the remaining Wilson coefficients. The residual leading  $\mu$  dependence in  $C_9(\mu)$  is cancelled by that contained in the matrix element of  $\mathcal{O}_9$ . The combination yields an effective value of  $C_9$  given by

$$C_9^{eff}(\hat{s}) = C_9(\mu)\eta(\hat{s}) + Y(\hat{s}), \quad (46)$$

with  $Y(\hat{s})$  being the one-loop matrix element of  $\mathcal{O}_9$ ,  $\eta(\hat{s})$  represents the single gluon corrections to this matrix element, and  $\hat{s} \equiv q^2/m_b^2$  is the scaled momentum transferred to the lepton pair. The effective value for  $C_7^{eff}(\mu)$  refers to the leading

order scheme-independent result obtained by Buras *et al.*<sup>34</sup> The corresponding formulae for  $C_i(\mu)$ ,  $Y(\hat{s})$ , and  $\eta(\hat{s})$  are collected in Refs. 43 and 64. The operator  $\mathcal{O}_{10}$  does not renormalize, and hence its corresponding coefficient does not depend on the value of  $\mu$  (except for the  $\mu$  dependence associated with the definition of the top-quark mass). The numerical estimates [in the naive dimensional regularization (NDR) scheme] for these coefficients are then (taking  $m_b^{pole} = 4.87$  GeV,  $m_t^{phys} = 175$  GeV, and  $\alpha_s(M_Z) = 0.118$ )

$$\begin{aligned} C_7^{eff}(\mu = m_b \frac{-m_s/2}{+m_s}) &= -0.312_{+0.034}^{-0.059}, \\ C_9(\mu = m_b \frac{-m_s/2}{+m_s}) &= 4.21_{-0.40}^{+0.31}, \end{aligned} \quad (47)$$

and

$$C_{10}(\mu) = -4.55. \quad (48)$$

The reduced scale dependence of the NLO versus the LO corrected coefficients is reflected in the deviations  $\Delta C_9(\mu) \lesssim \pm 10\%$  and  $\Delta C_7^{eff}(\mu) \approx \pm 20\%$  as  $\mu$  is varied in the range  $m_b/2 \leq \mu \leq 2m_b$ . We find that the coefficients are much less sensitive to the values of the remaining input parameters, with  $\Delta C_9(m_b)$ ,  $\Delta C_7^{eff}(m_b) \lesssim 3\%$ , varying  $\alpha_s(M_Z) = 0.118 \pm 0.003$  (Refs. 4 and 41), and  $m_t^{phys} = 175 \pm 6$  GeV (Ref. 13) corresponding to  $m_t(m_t) = 166 \pm 6$  GeV. The resulting inclusive branching fractions (which are computed by scaling the width for  $B \rightarrow X_s\ell^+\ell^-$  to that for  $B$  semileptonic decay) are found to be  $(6.25_{-0.93}^{+1.04}) \times 10^{-6}$ ,  $(5.73_{-0.78}^{+0.75}) \times 10^{-6}$ , and  $(3.24_{-0.54}^{+0.44}) \times 10^{-7}$  for  $\ell = e, \mu$ , and  $\tau$ , respectively, taking into account the above input parameter ranges, as well as  $B_{sl} \equiv B(B \rightarrow X\ell\nu) = (10.23 \pm 0.39)\%$  (Ref. 19), and  $m_c/m_b = 0.29 \pm 0.02$  (Refs. 36 and 4). There are also long-distance resonance contributions to  $B \rightarrow X_s\ell^+\ell^-$ , arising from  $B \rightarrow K^{(*)}\psi^{(\prime)} \rightarrow K^{(*)}\ell^+\ell^-$ . These appear as an effective  $(\bar{s}_L\gamma_\mu b_L)(\bar{\ell}\gamma_\mu \ell)$  interaction and are incorporated into  $C_9^{eff}$  via the modification  $Y(\hat{s}) \rightarrow Y'(\hat{s}) \equiv Y(\hat{s}) + Y_{res}(\hat{s})$ , where  $Y_{res}(\hat{s})$  is given in Ref. 65. These pole contributions lead to a significant interference between the dispersive part of the resonance and the short-distance contributions. However, suitable cuts on the lepton pair mass spectrum can cleanly separate the short-distance physics from the resonance contributions.

Various kinematic distributions associated with the final state lepton pair render  $B \rightarrow X_s\ell^+\ell^-$  an excellent SM testing ground. These distributions include the lepton pair invariant mass distribution,<sup>66</sup> the lepton pair forward-backward asymmetry,<sup>67</sup> and the tau polarization asymmetry<sup>68</sup> in the case  $\ell = \tau$ . They

are presented in Fig. 5, with and without the resonance contributions. Note that both asymmetries are large. As an example of how new physics can affect these distributions, we display in Fig. 5(d) the tau polarization asymmetry for various changes of sign of the contributing Wilson coefficients. Measurement of all three kinematic distributions as well as the rate for  $B \rightarrow X_s \gamma$  would allow for the determination of the sign and magnitude of all the Wilson coefficients for the contributing operators and thus provide a completely model-independent analysis. A 95% C.L. Monte Carlo fit to these coefficients has been performed<sup>42</sup> in order to ascertain how much quantitative information will be obtainable at future  $B$  factories. In this fit, "data" has been generated assuming the SM is realized, and by dividing the lepton pair invariant mass spectrum into bins, where six of the bins are taken to be in the low dilepton invariant mass region below the  $J/\psi$  resonance, and three of the bins above the  $\psi'$  pole. The "data" has been statistically fluctuated using a normalized Gaussian distributed random number procedure. The errors in each bin are expected to be statistics dominated. However, for  $B \rightarrow X_s \gamma$ , the statistical precision will eclipse the possible systematic and theoretical accuracy, and a flat 10% error in the determination of the branching fraction is thus assumed. A three-dimensional  $\chi^2$  fit to the coefficients  $C_{7,9,10}(\mu)$  is performed for three values of the integrated luminosity,  $3 \times 10^7$ ,  $10^8$ , and  $5 \times 10^8$   $B\bar{B}$  pairs, corresponding to one year at  $e^+e^-$   $B$  factory design luminosity, one year at an upgraded accelerator, and the total accumulated luminosity at the end of the program. Hadron colliders will, of course, also contribute to this program, but it is more difficult to assess their potential systematic and statistical weights without further study.

The 95% C.L. allowed regions as projected onto the  $C_9(\mu) - C_{10}(\mu)$  and  $C_7^{eff}(\mu) - C_{10}(\mu)$  planes are depicted in Figs. 6(a) and 6(b), where the diamond represents the expectations in the SM. We see that the determinations are relatively poor for  $3 \times 10^7$   $B\bar{B}$  pairs and that higher statistics are required in order to focus on regions centered around the SM. Clearly,  $C_9$  and  $C_{10}$  are highly correlated, whereas  $C_7^{eff}$  and  $C_{10}$  are not. We see that the sign, as well as the magnitude, of all the coefficients including  $C_7^{eff}$  can now be determined.

Supersymmetric contributions to  $B \rightarrow X_s \ell^+ \ell^-$  have recently been analyzed in Refs. 42 and 69. In Fig. 7, the correlation between  $R_9$  and  $R_{10}$  (recall  $R_i \equiv \frac{C_i^{new}(M_W)}{C_i^{SM}(M_W)} - 1$ ) is displayed using the same supersymmetric parameter space as in

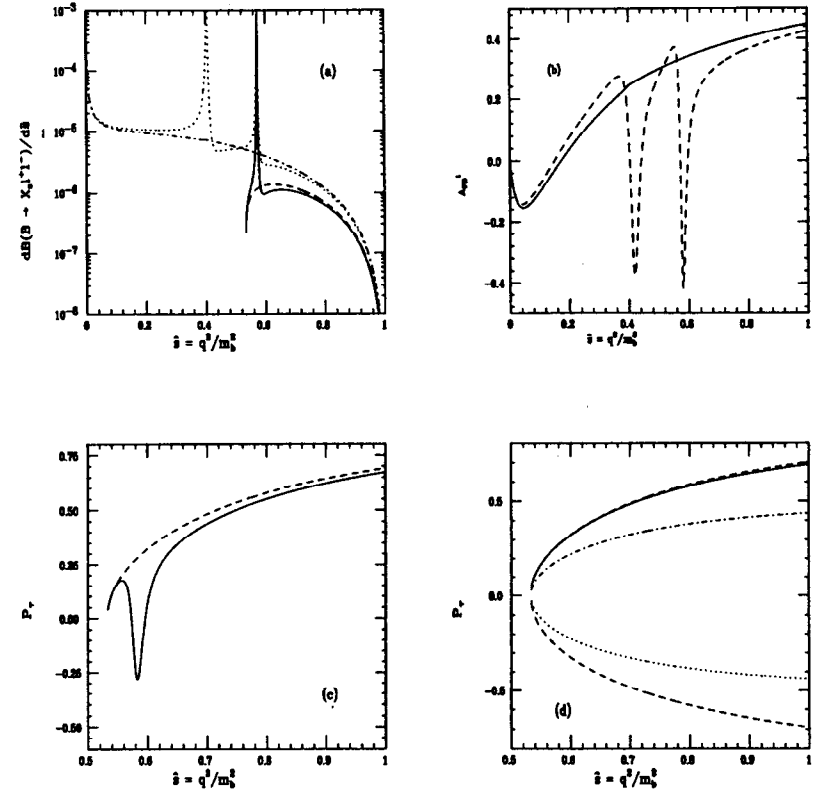


Figure 5: (a) Differential branching fraction, (b) lepton pair forward-backward asymmetry, and (c) tau polarization asymmetry as a function of  $\hat{s}$  for  $\ell = \tau$  (solid and dashed curves) and  $\ell = e$  (dotted and dash-dotted curves), with and without the long-distance contributions. (d) Tau polarization asymmetry with changes in sign of the Wilson coefficients at the electroweak scale, corresponding to  $C_{10}, C_9, C_{9,10}, SM$ , and  $C_{7,8}$  from bottom to top.

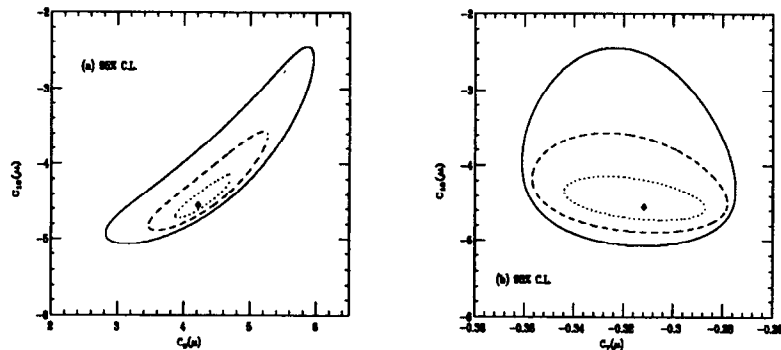


Figure 6: The 95% C.L. projections in the (a)  $C_9-C_{10}$  and (b)  $C_7^{eff}-C_{10}$  planes, where the allowed regions lie inside of the contours. The solid, dashed, and dotted contours correspond to  $3 \times 10^7$ ,  $10^8$ , and  $5 \times 10^8$   $B\bar{B}$  pairs. The SM prediction is labeled by the diamond.

Fig. 4(c). We see that  $R_9$  is always positive since the charged Higgs boson and chargino contributions always add constructively. We see that the values of  $R_9$  and  $R_{10}$  are bounded by about 0.04, a small number compared to the range found for  $R_7$  in Fig. 4(c), and rendering the minimal supergravity contributions to  $R_{9,10}$  essentially unobservable. The solid lines in this figure correspond to the 95% C.L. bounds obtainable with very high integrated luminosity ( $5 \times 10^8$   $B\bar{B}$  pairs) at  $B$  factories from the global fit shown above.

### 4.3 Other Rare $D$ Decays

While investigations of the  $K$  and  $B$  systems have and will continue to play a central role in our quest to understand flavor physics, in-depth examinations of the charm-quark sector have yet to be performed, leaving a gap in our knowledge. Since charm is the only heavy charged  $+2/3$  quark presently accessible to experiment in copious amounts, it provides the sole window of opportunity to examine flavor physics in this sector. In addition, charm allows a complementary probe of SM physics (and beyond) to that attainable from the down-quark sector.

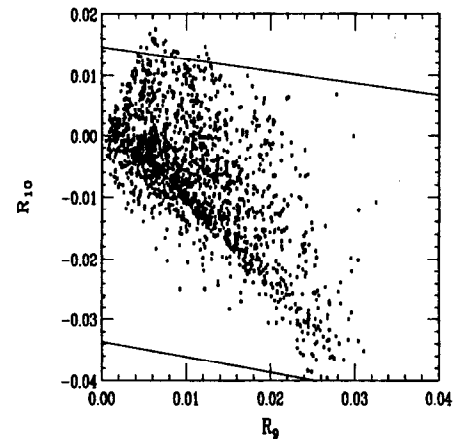


Figure 7: Parameter space scatter plot of  $R_9$  vs  $R_{10}$  in minimal supergravity model. The global fit to the coefficients obtained in Fig. 6 with  $5 \times 10^8$   $B\bar{B}$  pairs corresponds to the region inside the diagonal bands.

Due to the effectiveness of the GIM mechanism, short-distance SM contributions to rare charm processes are very small. Most reactions are thus dominated by long-range effects which are difficult to reliably calculate. However, for some interactions, there exists a window for the potential observation of new physics. In fact, it is precisely because the SM flavor changing neutral current rates are so small that charm provides an untapped opportunity to discover new effects and offers a detailed test of the SM in the up-quark sector.

FCNC decays of the  $D$  meson include the processes  $D^0 \rightarrow \ell^+ \ell^- \gamma \gamma$ , and  $D \rightarrow X + \ell^+ \ell^-$ ,  $X + \nu \bar{\nu}$ ,  $X + \gamma$ , with  $\ell = e, \mu$ , and with the radiative decays being discussed above. The calculation of the SM short-distance rates for these processes is straightforward and the transition amplitudes and standard loop integrals, which are categorized in Ref. 30 for rare  $K$  decays, are easily converted to the  $D$  system. The loop integrals relevant for  $D^0 \rightarrow \gamma \gamma$  may be found in Ref. 70. Employing the GIM mechanism results in a general expression for the loop integrals which can be written as

$$A = V_{cs} V_{us}^* [F(x_s) - F(x_d)] + V_{cb} V_{ub}^* [F(x_b) - F(x_d)], \quad (49)$$

with  $x_i \equiv m_i^2/M_W^2$  and  $F(x_d)$  usually being neglected (except in the  $2\gamma$  case). The  $s$ - and  $b$ -quark contributions are roughly equal as the larger CKM factors compensate for the small strange quark mass. The values of the resulting inclusive short-distance branching fractions are shown in Table 8, along with the current experimental bounds.<sup>4,71</sup> The corresponding exclusive rates are typically an order of magnitude less than the inclusive case. We note that the transition  $D^0 \rightarrow \ell^+ \ell^-$  is helicity suppressed and hence has the smallest branching fraction. The range given for this branching fraction,  $(1 - 20) \times 10^{-19}$ , indicates the effect of varying the parameters in the ranges  $f_D = 0.15 - 0.25$  GeV and  $m_s = 0.15 - 0.40$  GeV. It is clear that the typical branching fraction is indeed much smaller than that in the  $B$  meson system, illustrating the effectiveness of the GIM mechanism when there is no heavy top quark contributing inside the loop.

The calculation of the long-distance branching fractions are plagued with the usual hadronic uncertainties, and the estimates listed in the table convey an upper limit on the size of these effects rather than an actual value. These estimates have been computed by considering various intermediate particle states (e.g.,  $\pi, K, \bar{K}, \eta, \eta', \pi\pi$ , or  $K\bar{K}$ ) and inserting the known rates for the decay of the intermediate particles into the final state of interest. In all cases, we see

Decay Mode	Experimental Limit	$B_{S.D.}$	$B_{L.D.}$
$D^0 \rightarrow \mu^+ \mu^-$	$< 7.6 \times 10^{-6}$ (WA92)	$(1 - 20) \times 10^{-19}$	$< 3 \times 10^{-15}$
$D^0 \rightarrow e^+ e^-$	$< 1.3 \times 10^{-5}$ (CLEO)		
$D^0 \rightarrow \mu^+ e^-$	$< 1.9 \times 10^{-5}$ (CLEO)	0	0
$D^0 \rightarrow \gamma \gamma$	—	$10^{-16}$	$< 3 \times 10^{-9}$
$D \rightarrow X_u + \gamma$		$1.4 \times 10^{-17}$	
$D^0 \rightarrow \rho^0 \gamma$	$< 1.4 \times 10^{-4}$ (CLEO-prelim.)		$< 2 \times 10^{-5}$
$D^0 \rightarrow \phi^0 \gamma$	$< 2.0 \times 10^{-4}$ (CLEO-prelim.)		$< 10^{-4}$
$D^+ \rightarrow \rho^+ \gamma$	—		$< 2 \times 10^{-4}$
$D^+ \rightarrow \bar{K}^{*+} \gamma$	—		$3 \times 10^{-7}$
$D^0 \rightarrow \bar{K}^{*0} \gamma$	—		$1.6 \times 10^{-4}$
$D \rightarrow X_u + \ell^+ \ell^-$		$4 \times 10^{-9}$	
$D^0 \rightarrow \pi^0 ee/\mu\mu$	$< 4.5/18 \times 10^{-5}$ (CLEO/E653)		$< 2 \times 10^{-15}$
$D^0 \rightarrow \bar{K}^0 ee/\mu\mu$	$< 1.1/2.6 \times 10^{-4}$ (CLEO/E653)		
$D^0 \rightarrow \rho^0 ee/\mu\mu$	$< 1.0/2.3 \times 10^{-4}$ (CLEO/E653)		
$D^0 \rightarrow \eta ee/\mu\mu$	$< 1.1/5.3 \times 10^{-4}$ (CLEO)		
$D^+ \rightarrow \pi^+ ee/\mu\mu$	$< 6.6/1.8 \times 10^{-5}$ (CLEO/E653)	$\text{few} \times 10^{-10}$	$< 10^{-8}$
$D^+ \rightarrow K^+ ee/\mu\mu$	$< 480/3.2 \times 10^{-5}$ (MRK2/E653)		$< 10^{-15}$
$D^+ \rightarrow \rho^+ \mu\mu$	$< 5.6 \times 10^{-4}$ (E653)		
$D^0 \rightarrow X_u + \nu \bar{\nu}$		$2.0 \times 10^{-15}$	
$D^0 \rightarrow \pi^0 \nu \bar{\nu}$	—	$4.9 \times 10^{-16}$	$< 6 \times 10^{-16}$
$D^0 \rightarrow \bar{K}^0 \nu \bar{\nu}$	—		$< 10^{-12}$
$D^+ \rightarrow X_u + \nu \bar{\nu}$	—	$4.5 \times 10^{-15}$	
$D^+ \rightarrow \pi^+ \nu \bar{\nu}$	—	$3.9 \times 10^{-16}$	$< 8 \times 10^{-16}$
$D^+ \rightarrow K^+ \nu \bar{\nu}$	—		$< 10^{-14}$

Table 8: Standard Model predictions for the branching fractions due to short- and long-distance contributions for various rare  $D$  meson decays. Also shown are the 90% C.L. current experimental limits.<sup>71</sup>

that the long-distance contributions overwhelm those from the SM short-distance physics.

Lepton flavor violating decays, *e.g.*,  $D^0 \rightarrow \mu^\pm e^\mp$  and  $D \rightarrow X + \mu^\pm e^\mp$ , are strictly forbidden in the SM with massless neutrinos. In a model with massive nondegenerate neutrinos and nonvanishing neutrino mixings, such as in four-generation models,  $D^0 \rightarrow \mu^\pm e^\mp$  would be mediated by box diagrams with the massive neutrinos being exchanged internally. LEP data restricts<sup>72</sup> heavy neutrino mixing with  $e$  and  $\mu$  to be  $|U_{Ne}U_{N\mu}^*|^2 < 7 \times 10^{-6}$  for a neutrino with mass  $m_N > 45$  GeV. Consistency with this bound constrains the branching fraction to be  $B(D^0 \rightarrow \mu^\pm e^\mp) < 6 \times 10^{-22}$ . This same result also holds for a heavy singlet neutrino which is not accompanied by a charged lepton. The observation of this decay at a larger rate than the above bound would be a clear signal for the existence of a different class of models with new physics.

Examining Table 7, we see that there is a large window of opportunity to discover the existence of new physics in rare charm decays. Although the SM short-distance contributions are completely dominated by the long-distance effects, there are some modes where the size of the two contributions are not that far apart. The observation of any of these modes at a larger rate than what is predicted from long-distance interactions would provide a clear signal for new physics.

#### 4.4 Rare Decays in the Kaon System

The SM level for the theoretically clean decay  $K^+ \rightarrow \pi^+ \nu \bar{\nu}$  should be reached in the next decade, with the present bound<sup>73</sup> on the branching fraction being  $B(K^+ \rightarrow \pi^+ \nu \bar{\nu}) < 2.4 \times 10^{-9}$  from E787 at Brookhaven. This transition is theoretically clean as it is short-distance dominated;<sup>74</sup> the relevant hadronic operator is extracted from  $K^+ \rightarrow \pi^0 e^+ \nu$ , and the next-to-leading order QCD corrections are fully known.<sup>75</sup> The SM processes responsible for this decay are  $Z$ -mediated penguin graphs and  $W$  box diagrams with both charm and top quarks contributing internally. The full NLO expressions for this decay are given in Ref. 75. The impact of the NLO corrections are to reduce the scale uncertainties from  $\pm 22\%$  to  $\pm 7\%$ . Here we present the approximate result recently given by Buras,<sup>12</sup>

$$\begin{aligned} B(K^+ \rightarrow \pi^+ \nu \bar{\nu}) &= 0.7 \times 10^{-10} \left[ \left( \frac{|V_{td}|}{0.01} \right)^2 \left( \frac{|V_{cb}|}{0.04} \right)^2 \left( \frac{m_t(m_t)}{170 \text{ GeV}} \right)^{2.3} + cc + tc \right], \\ &= (9.1 \pm 3.2) \times 10^{-11}, \end{aligned} \quad (50)$$

where the  $cc$  and  $tc$  terms represent the pure charm and charm-top contributions, respectively. Measurement of this rare decay would provide a sensitive and direct determination of  $V_{td}$ . The theoretical error<sup>12,75</sup> on an evaluation of  $V_{td}$  from this channel is at the  $\pm 4\%$  level. Hence, this mode represents the most promising technique of determining  $V_{td}$ .

An enhancement over the SM rate would clearly signal new physics although such enhancements are not expected in most minimal extensions of the SM once the constraints from  $B - \bar{B}$  mixing,  $\epsilon_K$ , and  $b \rightarrow s \gamma$  are taken into account.<sup>76</sup> These processes are to a large extent governed by the same parameters, limiting the impact of new physics in this case. A possible exception concerns the MSSM with SUSY particles in the 100 GeV range where there can be some enhancement.<sup>77</sup> There remains the possibility of large enhancements in SUSY models with broken R-parity, models with family symmetry producing a new type of neutrino, as well as certain leptoquark models.<sup>76</sup> Typically, these models are more weakly constrained overall and could also lead to nonstandard signals in other rare processes (for example, B or D decays). The Three-Higgs-Doublet model also can lead to a moderate enhancement (by a factor of three) of the standard rate for this decay.<sup>78</sup> This is to be contrasted with the 2HDM where the existing constraints preclude any significant effect in future kaon decay measurements.<sup>46</sup>

The process  $K_L \rightarrow \mu^+ \mu^-$  shares several features of the preceding one as far as sensitivity to new physics is concerned. However, the bounds obtained are not as reliable due to large and uncertain long-distance contributions. One interesting aspect of this process is the sensitivity to other sources of CP violation in the measurement of the longitudinal polarization of the muon, which is expected to be  $P_L \approx 2 \times 10^{-3}$  in the SM.

Extensive discussions of other rare  $K$  decay modes can be found in Ref. 79.

#### 4.5 Rare Decays of the Top Quark

Loop-induced flavor changing top quark decays are small in the SM, as in the charm-quark system, due to the effectiveness of the GIM mechanism and the

small masses of the  $Q = -1/3$  quarks. However, these transitions are anticipated to be theoretically clean as long-distance effects are expected to be negligible. The SM rates for  $t \rightarrow c\gamma, cZ, cg$  are given by  $4.9 \times 10^{-13}, 1.4 \times 10^{-13}, 4.4 \times 10^{-11}$ , respectively, for  $m_t = 180$  GeV (Ref. 80). The branching fraction for  $t \rightarrow ch$  as a function of the Higgs mass is represented by the solid curve in Figs. 8(a) and 8(b). We see that this rate is also tiny, being in the  $10^{-13}$  range over the entire kinematically allowed region for the Higgs mass. Loop contributions from new physics have been studied in 2HDM<sup>80,81</sup> and in SUSY,<sup>82</sup> and generally can enhance these transition rates by three to four orders of magnitude for some regions of the parameter space. The effects of virtual  $H^\pm$  exchange in 2HDM of Type II on the reactions  $t \rightarrow cV, V = \gamma, Z, g$ , are displayed in Fig. 8(c) for  $m_t = 180$  GeV. We see that, indeed, enhancements are present for large values of  $\tan\beta$ . We also examine the decays  $t \rightarrow ch, cH$  in Model II, where  $h$  and  $H$  respectively represent the lightest and heaviest physical neutral scalars present in 2HDM. The resulting rates are depicted in Figs. 8(a) and 8(b) for the demonstrative case of  $m_{H^\pm} = 600$  GeV and  $\tan\beta = 2(30)$ , corresponding to the dashed (solid) curves. Here, we have made use of the SUSY Higgs mass relationships in order to reduce the number of free parameters. We note that the effects of super-partner virtual exchange should also be included (with, of course, a corresponding increase in the number of parameters). We have also studied these modes in Model I and found similar rate increases for regions of the parameter space. Even if new physics were to produce such enhancements, the resulting branching fractions would still lie below the observable level in future experiments at an upgraded Tevatron, the LHC, or the NLC.

On the other hand, if these FCNC decays were to be detected, they would provide an indisputable signal for new physics. Hence, a model-independent approach in probing anomalous FCNC top-quark couplings has recently been taken by a number of authors.<sup>83</sup> By parameterizing the general  $tcV$  vertex in a manner similar to that presented in Eq. (6), and performing a Monte Carlo study of the signal rate versus potential backgrounds, Han *et al.*<sup>83</sup> have found that such anomalous couplings can be probed down to the level of  $\kappa_{\gamma,Z} \equiv \sqrt{g_L^2 + g_R^2}|_{\gamma,Z} \simeq 0.1(0.01)$  at the Tevatron (LHC). This corresponds to values of the branching fractions for  $t \rightarrow cZ, c\gamma$  at the level of  $\text{few} \times 10^{-3}$  for the Tevatron bounds and  $10^{-4}$  for the

LHC. CDF has, in fact, already performed a search for these FCNC decays from their present top sample, and has placed the bounds<sup>84</sup>  $B(t \rightarrow c\gamma + u\gamma) < 2.9\%$  and  $B(t \rightarrow cZ + uZ) < 90\%$  at 95% and 90% C.L., respectively.

Potential non-SM tree-level decays of the top quark could feasibly occur at measurable rates in future colliders. Examples of these possible transitions are: (i) the decay of top into a charged Higgs,  $t \rightarrow bH^+$  in multi-Higgs models,<sup>85</sup> (ii) the tree-level flavor-changing decay  $t \rightarrow ch$ , which can occur, if kinematically accessible, in multi-Higgs models without natural flavor conservation,<sup>86,87</sup> (iii)  $t \rightarrow \tilde{t}\tilde{\chi}^0$  which can take place in supersymmetry if the top-squark is sufficiently light<sup>88</sup> (this possibility is related to the large value of the top Yukawa coupling, and is thus special to the top system), and (iv)  $t \rightarrow \tilde{\ell}^+ d$  in SUSY models with R-parity violation.<sup>89</sup> For favorable values of the parameters, each of these modes could be competitive with the SM decay  $t \rightarrow bW^+$ . The observation of the top quark by CDF and DØ, which relies heavily on the expected signal from SM top decay,<sup>13</sup> can thus restrict the values of the branching fractions for these potential new modes. The possible constraints that could be obtained on the models which would allow the decays (i)  $t \rightarrow bH^+$  and (ii)  $t \rightarrow ch$  to occur, if these collaborations were to make the statement that the observed  $t\bar{t}$  production rate is 50–90% of that expected in the SM, are given in Fig. 9. We have examined the case of the decay into a  $H^\pm$  in Model II, taking  $m_t = 180$  GeV, and find that the potentially excluded regions lie below the curves. Clearly, large regions of the parameter space have the potential to be ruled out. In the case of  $t \rightarrow ch$  decay, we have parameterized the tree-level  $tc$  coupling as  $(\sqrt{2}G_F)^{1/2}m_t(\alpha - \beta\gamma_5)$  and displayed the restrictions in the  $k \equiv \sqrt{\alpha^2 + \beta^2} - m_h$  plane. The region above the curves would be excluded.

## 5 Neutral Meson Mixing

For a neutral meson system, the mass and lifetime eigenstates,  $P_L, P_H$ , with masses  $m_{L,H}$  and widths  $\Gamma_{L,H}$ , are conventionally defined as mixtures of the two weak CP-conjugate eigenstates  $P^0, \bar{P}^0$  as

$$\begin{aligned} |P_L\rangle &= p|P^0\rangle + q|\bar{P}^0\rangle, \\ |P_H\rangle &= p|P^0\rangle - q|\bar{P}^0\rangle, \end{aligned} \quad (51)$$

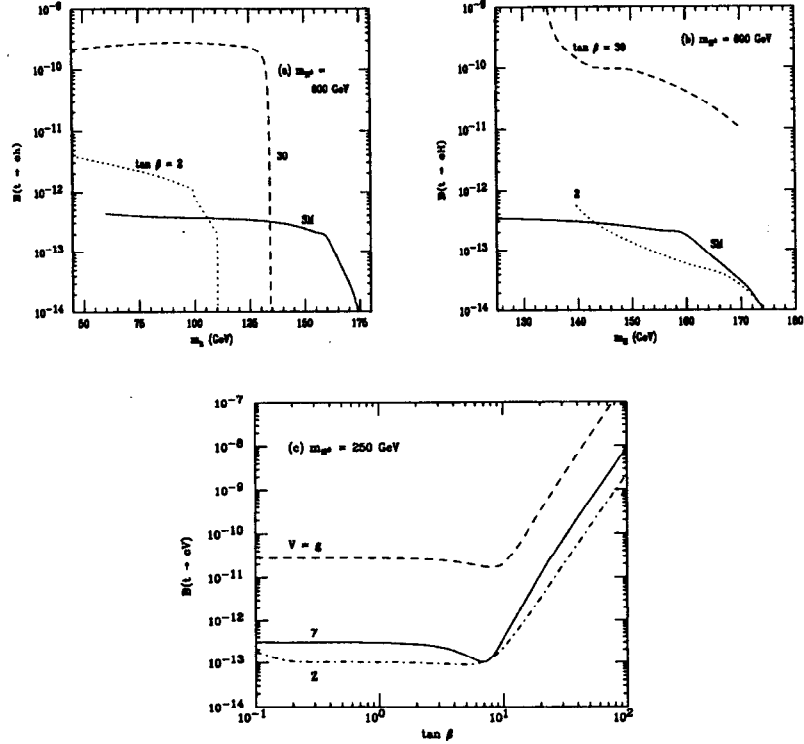


Figure 8: Branching fractions for (a)  $t \rightarrow ch$  and (b)  $t \rightarrow cH$  as a function of the neutral Higgs mass in 2HDM of Type II. The SM rate is represented by the solid curve. (c)  $B(t \rightarrow cV)$  where  $V = g, \gamma, Z$  as a function of  $\tan\beta$  in Model II. In all cases, the top-quark mass is taken to be 180 GeV.

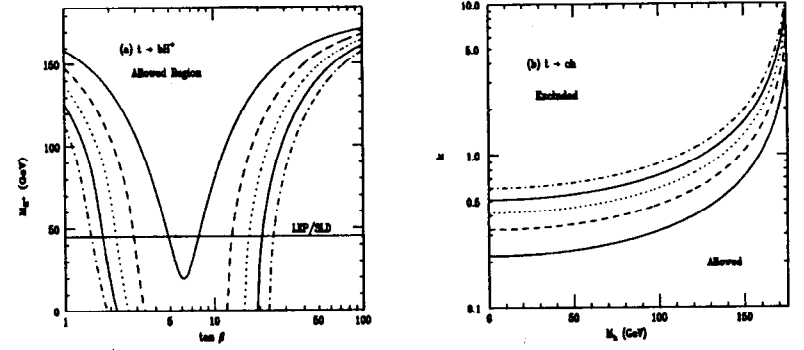


Figure 9: Constraints placed on the nonstandard decays (a)  $t \rightarrow bH^+$  and (b)  $t \rightarrow ch$  from demanding that the observed event rate for top-quark pair production is at least 50, 60, 70, 80, and 90% of that expected in the SM, corresponding to the dashed-dot, solid, dotted, dashed, and solid curves.  $m_t = 180$  GeV is assumed.

with the normalization  $|p|^2 + |q|^2 = 1$ , and the subscripts  $L$  and  $H$  denoting the light and heavy states, respectively. Here,  $P^0$  generically represents the pseudoscalar neutral meson systems  $K^0, D^0, B_d^0$ , and  $B_s^0$ . Note that there is no top-meson mixing as the top-quark decays too rapidly to form neutral meson bound states. There is also the equivalent definition

$$\begin{aligned} |P_L\rangle &= [(1 + \epsilon_P)|P^0\rangle + (1 - \epsilon_P)|\bar{P}^0\rangle]/\sqrt{2(1 + |\epsilon_P|^2)}, \\ |P_H\rangle &= [(1 + \epsilon_P)|P^0\rangle - (1 - \epsilon_P)|\bar{P}^0\rangle]/\sqrt{2(1 + |\epsilon_P|^2)}. \end{aligned} \quad (52)$$

The mixing parameters are related by  $q/p = (1 - \epsilon_P)/(1 + \epsilon_P)$ . In the limit of CP invariance,  $|p|^2 = |q|^2$ ,  $\text{Re}\epsilon_P = 0$ , and a phase convention can be found such that  $\text{Im}\epsilon_P = 0$  and  $p = q = 1/\sqrt{2}$ . Throughout our discussion, we will assume CPT invariance.

The Hamiltonian eigenvalue equation

$$\begin{pmatrix} M_{11} - \frac{i}{2}\Gamma_{11} & M_{12} - \frac{i}{2}\Gamma_{12} \\ M_{12}^* - \frac{i}{2}\Gamma_{12}^* & M_{22} - \frac{i}{2}\Gamma_{22} \end{pmatrix} \begin{pmatrix} p \\ \pm q \end{pmatrix} = \left( M_{L,H} - \frac{i}{2}\Gamma_{L,H} \right) \begin{pmatrix} p \\ \pm q \end{pmatrix} \quad (53)$$

	$K^0$	$D^0$	$B_d^0$	$B_s^0$
$x$	0.476	< 0.083	$0.72 \pm 0.03$	> 13.8

Table 9: Experimental measurements and constraints<sup>4,12</sup> on the parameter  $x \equiv \Delta M/\Gamma$  for the various meson systems.

has the solution

$$\frac{q}{p} = \left[ \frac{M_{12}^* - \frac{i}{2}\Gamma_{12}^*}{M_{12} - \frac{i}{2}\Gamma_{12}} \right]^{\frac{1}{2}} = \frac{-2(M_{12}^* - \frac{i}{2}\Gamma_{12}^*)}{\Delta M - \frac{i}{2}\Delta\Gamma}, \quad (54)$$

where  $\Delta M = M_H - M_L = 2|M_{12}|$  and  $\Delta\Gamma = \Gamma_H - \Gamma_L = 2|\Gamma_{12}|$ .  $M_{12}$  describes transitions between  $P^0$  and  $\bar{P}^0$  via virtual states, and  $\Gamma_{12}$  represents contributions to decay channels which are common to both  $P^0$  and  $\bar{P}^0$ . The parameter  $x \equiv \Delta M/\Gamma$  is often used to describe the competition between the  $P^0 - \bar{P}^0$  mixing and decay. The experimental measurements and constraints on  $x$  for the various meson systems are listed in Table 9.

The proper time evolution of an initially pure  $P^0$  or  $\bar{P}^0$  state is

$$\begin{aligned} |P^0(t)_{phys}\rangle &= e^{-\Gamma t/2} e^{-iMt} \left[ \cos\left(\frac{\Delta Mt}{2}\right) |P^0\rangle \right. \\ &\quad \left. + i\frac{q}{p} \sin\left(\frac{\Delta Mt}{2}\right) |\bar{P}^0\rangle \right], \quad (55) \\ |\bar{P}^0(t)_{phys}\rangle &= e^{-\Gamma t/2} e^{-iMt} \left[ i\frac{p}{q} \sin\left(\frac{\Delta Mt}{2}\right) |P^0\rangle \right. \\ &\quad \left. + \cos\left(\frac{\Delta Mt}{2}\right) |\bar{P}^0\rangle \right], \end{aligned}$$

where  $M$  is defined as  $M \equiv (M_H + M_L)/2$ . In systems where  $\Delta\Gamma$  can be neglected, the probability of mixing can then be written as

$$\mathcal{P}(t) = \frac{1}{2} e^{-\Gamma t} [1 - \cos(\Delta Mt)]. \quad (56)$$

Time-dependent measurements of mixing in the  $B_d$  system have only recently been performed at SLD, LEP, and the Tevatron with new vertexing technology,<sup>12</sup> and provide a direct determination of  $\Delta M$ . Previous results relied on the time-integrated mixing parameter

$$\chi = \int_0^\infty \mathcal{P}(t) dt = \frac{x^2}{2(1+x^2)}, \quad (57)$$

which is bounded to be  $\chi \leq 0.5$ , and determines the parameter  $x$ .  $\Upsilon(4S)$  experiments measure the pure time integrated  $\chi_d$  parameter of the  $B_d$  system, while high-energy experiments off the  $\Upsilon(4S)$  measure the mixture

$$\chi_B = f_d \chi_d + f_s \chi_s, \quad (58)$$

where  $f_{d,s}$  represent the fractions of produced b-quark hadrons that are  $B_d^0$  and  $B_s^0$ , respectively. The values of these hadronization fractions are not precisely known, they are approximately  $f_d \sim 0.39$  and  $f_s \sim 0.12$  at SLC/LEP energies, and hence introduce a source of uncertainty to the time-integrated mixing measurements. If  $\chi$  approaches its upper value of 0.5, as is expected for the  $B_s$  system, it clearly does not provide a good determination of  $x$ , and one must then rely on the time-dependent approach.

As in the case of rare decays, both short- and long-distance physics processes contribute to meson mixing within the SM. The short-distance contributions are mediated by box diagrams with internal quark and  $W$ -boson exchange and are calculated via the operator product expansion in Eq. 24. The  $\Delta Q = 2$  effective Lagrangian for a pseudoscalar meson  $P = Q\bar{q}$  is

$$\mathcal{L}_{eff}(\Delta Q = 2) = \frac{G_F^2 M_W^2}{16\pi^2} \sum_{i,j} V_{q_i'Q} V_{q_i'q}^* V_{q_j'Q} V_{q_j'q}^* \eta_{ij} S\left(\frac{m_{q_i'}^2}{M_W^2}, \frac{m_{q_j'}^2}{M_W^2}\right) \mathcal{O}_{LL}, \quad (59)$$

where the sum extends over the two contributing internal quarks  $q_{i,j}'$ ,  $\eta$  summarizes the QCD corrections, and  $S$  represents the Inami-Lim functions<sup>30</sup> from the evaluation of the box diagrams. Note that the GIM mechanism may be employed here as well, and hence we would expect sizable short-distance mixing in cases where the top quark contributes internally, such as in the  $K^0$ ,  $B_d^0$ , and  $B_s^0$  systems. The matrix element of the  $\Delta Q = 2$  operator can be evaluated as

$$\begin{aligned} \langle \bar{P}^0 | \mathcal{O}_{LL} | P^0 \rangle &= \langle \bar{P}^0 | \bar{q} \gamma_\mu (1 - \gamma_5) Q \bar{q} \gamma^\mu (1 - \gamma_5) Q | P^0 \rangle, \\ &= \frac{4}{3} f_P^2 B_P m_P, \quad (60) \end{aligned}$$

with  $f_P$  ( $m_P$ ) being the pseudoscalar meson decay constant (mass), which is measured in the purely leptonic decays as discussed above, and  $B_P$  being the so-called bag factor which represents the nonperturbative factors associated with the hadronic matrix element and comprises the major source of theoretical uncertainty in the calculation of meson mixing. These bag factors are estimated using

nonperturbative techniques such as lattice gauge theory, QCD sum rules,  $1/N$  expansion, or chiral perturbation theory, with the lattice gauge results giving the most accurate evaluations.<sup>21</sup>

The long-distance contributions may be generally represented as the sum of common intermediate states  $I$ , which interact with the pseudoscalar mesons via an effective weak Hamiltonian  $\mathcal{H}_{eff}$

$$\langle \bar{P}^0 | \mathcal{A} | P^0 \rangle = \sum_I \frac{\langle \bar{P}^0 | \mathcal{H}_{eff} | I \rangle \langle I | \mathcal{H}_{eff} | P^0 \rangle}{m_P^2 - m_I^2 + i\epsilon}. \quad (61)$$

The dominant classes of contributions of this type arise from (i) single particle intermediate states, called pole contributions, and (ii) two particle intermediate states, denoted as dispersive contributions. Due to the effectiveness of the GIM mechanism in reducing the size of the short-distance effects in the charm system, one expects long-distance processes to dominate  $D^0 - \bar{D}^0$  mixing.

### 5.1 $K^0 - \bar{K}^0$ Mixing

The neutral kaon system provides a special laboratory for the study of mixing. The dominant CP conserving decays of the two physical states are  $K_L \rightarrow 3\pi$  and  $K_S \rightarrow 2\pi$ . Due to the strong phase space suppression for the  $K_L$  decay,  $K_L$  and  $K_S$  have very different lifetimes, providing a clean separation of these two eigenmodes in the laboratory. The SM short-distance contributions to the  $K_L - K_S$  mass difference arises from top- and charm-quark contributions to the  $W$  box diagram, giving

$$M_{12}(\Delta S = 2) = \frac{G_F^2 M_W^2 f_K^2 B_K m_K}{12\pi^2} \left[ (V_{cs} V_{cd}^*)^2 \eta_c S(x_t) + (V_{ts} V_{td}^*)^2 \eta_t S(x_t) + 2V_{cs} V_{cd}^* V_{ts} V_{td}^* \eta_{ct} S(x_c, x_t) \right]. \quad (62)$$

Here,  $S(x)$  represents the Inami-Lim functions,<sup>30</sup>  $x_i \equiv m_i^2/M_W^2$ , and the  $\eta_i$  correspond to the QCD correction factors which have been computed<sup>90,91</sup> to NLO for each contribution, with their numerical values being  $\eta_c = 1.38 \pm 0.20$ ,  $\eta_{c,t} = 0.47 \pm 0.04$ , and  $\eta_t = 0.57 \pm 0.01$ . The hadronic matrix element (or bag factor),  $B_K$ , represents a large uncertainty in the computation of  $M_{12}$ , with the results from various approaches being summarized in Table 10. Buras<sup>12</sup> advocates use of the value  $B_K = 0.75 \pm 0.15$ . The mass difference is then  $\Delta M_K = 2|M_{12}|$ .

Approach	$B_K$
Lattice	$0.90 \pm 0.06$
$1/N$	$0.70 \pm 0.10$
QCD Sum Rules	$\sim 0.60$
Chiral Quark Model	$0.87 \pm 0.25$
QCD Hadronic Duality	$0.39 \pm 0.10$
SU(3) Symmetry	1/3

Table 10: Compilation of various determinations<sup>21,92</sup> of  $B_K$ .

The calculation of  $\Delta M_K$  is unfortunately plagued with uncertainties from the potentially sizable long-distance contributions.<sup>93</sup> Even so, the  $K_L - K_S$  mass difference has played a strong and historical role in constraining new physics. For example, the strongest bound<sup>94</sup> (albeit assumption dependent) on the mass of a right-handed  $W$  boson in the Left-Right Symmetric Model of  $M_{W_R} \gtrsim 1.6$  TeV, the requirement of near degeneracy of the squark masses in supersymmetry,<sup>95</sup> and severe constraints on technicolor model building<sup>96</sup> such as the introduction of the Techni-GIM mechanism, are all obtained from  $K^0 - \bar{K}^0$  mixing.

### 5.2 $B_d^0 - \bar{B}_d^0$ and $B_s^0 - \bar{B}_s^0$ Mixing

The quark level process which is dominantly responsible for  $B^0 - \bar{B}^0$  mixing in the SM is that of top-quark exchange in a  $W$  box diagram. The mass difference for  $B_d$  meson mixing is then given by

$$\Delta M_d = \frac{G_F^2 M_W^2 m_B}{6\pi^2} f_{B_d}^2 B_{B_d} \eta_{B_d} |V_{tb} V_{td}^*|^2 F(m_t^2/M_W^2), \quad (63)$$

with  $\eta_{B_d} = 0.55 \pm 0.01$  being the QCD correction factor which is calculated to NLO,<sup>91</sup> and  $F(x)$  being the usual Inami-Lim function.<sup>30</sup> For consistency with the NLO QCD calculations, the running top-quark mass evaluated at  $m_t$  should be used. An equivalent expression for  $B_s$  mixing is obtained with  $d \rightarrow s$ . This yields the SM values of  $\Delta M_d = (3.0_{-2.7}^{+9.0}) \times 10^{-13}$  GeV and  $\Delta M_s = (7.4_{-4.3}^{+8.6}) \times 10^{-12}$  GeV, where the ranges correspond to taking  $m_t^{phys} = 175 \pm 6$  GeV,  $|V_{td}| = 0.009 \pm 0.005$  and  $|V_{ts}| = 0.040 \pm 0.006$  as given in Ref. 4, and  $f_{B_d} = 175 \pm 25$  MeV,  $B_{B_d} = 1.31 \pm 0.03$ , (the combined quantity is quoted to be  $f_{B_d} \sqrt{B_{B_d}} = 207 \pm 30$  MeV)  $f_{B_s} = 200 \pm 25$  MeV, and  $B_{B_s} = (1.01 \pm 0.01) B_{B_d}$  as suggested by a global summary

of lattice gauge theory results.<sup>21</sup> This agrees well with the experimental bounds<sup>12</sup> of  $\Delta M_d = (0.464 \pm 0.012 \pm 0.013) \text{ ps}^{-1}$  and  $\Delta M_s > 9.2 \text{ ps}^{-1}$ , corresponding to the  $x$  parameter values in Table 9. This situation is summarized in Fig. 10.

$B_d^0 - \bar{B}_d^0$  mixing is measured with impressive accuracy and can be used to determine the value of  $V_{td}$ , giving<sup>12</sup> (in the Wolfenstein CKM parameterization)

$$\begin{aligned} |V_{td}| &= A\lambda^3[(1-\rho)^2 + \eta^2]^{1/2}, \\ &= 8.54 \times 10^{-3} \left[ \frac{207 \text{ MeV}}{f_{B_d} \sqrt{B_{B_d}}} \right] \left[ \frac{170 \text{ GeV}}{\bar{m}_t(m_t)} \right]^{0.76} \left[ \frac{\Delta M_d}{0.464 \text{ ps}^{-1}} \right] \sqrt{\frac{0.55}{\eta}}. \end{aligned} \quad (64)$$

Setting the input parameters at their  $1\sigma$  values gives the range  $|V_{td}| = 0.007 - 0.010$ . Unfortunately, this evaluation of  $V_{td}$  is dominated by the uncertainties associated with the hadronic matrix elements and assumes that new physics does not contribute to  $B_d^0 - \bar{B}_d^0$  mixing.

A measurement of  $B_s^0 - \bar{B}_s^0$  mixing could also yield a value for the ratio of CKM elements  $|V_{td}/V_{ts}|$  via

$$\frac{\Delta M_d}{\Delta M_s} = \frac{f_{B_d}^2 B_{B_d} \eta_{B_d} m_{B_d} |V_{td}|^2}{f_{B_s}^2 B_{B_s} \eta_{B_s} m_{B_s} |V_{ts}|^2} = \xi^2 \lambda^2 [(1-\rho)^2 + \eta^2]. \quad (65)$$

The factor which multiplies the ratio of CKM elements,  $\xi$ , measures the amount of SU(3) breaking effects. The ratio of hadronic matrix elements,  $f_{B_d} \sqrt{B_{B_d}}/f_{B_s} \sqrt{B_{B_s}}$ , is more accurately determined in lattice gauge theory than the individual quantities with the current global value<sup>21</sup> being  $1.15 \pm 0.05$  in quenched calculations. However, unquenching is expected to increase this result by 10%. The LEP bound on  $\Delta M_s$  then yields<sup>12</sup> the 95% C.L. constraint

$$\left| \frac{V_{td}}{V_{ts}} \right| < 0.29. \quad (66)$$

We note that if  $V_{ts}$  is relatively large, a sensitive technique<sup>97</sup> of extracting  $|V_{td}/V_{ts}|$  could be obtained from a measurement of  $\Delta\Gamma/\Gamma$  for the  $B_s$  meson.

Remarkably, the above technique for extracting  $|V_{td}/V_{ts}|$  remains valid in many scenarios beyond the SM. In this class of models, the virtual exchange of new particles alters the Inami-Lim function in Eq. (63) above, but not the factors in front of the function. The effects of the new physics then cancels in the ratio  $\Delta M_d/\Delta M_s$ . Models of this type include Two-Higgs-Doublet models and supersymmetry in the super-CKM basis. Notable exceptions to this feature can be found in models which (i) change the structure of the CKM matrix, such as the addition of a fourth

generation, or extra singlet quarks, and in Left-Right Symmetric models, (ii) have couplings proportional to fermion masses, such as flavor changing Higgs models, or (iii) have generational dependent couplings, *e.g.*, leptoquarks or supersymmetry with R-parity violation.

It is difficult to use  $\Delta M_d$  alone to restrict new physics due to the errors on the theoretical predictions for this quantity from the imprecisely determined CKM factors and  $B$  hadronic matrix elements. (This is unfortunate as  $\Delta M_d$  is so precisely measured!) In most cases, the restrictions obtained from  $B \rightarrow X_s \gamma$  surpass those from  $B^0 - \bar{B}^0$  mixing.

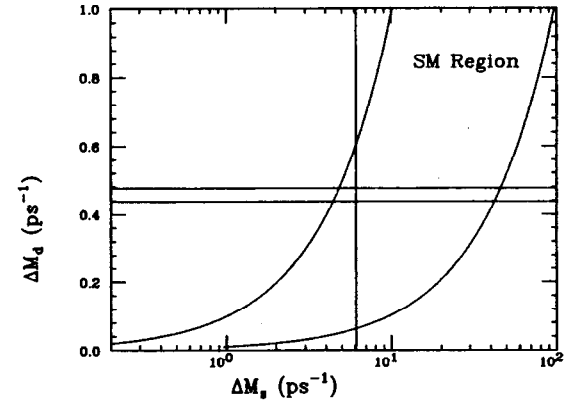


Figure 10: The SM expectation for the  $\Delta M_d - \Delta M_s$  plane, where the predicted region lies inside the solid curves. The experimental bounds lie in between the solid horizontal lines and to the right of the solid vertical line.

### 5.3 $D^0 - \bar{D}^0$ Mixing

Currently, the limits<sup>98</sup> on  $D^0 - \bar{D}^0$  mixing are from fixed target experiments, with  $x_D \equiv \Delta m_D/\Gamma < 0.083$ , implying  $\Delta m_D < 1.3 \times 10^{-13} \text{ GeV}$ , from an analysis which assumes there is no interference between doubly-Cabibbo suppressed decays and the mixing amplitude. A more recent result,<sup>99</sup> which takes these interference

effects into account, obtains the bound on the ratio of wrong-sign to right-sign final states of  $r_D \equiv \Gamma(D^0 \rightarrow \ell^- X)/\Gamma(D^0 \rightarrow \ell^+ X) < 0.50\%$  at 90% C.L., where

$$r_D \approx \frac{1}{2} \left| \frac{q}{p} \right|^2 \left[ \left( \frac{\Delta m_D}{\Gamma} \right)^2 + \left( \frac{\Delta \Gamma}{2\Gamma} \right)^2 \right]. \quad (67)$$

This gives  $\Delta M_D < 1.58 \times 10^{-13}$  GeV, assuming  $|q/p|^2 = 1$  and  $\Delta \Gamma \approx 0$ .

The short-distance SM contributions to  $\Delta m_D$  proceed through a  $W$  box diagram with internal  $d, s, b$  quarks. In this case, the external momentum, which is of order  $m_c$ , is communicated to the light quarks in the loop and cannot be neglected. The effective Hamiltonian becomes

$$\mathcal{H}_{eff}^{\Delta c=2} = \frac{G_F \alpha}{8\sqrt{2}\pi x_w} \left[ |V_{cs} V_{us}^*|^2 (I_1^s \mathcal{O}_{LL} - m_c^2 I_2^s \mathcal{O}_{RR}) + |V_{cb} V_{ub}^*|^2 (I_3^b \mathcal{O}_{LL} - m_c^2 I_4^b \mathcal{O}_{RR}) \right], \quad (68)$$

where the  $I_j^q$  represent integrals<sup>100</sup> that are functions of  $m_q^2/M_W^2$  and  $m_q^2/m_c^2$ , and  $\mathcal{O}_{LL} = [\bar{u}\gamma_\mu(1 - \gamma_5)c]^2$  is the usual mixing operator while  $\mathcal{O}_{RR} = [\bar{u}(1 + \gamma_5)c]^2$  arises in the case of nonvanishing external momentum. The numerical value of the short-distance contribution is  $\Delta m_D \sim 5 \times 10^{-18}$  GeV (taking  $f_D = 200$  MeV). The long-distance contributions have been computed via two different techniques: (i) the intermediate particle dispersive approach (using current data on the intermediate states) yields  $\Delta m_D \sim 10^{-4}\Gamma \simeq 10^{-16}$  GeV (Ref. 101), and (ii) heavy quark effective theory which results in  $\Delta m_D \sim (1-2) \times 10^{-5}\Gamma \simeq 10^{-17}$  GeV (Ref. 102). Clearly, the long-distance contributions overwhelm those from short-distance SM physics in  $D^0 - \bar{D}^0$  mixing, and both contributions lie far below the present experimental sensitivity.

One reason the SM expectations for  $D^0 - \bar{D}^0$  mixing are so small is that there are no heavy particles participating in the box diagram to enhance the rate. Hence, the first extension to the SM that we consider is the addition<sup>103</sup> of a heavy  $Q = -1/3$  quark. We can now neglect the external momentum, and  $\Delta m_D$  is given by the usual expression<sup>30</sup>

$$\Delta m_D = \frac{G_F^2 M_W^2 m_D}{6\pi^2} f_D^2 B_D |V_{c\ell} V_{u\ell}^*|^2 F(m_\ell^2/M_W^2). \quad (69)$$

The value of  $\Delta m_D$  is displayed in this model in Fig. 11(a) as a function of the overall CKM mixing factor for various values of the heavy quark mass. We see that  $\Delta m_D$  approaches the experimental bound for large values of the mixing factor.

Another simple extension of the SM is to enlarge the Higgs sector by an additional doublet. First, we examine two-Higgs-doublet models which avoid tree-level

FCNC by introducing a global symmetry; such models are discussed above in the sections on leptonic and radiative decays. The expression for  $\Delta m_D$  in this case can be found in Ref. 46. From the Lagrangian in Eq. (17), it is clear that Model I will only modify the SM result for  $\Delta m_D$  for very small values of  $\tan \beta$ , and this region is already excluded from existing data on  $B \rightarrow X_s \gamma$ . However, enhancements can occur in Model II for large values of  $\tan \beta$ , as demonstrated in Fig. 11(b).

Next, we consider the case of extended Higgs sectors without natural flavor conservation. In these models, the above requirement of a global symmetry which restricts each fermion type to receive mass from only one doublet is replaced<sup>104</sup> by approximate flavor symmetries which act on the fermion sector. The Yukawa couplings can then possess a structure which reflects the observed fermion mass and mixing hierarchy. This allows the low-energy FCNC limits to be evaded as the flavor changing couplings to the light fermions are small. We employ the Cheng-Sher ansatz,<sup>86</sup> where the flavor changing couplings of the neutral Higgs are  $\lambda_{h^0 f_i f_j} \approx (\sqrt{2}G_F)^{1/2} \sqrt{m_i m_j} \Delta_{ij}$ , with the  $m_{i(j)}$  being the relevant fermion masses and  $\Delta_{ij}$  representing a combination of mixing angles.  $h^0$  can now contribute to  $\Delta m_D$  through tree-level exchange as well as mediating  $D^0 - \bar{D}^0$  mixing by  $h^0$  and t-quark virtual exchange in a box diagram. These latter contributions only compete with those from the tree-level process for large values of  $\Delta_{ij}$ . In Figs. 11(c) and 11(d), we show the constraints placed on the parameters of this model from the present experimental bound on  $\Delta m_D$  for both the tree-level and box diagram contributions.

The last contribution to  $D^0 - \bar{D}^0$  mixing that we consider here is that of scalar leptoquark bosons. They participate in  $\Delta m_D$  via virtual exchange inside a box diagram,<sup>62</sup> together with a charged lepton or neutrino. Assuming that there is no leptoquark-GIM mechanism, and taking both exchanged leptons to be the same type, we obtain the restriction

$$\frac{F_{\ell c} F_{\ell u}}{m_{LQ}^2} < \frac{196\pi^2 \Delta m_D}{(4\pi\alpha f_D)^2 m_D}, \quad (70)$$

where  $F_{\ell q}$  parameterize the a priori unknown leptoquark Yukawa couplings as  $\lambda_{\ell q}^2/4\pi = F_{\ell q}\alpha$ . The resulting bounds in the leptoquark coupling-mass plane are presented in Fig. 11(e).

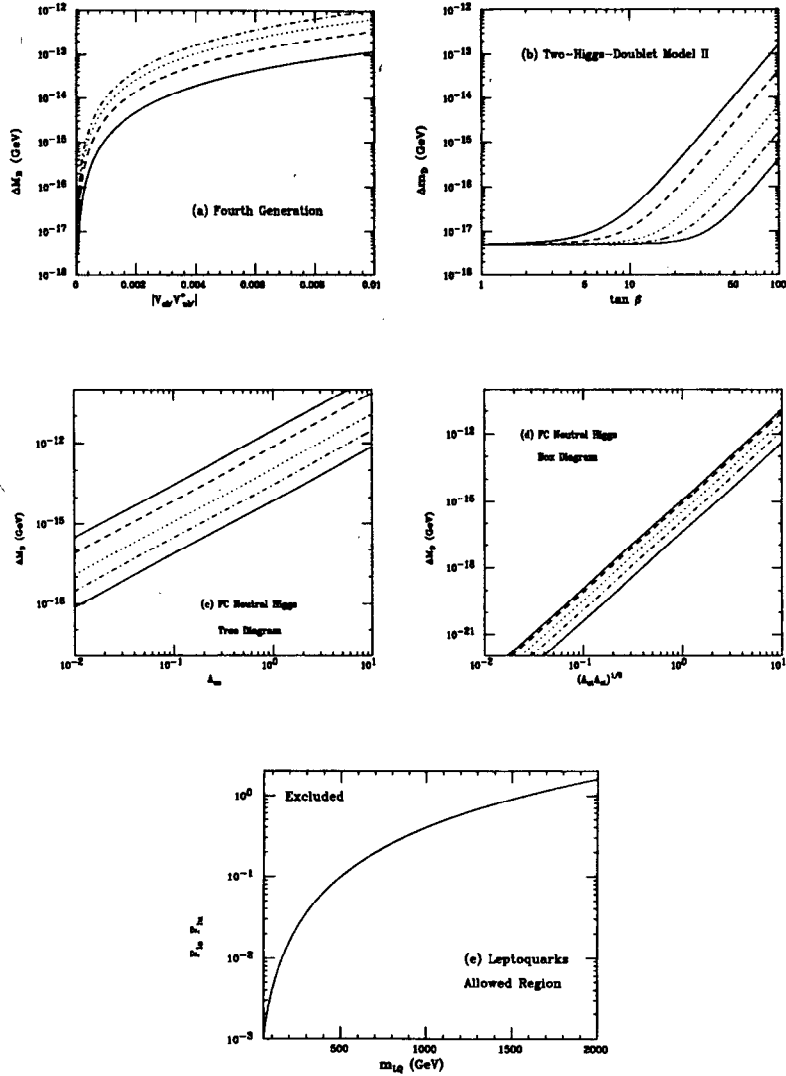


Figure 11:  $\Delta m_D$  in (a) the four-generation SM with the solid, dashed, dotted, dash-dotted curve corresponding to fourth generation quark masses  $M_{\nu} = 100, 200, 300,$  and  $400$  GeV, respectively. (b) The two-Higgs-doublet Model II as a function of  $\tan \beta$  with, from top to bottom, the solid, dashed, dotted, dash-dotted, solid curve representing  $m_{H^{\pm}} = 50, 100, 250, 500,$  and  $1000$  GeV. (c) Tree-level and (d) box diagram contributions to  $\Delta m_D$  in the flavor changing Higgs model described in the text as a function of the mixing factor for  $m_h = 50, 100, 250, 500,$  and  $1000$  GeV corresponding to the solid, dashed, dotted, dash-dotted, and solid curves from top to bottom. (e) Constraints in the leptoquark coupling-mass plane from  $\Delta m_D$ .

## 6 CP Violation

The symmetries C, charge conjugation (which describes particle-antiparticle interchange), P, parity (which relates left- to right-handed particles), and T, time reversal (which correlates a process with its time-reversed state), are all preserved under the strong and electromagnetic interactions. Weak processes, however, are known to violate each of these symmetries separately, while conserving the product CPT, which is an exact symmetry of the equations of motion. Weak decays violate C and P at a fairly large level, while the product CP has been observed to be violated at a much smaller rate.

CP violation arises in the SM from the existence of the phase in the three-generation CKM matrix as first postulated by Kobayashi and Maskawa.<sup>2</sup> Unitarity of the CKM matrix can be represented geometrically in terms of triangles in the complex plane. For example, the relation  $V_{ib}V_{id}^* + V_{cb}V_{cd}^* + V_{ub}V_{ud}^* = 0$ , can be depicted as the triangle displayed in Fig. 12. The figure depicts the rescaled triangle, where the length of all sides are scaled to  $|V_{cd}V_{cb}^*|$ , and hence the length of the base is unity. In this case, it can be shown that the apex of the triangle is located at the point  $(\rho, \eta)$  in the complex plane, where  $\rho$  and  $\eta$  are the Wolfenstein parameters describing the CKM matrix. Here, the unitarity angles  $\alpha, \beta,$  and  $\gamma$  are related to the magnitudes of the sides of the triangle by

$$\alpha = \arg \left( \frac{V_{td}V_{tb}^*}{V_{ud}V_{ub}^*} \right), \quad \beta = \arg \left( \frac{V_{cd}V_{cb}^*}{V_{td}V_{tb}^*} \right), \quad \gamma = \arg \left( \frac{V_{ud}V_{ub}^*}{V_{cd}V_{cb}^*} \right). \quad (71)$$

The values of these angles are rather poorly constrained at present, as will be discussed below. The area of the triangle represents the amount of CP violation in the SM, and can be described by the Jarlskog<sup>105</sup> parameter

$$J = 2 \times \text{area of triangle}, \quad (72)$$

$$= |V_{ud}||V_{us}||V_{ub}||V_{cb}|\sin \delta = A^2 \lambda^6 \eta \simeq \mathcal{O}(10^{-5}).$$

Similar unitarity triangles, representing other orthogonality relations of the CKM matrix, may also be drawn. All such triangles clearly have the same area in the SM; however, the remaining triangles involve one side which is much shorter than the other two, and consequently one of their unitarity angles is extremely small. This is in contrast to the above triangle, where all three sides are of comparable magnitude,  $\mathcal{O}(\lambda^3)$ , and hence all three angles are naturally large.

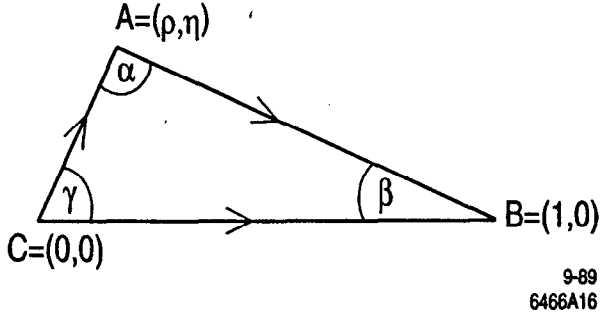


Figure 12: The rescaled unitarity triangle.

This explains why CP asymmetries are predicted to be large in neutral  $B_d$  decays. For example, the triangle representing the neutral  $K$  meson system, which is built from the relation  $\sum_q V_{qd}V_{qs}^* = 0$ , has two long sides of length  $\mathcal{O}(\lambda)$  and a third side of length  $\mathcal{O}(\lambda^5)$ . Hence, CP asymmetries in this system are related to the small angle of this unitarity triangle and are of order  $10^{-3}$ .

There are many additional sources of CP violation in theories beyond the SM, such as multi-Higgs-Doublet models, supersymmetry, and Left-Right Symmetric models.<sup>106</sup> It is worth noting that the observed matter-antimatter asymmetry of the universe may require additional sources of CP violation beyond the CKM phase.<sup>107</sup>

There is a vast literature on CP violation<sup>108</sup> to which we refer the reader for a more detailed discussion. Here, we now describe the three manifestations of CP violation and how they are observed in the various meson systems. In all cases, one should keep in mind the experimentally relevant number for measurement of a CP asymmetry at the  $n\sigma$  level,

$$N = \frac{n^2}{Ba^2}, \quad (73)$$

where  $N$  is the number of identified  $P$  mesons required for observation of the asymmetry (not including efficiency reductions),  $B$  represents the branching fraction of the decay mode, and  $a$  is the value of the CP violating asymmetry.

## 6.1 CP Violation in Decays

CP violating effects may be observed directly in the decays of charged or neutral mesons. This is referred to as Direct CP Violation, or CP Violation in Decays. CPT symmetry assures us that the total width of a particle and its antiparticle are identical, i.e.,

$$\Gamma_{\text{total}} = \bar{\Gamma}_{\text{total}}. \quad (74)$$

If CP were conserved, this would also hold true for the partial decay width of a meson to a particular final state,  $P \rightarrow f$ , versus the time-reversed process,  $\bar{P} \rightarrow \bar{f}$ . For CP to be violated, these two partial widths must be different, i.e.,

$$\Gamma(P \rightarrow f) \neq \Gamma(\bar{P} \rightarrow \bar{f}). \quad (75)$$

In order for direct CP violation to occur, the decay amplitudes must have contributions from (at least) two different weak phases, and two separate strong phases. This can easily be seen as follows. Let us assume that the decay amplitude to the final state  $f$  has the form

$$A_f = A_1 e^{i\delta_1} + A_2 e^{i\delta_2}, \quad (76)$$

with  $A_{1,2}$  being the two weak amplitudes after the strong phases  $\delta_{1,2}$  have been factored out. In the SM, all tree-level contributions to a given transition enter with the same weak phase, whereas penguin diagrams can contribute with a different phase. Here, we identify  $A_1$  as the tree-level amplitude, while  $A_2$  represents the penguin transition. For the CP conjugate amplitude, the weak phases are conjugated,  $A_{1,2} \rightarrow A_{1,2}^*$ , but the strong phases are not. The CP asymmetry is then given by

$$\frac{|A_f|^2 - |\bar{A}_f|^2}{|A_f|^2 + |\bar{A}_f|^2} = \frac{2\text{Im}(A_1^* A_2) \sin(\delta_1 - \delta_2)}{|A_1|^2 + |A_2|^2 + 2\text{Re}(A_1^* A_2) \cos(\delta_1 - \delta_2)}, \quad (77)$$

which clearly vanishes if  $A_{1,2}$  contain the same weak phase and if  $\delta_1 = \delta_2$ . Hence, direct CP violation arises from the product of the weak phase difference, which is odd under CP, and the strong phase difference from final state interactions, which is even under CP. Since this results from the interference between the tree-level and penguin transitions, the magnitude of direct CP violation is related to the size of the penguin contributions. Unfortunately, there is at present no unambiguous experimental signal for direct CP violation.

## 6.2 CP Violation in Mixing

Indirect CP violation, or CP violation due to mixing, is a consequence of the fact that the mass eigenstates  $P_{L,H}$  are not CP eigenstates and is represented by the potential deviation of  $|q/p|$  from unity. Clearly, these effects only arise in neutral meson decays. This process is theoretically clean as it is independent of the strong phases and thus provides a direct measurement of the CKM phase<sup>109</sup> (at least within the SM).

The CP violating observable that can be defined in this case is given by

$$\frac{1 - |q/p|^2}{1 + |q/p|^2} = \frac{2\text{Re}\epsilon_P}{1 + |\epsilon_P|^2} = \frac{2\text{Im}(M_{12}^*\Gamma_{12}/2)}{|\Gamma_{12}/2|^2 + |M_{12}|^2 + [(\Delta m_P)^2 + (\Delta\Gamma_P/2)^2]/4}, \quad (78)$$

where we give the expression in terms of  $M_{12}$  and  $\Gamma_{12}$ , which are defined in the previous sections. This quantity is independent of the phase convention and is directly observable. As noted by Ma *et al.*,<sup>110</sup> this observable demonstrates that CP nonconservation is determined by the relative phase between  $M_{12}$  and  $\Gamma_{12}$ . Defining  $\Delta\Gamma_P/\Delta M_P \equiv a$  and taking the approximation (which is valid in the SM only) that  $\Delta M \simeq 2\text{Re}M_{12}$  and  $\Delta\Gamma \simeq 2\text{Re}\Gamma_{12}$ , the above expression can be written in the more convenient form

$$\frac{2\text{Re}\epsilon_P}{1 + |\epsilon_P|^2} = \frac{a}{2(1 + a^2/4)} \left[ \frac{\text{Im}\Gamma_{12}}{\text{Re}\Gamma_{12}} - \frac{\text{Im}M_{12}}{\text{Re}M_{12}} \right]. \quad (79)$$

## 6.3 CP Violation in the Interference Between Mixing and Decay

Additional CP violating effects can arise from the interference of a pseudoscalar meson  $P^0$  decaying to a final state  $f$  at time  $t$ , with a  $P^0$  which mixes into a  $\bar{P}^0$  state which then decays to  $f$  at time  $t$ . We define the phase convention independent quantity

$$r_f \equiv \frac{q\bar{A}_f}{pA_f}. \quad (80)$$

When CP is conserved,  $|q/p| = 1$ ,  $|\bar{A}_f/A_f| = 1$ , and the relative phase between these two quantities vanishes. If any one of these three conditions are not met, then  $r_f \neq 1$  and CP is violated. As discussed above, if the first condition (the deviation of  $|q/p|$  from unity) doesn't hold, then CP violation occurs through mixing, while if the magnitudes of the amplitudes differ, then CP violation occurs in decay. However, even if these first two conditions hold, it is possible that the

relative phase between these two quantities is nonzero resulting in  $\text{Im}r_f \neq 0$  while  $|r_f| = 1$ . It is this case that we call CP violation in the interference between mixing and decay. This case is also independent of hadronic uncertainties and hence is theoretically clean and can be directly related to the CKM matrix elements. We will discuss the significance and potential measurements of this third type of CP violation in the kaon and  $B$  meson systems separately.

## 6.4 CP Violation in the Kaon System

The kaon system has provided our only experimental observation of CP violation. The charge asymmetry in semileptonic decay,  $K_L^0 \rightarrow \ell\nu_\ell + X$ ,

$$a_{sl} = \frac{\Gamma(K_L \rightarrow \ell^+\nu_\ell X) - \Gamma(K_L \rightarrow \ell^-\bar{\nu}_\ell X)}{\Gamma(K_L \rightarrow \ell^+\nu_\ell X) + \Gamma(K_L \rightarrow \ell^-\bar{\nu}_\ell X)}, \quad (81)$$

has been measured<sup>4</sup> to have the value  $a_{sl} = (3.27 \pm 0.12) \times 10^{-3}$ . Since we can relate  $\langle \ell^+\nu_\ell X | H | K_L \rangle = pA$ , while  $\langle \ell^-\bar{\nu}_\ell X | H | K_L \rangle = qA^*$ , the charge asymmetry can be identified as a determination of  $|q/p| \neq 1$  with

$$a_{sl} = \frac{2\text{Re}\epsilon_K}{1 + |\epsilon_K|^2}. \quad (82)$$

CP violation has also been measured in the decay of  $K_L \rightarrow \pi\pi$ . The amplitudes in the CP eigenstate basis can be written as

$$\begin{aligned} \mathcal{A}(K^0 \rightarrow \pi\pi(I)) &= A_I e^{i\delta_I}, \\ \mathcal{A}(\bar{K}^0 \rightarrow \pi\pi(I)) &= A_I^* e^{i\delta_I}, \end{aligned} \quad (83)$$

where  $I$  denotes the isospin of the  $\pi\pi$  final state,  $\delta_I$  is the final state phase shift, and  $A_I$  would be real if CP were conserved. It is interesting to note that experimentally,  $|\mathcal{A}_0/\mathcal{A}_2| = 20$ . The following ratios of CP violating to CP conserving amplitudes have been measured

$$\begin{aligned} \eta_{+-} &= \frac{\mathcal{A}(K_L^0 \rightarrow \pi^+\pi^-)}{\mathcal{A}(K_S^0 \rightarrow \pi^+\pi^-)}, \\ \eta_{00} &= \frac{\mathcal{A}(K_L^0 \rightarrow \pi^0\pi^0)}{\mathcal{A}(K_S^0 \rightarrow \pi^0\pi^0)}. \end{aligned} \quad (84)$$

These differences in these quantities can be parameterized as

$$\begin{aligned} \eta_{+-} &= \epsilon + \epsilon', \\ \eta_{00} &= \epsilon - 2\epsilon', \end{aligned} \quad (85)$$

where  $\epsilon$  and  $\epsilon'$  are defined by

$$\begin{aligned}\epsilon &= \epsilon_K + i \frac{\text{Im} A_0}{\text{Re} A_0}, \\ |\epsilon'| &= \frac{1}{\sqrt{2}} \frac{\text{Re} A_2}{\text{Re} A_0} \left[ \frac{\text{Im} A_2}{\text{Re} A_2} - \frac{\text{Im} A_0}{\text{Re} A_0} \right].\end{aligned}\quad (86)$$

These parameters,  $\epsilon$  and  $\epsilon'$ , are defined so that the potentially direct CP violating effects are isolated and affect only  $\epsilon'$ . In superweak models,<sup>111</sup> CP violation is confined to the mass matrix and  $\epsilon'$  is predicted to vanish. As shown by Wu and Yang,<sup>112</sup> it is possible to adopt a phase convention such that  $\text{Im} A_0 = 0$ . In this case, we then have

$$\begin{aligned}\epsilon &= \epsilon_K, \\ |\epsilon'| &= \frac{1}{\sqrt{2}} \frac{\text{Re} A_2}{\text{Re} A_0} \frac{\text{Im} A_2}{\text{Re} A - 2}.\end{aligned}\quad (87)$$

$\epsilon$  is then given by the CP violation effects due to mixing and can be calculated as

$$\begin{aligned}\epsilon &= \epsilon_K = \frac{e^{i\pi/4}}{\sqrt{2} \Delta M_K} \text{Im} M_{12}, \\ &= \frac{G_F^2 M_W^2 f_K^2 B_K m_K}{6 \sqrt{s} \pi^2 \Delta M_K} A^2 \lambda^6 \eta \left[ \eta_c S(x_c, x_t) - \eta_c S(x_c) + \eta_t A^2 \lambda^4 (1 - \rho) S(x_t) \right],\end{aligned}\quad (88)$$

in the Wolfenstein parameterization. We see that the measurement of  $\epsilon_K$  guarantees that  $\eta \neq 0$ ! The uncertainties in the calculation of  $\epsilon_K$  are equivalent to those outlined above in the case of  $K_L - K_S$  mixing.

Returning to direct CP violation in K decays, we see that  $\epsilon'/\epsilon$  can be expressed in terms of the operator product expansion<sup>113</sup> by relating  $\text{Re} A_{0,2}$  and  $\text{Im} A_{0,2}$  to the appropriate Wilson coefficients and hadronic matrix elements. The effective Hamiltonian for this process can then be written as

$$\mathcal{H}_{eff} = \frac{G_F}{\sqrt{2}} V_{us} V_{ud}^* \sum_{i=1}^{10} \left[ Z_i(\mu) - \frac{V_{ts} V_{td}^*}{V_{us} V_{ud}^*} y_i(\mu) \right] \mathcal{O}_i(\mu), \quad (89)$$

where the sum extends over the set of operators given by the current-current operators  $\mathcal{O}_{1,2}$ , the QCD penguin operators  $\mathcal{O}_{3-6}$ , and the electroweak operators  $\mathcal{O}_{7-10}$ . The functions  $z_i$  and  $y_i$  are related to the Wilson coefficients; their forms are given explicitly in Ref. 113. In this formalism, it is easy to see that  $\epsilon'/\epsilon$  is governed by both QCD and electroweak penguin transitions. In fact, due to the large value of the top quark mass, the electroweak penguin amplitudes play an

important role<sup>114</sup> and enter  $\epsilon'/\epsilon$  with the opposite sign of the QCD penguin contributions. This serves to suppress the prediction of  $\epsilon'/\epsilon$  within the SM. In fact, for  $m_t = 200$  GeV, the SM prediction for  $\epsilon'/\epsilon$  is zero! Due to this strong cancellation for large values of  $m_t$  and the uncertainties associated with the hadronic matrix elements, a precise SM prediction for  $\epsilon'/\epsilon$  is very difficult. However, a simplified analytic expression which highlights these uncertainties may be written as<sup>12</sup>

$$\frac{\epsilon'}{\epsilon} = 11 \times 10^{-4} \left[ \frac{\eta \lambda^5 A^2}{1.3 \times 10^{-4}} \right] \left[ \frac{140 \text{ MeV}}{m_2 (2 \text{ GeV})} \right] \left[ \Lambda_{MS}^{(4)} \right] [B_6 - Z(x_t) B_8], \quad (90)$$

where  $Z(x_t) \approx 0.18(m_t/M_W)^{1.86}$ , and  $B_{6,8}$  represent the hadronic matrix elements corresponding to operators  $\mathcal{O}_{6,8}$ . The most recent analysis,<sup>115</sup> which incorporates the latest determinations of all the input parameters, predicts the range

$$-1.2 \times 10^{-4} \leq \epsilon'/\epsilon \leq 16.0 \times 10^{-4}. \quad (91)$$

This prediction may be altered, however, if the value of the strange quark mass is as low as presently calculated in lattice gauge theories.<sup>21</sup>

The importance of the measurement of  $\epsilon'/\epsilon$  to understand more about the mechanism of CP violation cannot be overemphasized, although, due to presently conflicting experimental results, constraints on new physics from  $\epsilon'/\epsilon$  will not be taken into account here. The next round of experiments, which will reach a precision of  $10^{-4}$ , might settle the issue of whether or not  $\epsilon'/\epsilon \neq 0$ . As shown above, the SM prediction allows for a wide range of values for  $\epsilon'/\epsilon$ . Ultimately, one wants to establish whether CP violation is milliweak ( $\Delta S = 1$ ) as in the SM and/or superweak ( $\Delta S = 2$ ). The latter occurs in multi-Higgs doublet models through scalar interactions, in SUSY models,<sup>116</sup> or in the LRM to give a few examples.<sup>117</sup>

We note briefly that the decay  $K_L \rightarrow \pi^0 \nu \bar{\nu}$ , which is related to  $K^+ \rightarrow \pi^+ \nu \bar{\nu}$  discussed above, proceeds almost exclusively through direct CP violation and would provide a clean laboratory to measure this phenomenon. Unfortunately, the branching fraction is extremely small in the SM at  $B(K_L \rightarrow \pi^0 \nu \bar{\nu}) \approx 2.8 \times 10^{-11}$ , and the present experimental limits<sup>4</sup> lie above this prediction by roughly six orders of magnitude.

## 6.5 CP Violation in B Decays

CP violation in the B system will be examined<sup>118</sup> during the next decade at dedicated  $e^+e^-$  B factories and at hadron colliders. A theoretically clean technique

is offered<sup>109</sup> by the measurement of the time-dependent CP asymmetry, which involves the CP violating effects from the interference of mixing and decay. Given the proper time evolution of a neutral pseudoscalar meson state of Eq. (56) and the definition of  $r_f$  in Eq. (80), we can write the time-dependent rate for the decay of initially pure  $B^0$  or  $\bar{B}^0$  states into a CP eigenstate as

$$\begin{aligned}\Gamma(B_{phys}^0 \rightarrow f_{CP}) &= |A|^2 e^{-\Gamma t} \left[ \frac{1 + |r_f|^2}{2} + \frac{1 - |r_f|^2}{2} \cos(\Delta Mt) - \mathcal{I}m r_f \sin(\Delta Mt) \right], \\ \Gamma(\bar{B}_{phys}^0 \rightarrow f_{CP}) &= |A|^2 e^{-\Gamma t} \left[ \frac{1 + |r_f|^2}{2} - \frac{1 - |r_f|^2}{2} \cos(\Delta Mt) + \mathcal{I}m r_f \sin(\Delta Mt) \right].\end{aligned}\quad (92)$$

The time-dependent CP asymmetry can then be expressed as

$$\begin{aligned}a_f(t) &= \frac{\Gamma(B_{phys}^0 \rightarrow f_{CP}) - \Gamma(\bar{B}_{phys}^0 \rightarrow f_{CP})}{\Gamma(B_{phys}^0 \rightarrow f_{CP}) + \Gamma(\bar{B}_{phys}^0 \rightarrow f_{CP})}, \\ &= \frac{(1 - |r_f|^2) \cos(\Delta Mt) - 2\mathcal{I}m r_f \sin(\Delta Mt)}{1 + |r_f|^2},\end{aligned}\quad (93)$$

and hence is directly related to  $\mathcal{I}m r_f$ . In fact, for decay modes which have  $|r_f| = 1$ , the time-dependent asymmetry reduces to

$$a_f(t) = -\mathcal{I}m r_f \sin(\Delta Mt). \quad (94)$$

Recall that when there is no direct CP violation in a channel, all amplitudes that contribute to the decay mode have the same CKM phase, denoted generically here as  $\phi_D$ , and hence  $|\bar{A}_f/A_f| = |e^{-2i\phi_D}| = 1$ . In this case,  $r_f$  can be completely expressed in terms of the CKM matrix elements as  $r_f = \pm \exp -2i(\phi_D + \phi_M)$ , where  $\phi_M$  represents the mixing phase from  $q/p = \sqrt{M_{12}^*/M_{12}} = e^{-2i\phi_M}$  (for  $\Gamma_{12} \ll M_{12}$ ), and the overall sign is determined by the CP eigenvalue of the final state  $f$ . Clearly, the asymmetry is simply

$$a_f(t) = \pm \sin(2(\phi_D + \phi_M)) \sin(\Delta Mt). \quad (95)$$

In order to relate the time-dependent CP asymmetry to the CKM parameters, one needs to examine the CKM dependence of mixing and of the amplitudes of the relevant decay channels. An extensive summary of these relations for various decay modes is given in the Particle Data Book.<sup>4</sup> Here, we briefly discuss two important cases,  $B_d \rightarrow J/\psi K_s$  and  $B_d \rightarrow \pi\pi$ . In the first case, the quark subprocess

responsible for the decay is  $b \rightarrow c\bar{c}s$ , which is dominated by a tree-level diagram mediated by  $W$ -boson exchange. There are small penguin contributions as well; however, the penguin weak phase,  $\arg(V_{tb}V_{ts}^*)$ , is similar (modulo  $\pi$ ) to the weak phase of the tree-level contribution. We thus have contributions to the weak phase from the CKM structure of the decay diagram, from  $B_d^0 - \bar{B}_d^0$  mixing, and from  $K^0 - \bar{K}^0$  mixing in the final state. This gives

$$\begin{aligned}r_f &= -\left(\frac{q}{p}\right)_{B_d} \frac{\bar{A}_{J/\psi K_S}}{A_{J/\psi K_S}} \left(\frac{q}{p}\right)_K, \\ &= \frac{V_{tb}^* V_{td}}{V_{cb}^* V_{cb}}, \frac{V_{cs} V_{cb}^*}{V_{cs}^* V_{cb}}, \frac{V_{cs}^* V_{cd}}{V_{cs} V_{cd}},\end{aligned}\quad (96)$$

where the minus sign arises since  $J/\psi K_S$  is CP-odd. Comparing this with Eq. (71) yields  $\mathcal{I}m r_f = -\sin 2\beta$ . This gives the theoretically cleanest determination of a unitarity angle! In the latter example,  $B_d \rightarrow \pi\pi$ , the quark subprocess is  $b \rightarrow u\bar{u}d$ , which is again dominated by tree-level  $W$  exchange. In this case, we have

$$\begin{aligned}r_f &= \left(\frac{q}{p}\right)_{B_d} \frac{\bar{A}_{\pi\pi}}{A_{\pi\pi}}, \\ &= \frac{V_{tb}^* V_{td}}{V_{cb}^* V_{cb}}, \frac{V_{ub} V_{ud}^*}{V_{ud} V_{ub}^*},\end{aligned}\quad (97)$$

which then gives  $\mathcal{I}m r_f = \sin 2\alpha$ . Unfortunately, this process is not as clean as  $B_d \rightarrow J/\psi K_S$ , as both the gluonic and electroweak penguin contributions enter with a different phase at an unknown size.  $B_d \rightarrow \pi\pi$  thus suffers from what is called penguin contamination. The amount of this contamination needs to be separately determined.<sup>119</sup>

The present status of the unitarity triangle in the  $\rho - \eta$  plane is summarized in Fig. 13(a), where the shaded area is that allowed in the SM. This region is determined by measurements of the quantities (i)  $|V_{ub}|$  and  $|V_{cb}|$ , (ii)  $\epsilon_K$ , and (iii) the rates for  $B_d^0 - \bar{B}_d^0$  and  $B_s^0 - \bar{B}_s^0$  mixing, as discussed above, together with theoretical estimates for the parameters which relate these measurements to the underlying theory, such as  $B_K$ ,  $f_B$ , and  $B_B$ . The value of  $\bar{m}_t(m_t)$  is taken to be consistent with the physical range  $175 \pm 6$  GeV. Here we have employed the scanning technique, where both the experimental measurements and theoretical input parameters are scanned independently within their  $1\sigma$  errors. This method yields the SM ranges for the angles of the unitarity triangle:  $-0.89 \leq \sin 2\alpha \leq 1.00$ ,  $0.18 \leq \sin 2\beta \leq 0.81$ , and  $-1.00 \leq \sin 2\gamma \leq 1.00$ . Since

the ratio  $\Delta M_{B_s}/\Delta M_{B_c}$  is more accurately related to the theoretical predictions than the separate quantities, we see that a measurement of  $B_s^0 - \bar{B}_s^0$  mixing would be an invaluable tool in determining the angles of this triangle.

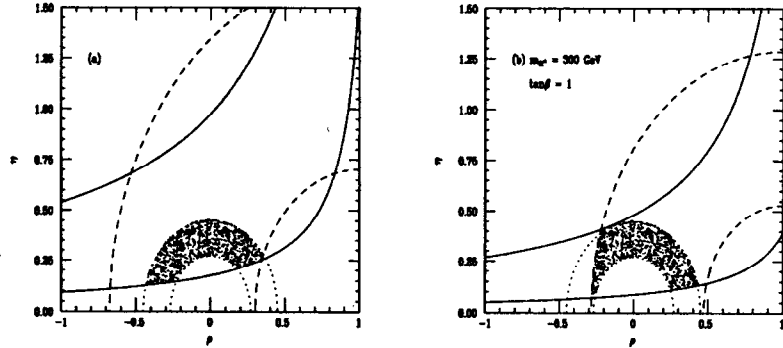


Figure 13: Constraints in the (a) SM and (b) two-Higgs-doublet Model II in the  $\rho - \eta$  plane from  $|V_{ub}|/|V_{cb}|$  (dotted circles),  $B_d^0 - \bar{B}_d^0$  mixing (dashed circles), and  $\epsilon$  (solid hyperbolas). The shaded area corresponds to that allowed for the apex of the unitarity triangle.

It is important to remember that this picture can be dramatically altered if new physics is present, even if there are no new sources of CP violation. Figure 13(b) displays the constraints in the  $\rho - \eta$  plane in the two-Higgs-doublet Model II. In this case, the presence of the extra Higgs doublet is felt by the virtual exchange of the  $H^\pm$  boson in the box diagram which mediates  $B_d^0 - \bar{B}_d^0$  and  $B_s^0 - \bar{B}_s^0$  mixing and governs the value of  $\epsilon_K$ . For this  $\rho - \eta$  region, the allowed ranges of the angles of the unitarity triangle become  $-1.00 \leq \sin 2\alpha \leq 1.00$ ,  $0.12 \leq \sin 2\beta \leq 0.81$ , and  $-1.00 \leq \sin 2\gamma \leq 1.00$ . In fact, this opens up a new allowed region in the  $\sin 2\alpha - \sin 2\beta$  plane, as shown in Fig. 14 from Ref. 120. Similar effects have also been pointed out in supersymmetric models.<sup>121</sup> Clearly, caution must be exercised when relating the results of future CP violation experiments to the  $\rho - \eta$  plane.

The B factories presently under construction should be able to discern whether new physics contributes to CP violation. Signals for new sources of CP violation include (i) nonclosure of the three-generation unitarity triangle, (ii) new contributions to  $B^0 - \bar{B}^0$  mixing which yield a nonvanishing phase for this process, (iii) nonvanishing CP asymmetries for the channels  $B_d^0 \rightarrow \phi\pi^0, K_S^0 K_S^0$ , (iv) inconsistency of separate measurements of the angles of the unitarity triangle, and (v) a deviation of CP rates from SM predictions. Models which contain additional CP phases include nonminimal Supersymmetry, Multi-Higgs Doublets, Left-Right Symmetric Models, and the Superweak Model. A concise review of the effects of these models on CP violating observables is given by *Grossman et al.*<sup>106</sup> We present here, as an example, the case of multi-Higgs models with three or more Higgs doublets. In this scenario,  $B^0 - \bar{B}^0$  mixing receives additional contributions from the  $H_{1,2}^\pm$  exchange which depends on the phase in the charged scalar mixing matrix. Interference between these contributions and the SM yield an overall nonzero phase in  $\Delta M_{B_s}$ . Denoting this phase as  $\theta_H$ , the unitarity angles measured by CP asymmetries in B decays are thus shifted by

$$a_{CP}(B \rightarrow J/\psi K_S) = -\sin(2\beta + \theta_H), \quad a_{CP}(B \rightarrow \pi\pi) = \sin(2\alpha + \theta_H). \quad (98)$$

The magnitude of this effect depends on the size of  $\theta_H$ , which has recently<sup>120</sup> been constrained by  $B \rightarrow X_s \gamma$ . Another interesting example is provided in models with an extra iso-singlet down quark; in this scenario, it has been found<sup>122</sup> that measurements of the unitarity angles  $\alpha$  and  $\beta$  alone are not enough to distinguish and bound the new contributions, and that observation of both the third angle  $\gamma$  and  $B_s$  mixing are also needed. In summary, the large data sample which will become available will provide a series of unique consistency tests of the quark sector and will challenge the SM in a new and quantitatively precise manner.

## 6.6 CP Violation in the D Meson System

CP violation in the  $Q = 2/3$  quark sector is complementary to that of the K and B systems, but has yet to be explored. In the SM, the CKM phase is responsible for generating CP violation, and in the charm system, the resulting rates are small. However, new sources of CP violating phases could greatly enhance the rates, thus rendering CP violation in the charm system a sensitive probe for physics beyond the SM.

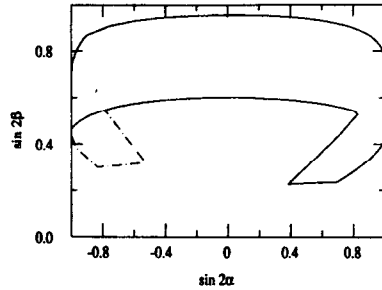


Figure 14: The allowed region in the  $\sin 2\alpha - \sin 2\beta$  plane in the SM (solid) and in 2HDM (dot-dashed). From Ref. 120.

#### • Indirect CP Violation

However, since  $\Delta m_D$  is extremely small in the SM, the induced CP violation is negligible. If new physics were to enhance  $D^0 - \bar{D}^0$  mixing, as seen to occur in the previous section for some models, then this mechanism could yield sizable CP violating effects. This interaction between mixing and CP violation in the  $D$  meson system has recently received attention in the literature.<sup>123,124</sup>

#### • Direct CP Violation

Before estimating the typical size of this asymmetry in the SM, we first note that in contrast to  $B$  decays, the branching fractions for the relevant modes, *i.e.*,  $\pi^+\pi^-$ ,  $K^+K^-$ , etc., are rather sizable in the charm system, and for once, the large effects of final state interactions are welcomed! The size of the CP asymmetry in the SM is estimated<sup>125</sup> to be at most a few  $\times 10^{-3}$ . The present experimental sensitivity for various modes is in the vicinity of 10% (Ref. 126).

An interesting example of the potential size of CP violating effects from new physics is that of left-right symmetric models.<sup>127</sup> In this case, reasonably large values for CP asymmetries can be obtained for the Cabibbo allowed decay modes. This occurs due to the existence of an additional amplitude from the  $W_R$  exchange, which carries a different weak phase from that of the  $W_L$  mediated decay. The estimated values of the CP asymmetries in these models is of an order of a few  $\times 10^{-2}$ . CP asymmetries at the percent level are expected<sup>128</sup> in some nonminimal SUSY models for the decays  $D^0 \rightarrow K_S^0 \pi^0, K_S^0 \phi$ .

## 6.7 CP Violation in the Top-Quark Decays

CP violation in top-quark production and decay is expected to be very small in the SM,<sup>129</sup> however, numerous models with new interactions, such as multi-Higgs models and supersymmetry, can give rise to CP violation in the top system at interesting levels. Since the top-quark decays before it has time to hadronize, it provides a particularly good laboratory for the study of such effects. Searches for CP violating effects can be carried out by studying CP-odd spin-momentum correlations in the top-quark decay products.  $e^+e^-$  colliders, with polarized beams, are especially suited to carry out such investigations. Numerous studies of CP symmetry tests can be found in Refs. 130 and 131.

## 7 Conclusion

Rare processes in the kaon sector will be investigated with more precision with the large data sample which will be collected at DAPHNE. In particular, the CP violating parameter  $\epsilon'/\epsilon$  will be explored at the  $10^{-4}$  level. Future runs of the AGS at Brookhaven could increase their total integrated luminosity by a factor of three to six, and hence, finally place the SM prediction for the long sought-after decay  $K^+ \rightarrow \pi^+ \nu \bar{\nu}$  within experimental reach.

A large amount of data on the  $B$ -meson system has been and will continue to be acquired during the next decade at CESR, the Tevatron, HERA, the SLAC and KEK B factories, as well as the LHC, and promises to yield exciting new tests of the SM. FCNC processes in the  $B$  sector are not as suppressed as in the other meson systems and can occur at reasonable rates in the SM. This is due to a sizable loop-level contribution from the top quark, which results from the combination of the large top mass (giving a big GIM splitting) and the diagonal nature of the CKM matrix. Long-distance effects are expected to play less of a role due to the heavy  $B$  mass, and hence rare processes are essentially short-distance dominated. Many classes of new models can also give significant and testable contributions to rare  $B$  transitions. The benchmark process for this type of new physics search is the inclusive decay  $B \rightarrow X_s \gamma$  (and the related exclusive process  $B \rightarrow K^* \gamma$ ) which has been recently observed by CLEO.<sup>31</sup> It has since provided strong restrictions on the parameters of several theories beyond the SM. This constitutes the first direct observation of a penguin mediated process and

demonstrates the fertile ground ahead for the detailed exploration of the SM in rare  $B$  transitions.

FCNC in the  $Q = 2/3$  quark systems will also be explored at a deeper level within the next decade. Increased statistics in the  $D$  meson sector will be collected at the  $e^+e^- B$  factories and in a possible fixed target run of the Tevatron main injector or at a possible new dedicated heavy flavor experiment for the Tevatron collider. While it is not expected that the data sample will be large enough to reach the miniscule SM rates for the  $D$  meson FCNC transitions, important restrictions on new physics can be placed.

And, lastly, the physics of the top quark is just beginning to be explored. In the near future, the Tevatron main injector will produce roughly  $7 \times 10^3 t\bar{t}$  pairs with  $1 \text{ fb}^{-1}$  of integrated luminosity, while in the longer term, the LHC and NLC will be top-quark factories. Since the top quark is the heaviest SM fermion with a mass at the electroweak symmetry breaking scale, it might provide a unique window to new physics.

In summary, we look forward to an exciting future in heavy flavor physics!

## References

- [1] For a review and original references, see R. N. Mohapatra, *Unification and Supersymmetry* (Springer, New York, 1986).
- [2] M. Kobayashi and T. Maskawa, *Prog. Theor. Phys.* **49**, 652 (1973).
- [3] L. Wolfenstein, *Phys. Rev. Lett.* **51**, 1945 (1983).
- [4] R. M. Barnett *et al.* (Particle Data Group), *Phys. Rev. D* **54**, 1 (1996).
- [5] W. J. Marciano in *Proceedings of the 5th International Symposium on Heavy Flavor Physics*, Montreal, Canada, edited by D. I. Britton (Editions Frontieres, France, 1994).
- [6] F. C. Barker, *Nucl. Phys. A* **579**, 62 (1994), and **540**, 501 (1992); I. S. Towner, *Nucl. Phys. A* **540**, 478 (1992); E. Hagberg *et al.*, *Nucl. Phys. A* **509**, 429 (1990); B. A. Brown and W. E. Ormand, *Phys. Rev. Lett* **62**, 866 (1989).
- [7] H. Leutwyler and M. Roos, *Z. Phys. C* **25**, 91 (1984); M. Bourquin *et al.*, *Z. Phys. C* **21**, 27 (1983).
- [8] H. Albrecht *et al.* (ARGUS Collaboration), *Phys. Lett. B* **255**, 297 (1991); J. Bartelt *et al.* (CLEO Collaboration), *Phys. Rev. Lett.* **71**, 4111 (1993).
- [9] J. P. Alexander *et al.* (CLEO Collaboration), *Phys. Rev. Lett.* **77**, 5000 (1996).
- [10] V. Barger, C. S. Kim, and R. J. N. Phillips, *Phys. Lett. B* **251**, 629 (1990); C. Greub and S.-J. Rey, SLAC-PUB-7245, hep-ph/9608247.
- [11] H. Abramowicz *et al.*, *Z. Phys. C* **15**, 19 (1982); S. A. Rabinowitz *et al.*, *Phys. Rev. Lett.* **70**, 134 (1993); A. O. Bazarko *et al.*, *Z. Phys. C* **65**, 189 (1995).
- [12] L. Gibbons, presented at the *28th International Conference on High Energy Physics*, Warsaw, Poland, July 1996; A. Buras, *ibid.*
- [13] P. Tipton, presented at the *28th International Conference on High Energy Physics*, Warsaw, Poland, July 1996.
- [14] J. Adler *et al.* (MARK III Collaboration), *Phys. Rev. Lett.* **60**, 1375 (1988).
- [15] J. Z. Bai *et al.* (BES Collaboration), SLAC-PUB-7147 (1996).
- [16] D. Acosta *et al.* (CLEO Collaboration), *Phys. Rev. D* **49**, 5690 (1993).
- [17] A. Aoki *et al.*, *Prog. Theor. Phys.* **89**, 131 (1993); K. Kodama *et al.* (FNAL E635 Collaboration), *Phys. Lett. B* **382**, 299 (1996).
- [18] J. Z. Bai *et al.* (BES Collaboration), *Phys. Rev. Lett.* **74**, 4599 (1995).
- [19] J. Richman, presented at the *28th International Conference on High Energy Physics*, Warsaw, Poland, July 1996.
- [20] L3 Collaboration, CERN-PPE/96-198 (1996).
- [21] J. M. Flynn, presented at the *28th International Conference on High Energy Physics*, Warsaw, Poland, July 1996, hep-lat/9611016.
- [22] J. Amundson *et al.*, *Phys. Rev. D* **47**, 3059 (1993); J. Rosner, *Phys. Rev. D* **42**, 3732 (1990).
- [23] S. Capstick and S. Godfrey, *Phys. Rev. D* **41**, 2856 (1990).
- [24] C. A. Dominguez and N. Paver, *Phys. Lett. B* **318**, 629 (1993).
- [25] Y. Grossman, H. Haber, and Y. Nir, *Phys. Lett. B* **357**, 630 (1995); W.-S. Hou, *Phys. Rev. D* **48**, 2342 (1993); P. Krawczyk and S. Pokorski, *Phys. Rev. Lett.* **60**, 182 (1988); J. L. Hewett, in *Proceedings of the 1992 DPF Meeting*, Fermilab, edited by J. Yoh (World Scientific, 1993).
- [26] M. Artuso *et al.* (CLEO Collaboration), *Phys. Rev. Lett.* **75**, 785 (1995); D. Buskulic *et al.* (ALEPH Collaboration), *Phys. Lett. B* **343**, 444 (1995).
- [27] S. L. Glashow and S. Weinberg, *Phys. Rev. D* **15**, 1958 (1977); E. Pachos, *Phys. Rev. D* **15**, 1966 (1977).
- [28] S. L. Glashow, J. Iliopoulos, and L. Maiani, *Phys. Rev. D* **2**, 1285 (1970).
- [29] See, for example, the recent review, G. Buchalla, A. J. Buras, and M. E. Lautenbacher, *Rev. Mod. Phys.* **68**, 1125 (1996); as well as F. J. Gilman and M. Wise, *Phys. Rev. D* **20**, 2392 (1979); *ibid.*, **D 27**, 1128 (1983).
- [30] T. Inami and C. S. Lim, *Prog. Theor. Phys.* **65**, 297 (1981).
- [31] M. S. Alam *et al.*, CLEO Collaboration, *Phys. Rev. Lett.* **74**, 2885 (1995); R. Ammar *et al.*, CLEO Collaboration, *Phys. Rev. Lett.* **71**, 674 (1993); K. W. Edwards *et al.*, CLEO Collaboration, presented at the *1995 Meeting of the European Physical Society Conference on High Energy Physics*, Brussels, Belgium, July 1995, CLEO-CONF95-6.
- [32] R. Ammar *et al.*, (CLEO Collaboration), presented at the *28th International Conference on High Energy Physics*, Warsaw, Poland, July 1996, CLEO-CONF-96-05.

- [33] For a review of implications of non-SM physics in  $B \rightarrow X_s \gamma$ , see J. L. Hewett, in *The 21st SLAC Summer Institute on Particle Physics*, Stanford, CA, July 1993, hep-ph/9406302.
- [34] N. G. Deshpande, P. Lo, J. Trampetic, G. Eilam, and P. Singer, *Phys. Rev. Lett.* **59**, 183 (1987); S. Bertolini, F. Borzumati, and A. Masiero, *Phys. Rev. Lett.* **59**, 180 (1987); B. Grinstein, R. Springer, and M. Wise, *Phys. Lett. B* **202**, 138 (1988); *Nucl. Phys. B* **339**, 269 (1988); A. Buras, M. Misiak, M. Münz, and S. Pokorski, *Nucl. Phys. B* **424**, 374 (1994).
- [35] A. Ali and C. Greub, *Z. Phys. C* **49**, 431 (1991); *Phys. Lett. B* **259**, 182 (1991); *Phys. Lett. B* **361**, 146 (1995); N. Pott, *Phys. Rev. D* **54**, 938 (1996).
- [36] C. Greub, T. Hurth, and D. Wyler, *Phys. Lett. B* **380**, 385 (1996); *Phys. Rev. D* **54**, 3350 (1996); C. Greub and T. Hurth, presented at DPF96, Minneapolis, MN, August 1996, hep-ph/9608449.
- [37] K. Adel and Y.-P. Yao, *Phys. Rev. D* **49**, 4945 (1994).
- [38] K. G. Chetyrkin, M. Misiak, and M. Münz, hep-ph/9612313; M. Misiak, presented at the *28th International Conference on High Energy Physics*, Warsaw, Poland, July 1996.
- [39] J. Chay, H. Georgi, and B. Grinstein, *Phys. Lett. B* **247**, 399 (1990); I. Bigi, N. Uraltsev, and A. Vainshtein, *Phys. Lett. B* **243**, 430 (1992); B. Blok and M. Shifman, *Nucl. Phys. B* **399**, 441 (1993); I. Bigi *et al.*, *Phys. Rev. Lett.* **71**, 496 (1993).
- [40] P. N. Burrows, presented at the *3rd International Symposium on Radiative Corrections*, Cracow, Poland, August 1996, hep-ex/9612007.
- [41] M. Schmelling, presented at the *28th International Conference on High Energy Physics*, Warsaw, Poland, July 1996.
- [42] J. L. Hewett and J. D. Wells, *Phys. Rev. D* (in press), hep-ph/9610323.
- [43] A. Ali, in *The 20th International Nathiagali Summer College on Physics and Contemporary Needs*, Bhurban, Pakistan, 1995, hep-ph/9606324.
- [44] J. L. Hewett, *Phys. Lett. B* **193**, 327 (1987); W.-S. Hou, A. Soni, and H. Steger, *Phys. Lett. B* **192**, 441 (1987).
- [45] T. G. Rizzo, *Phys. Rev. D* **38**, 820 (1988); X. G. He, T. D. Nguyen, and R. R. Volkas, *Phys. Rev. D* **38**, 814 (1988); W.-S. Hou and R. S. Willey, *Phys. Lett. B* **202**, 591 (1988); C. Q. Geng and J. N. Ng, *Phys. Rev. D* **38**, 2858 (1988); B. Grinstein, R. Springer, and M. Wise, *Nucl. Phys. B* **339**, 269 (1990); J. L. Hewett, *Phys. Rev. Lett.* **70**, 1045 (1993); V. Barger, M. Berger, and R. J. N. Phillips, *Phys. Rev. Lett.* **70**, 1368 (1993).
- [46] V. Barger, J. L. Hewett, and R. J. N. Phillips, *Phys. Rev. D* **41**, 3421 (1990); A. Buras *et al.*, *Nucl. Phys. B* **337**, 284 (1990); J. F. Gunion and B. Grzadkowski, *Phys. Lett. B* **243**, 301 (1990).
- [47] S. Bertolini *et al.*, *Nucl. Phys. B* **294**, 321 (1987), and *Nucl. Phys. B* **353**, 591 (1991); R. Barbieri and G. F. Giudice, *Phys. Lett. B* **309**, 86 (1993); R. Garisto and J. N. Ng, *Phys. Lett. B* **315**, 119 (1993); M. A. Diaz, *Phys. Lett. B* **322**, 207 (1994); F. M. Borzumati, *Z. Phys. C* **63**, 291 (1994); S. Bertolini and F. Vissani, *Z. Phys. C* **67**, 513 (1995); J. L. Lopez *et al.*, *Phys. Rev. D* **48**, 974 (1993); H. Anlauf, *Nucl. Phys. B* **430**, 245 (1994); H. Baer and M. Brhlik, hep-ph/9610224.
- [48] T. Goto and Y. Okada, *Prog. Theor. Phys.* **94**, 407 (1995).
- [49] G. L. Kane, C. Kolda, L. Roszkowski, and J. D. Wells, *Phys. Rev. D* **49**, 6173 (1994).
- [50] J. L. Hewett and T. G. Rizzo, *Phys. Rev. D* **49**, 319 (1994).
- [51] J. L. Hewett, T. Takeuchi, and S. Thomas, to appear in *Electroweak Symmetry Breaking and Beyond the Standard Model*, edited by T. Barklow *et al.*, SLAC-PUB-7088, hep-ph/9603391.
- [52] For a review, see R. Frey, D. Gerdes, and J. Jaros, to appear in *Proceedings of the 1996 DPF/DPB Summer Study on Future Directions for High Energy Physics*, Snowmass, CO, July 1996.
- [53] A. Ali, V. M. Braun, and H. Simma, *Z. Phys. C* **63**, 437 (1994); S. Narrison, *Phys. Lett. B* **327**, 354 (1994); J. M. Soares, *Phys. Rev. D* **49**, 283 (1994).
- [54] See, for example, D. Atwood, B. Blok, and A. Soni, *Int. J. Mod. Phys. A* **11**, 3743 (1996); N. G. Deshpande, X.-G. He, and J. Trampetic, *Phys. Lett. B* **367**, 362 (1996); H.-Y. Cheng, Report IP-ASTP-23-94; J. Milana, *Phys. Rev. D* **53**, 1403 (1996); G. Ricciardi, *Phys. Lett. B* **358**, 129 (1995); A. Ali and V. M. Braun, *Phys. Lett. B* **359**, 223 (1995).
- [55] E. Golowich and S. Pakvasa, *Phys. Rev. D* **51**, 3518 (1995); Z. Ligeti, L. Randall, and M. B. Wise, hep-ph/9702322; A. Khodjamirian *et al.*, hep-ph/9702318.
- [56] G. Burdman, E. Golowich, J. L. Hewett, and S. Pakvasa, *Phys. Rev. D* **52**, 6883 (1995).
- [57] C. Greub, T. Hurth, M. Misiak, and D. Wyler, *Phys. Lett. B* **382**, 415 (1996).
- [58] For a review of present experiment results on rare  $B$  physics, see, T. E. Browder, K. Honscheid, and S. Playfer, in *B Decays*, 2nd edition, edited by S. Stone (World Scientific, 1995).
- [59] S. Abachi *et al.* (DØ Collaboration), DØnote-2023 (1996); F. Abe *et al.* (CDF Collaboration), Fermilab-PUB-96/1040-E; P. Perrodo *et al.* (ALEPH Collaboration), Warsaw, Poland, July 1996; Acciani *et al.* (L3 Collaboration), *Phys. Lett. B* **363**, 137 (1995); R. Ammar *et al.* (CLEO Collaboration), *Phys. Rev. D* **49**, 5701 (1994); E. Thorndike *et al.* (CLEO Collaboration), in the *Proceedings of the 27th International Conference on High Energy Physics*, Glasgow, Scotland, July 1994, edited by P. J. Bussey and I. G. Knowles (Institute of Physics, Bristol, 1995).
- [60] L. Randall and R. Sundrum, *Phys. Lett. B* **312**, 148 (1993).
- [61] J. L. Hewett, S. Nandi, and T. G. Rizzo, *Phys. Rev. D* **39**, 250 (1989); M. Savage, *Phys. Lett. B* **266**, 135 (1991).
- [62] S. Davidson, D. Bailey, and B. A. Campbell, *Z. Phys. C* **61**, 613 (1994); M. Leurer, *Phys. Rev. D* **50**, 536 (1994), and *D* **49**, 333 (1994).
- [63] B. Grinstein, Y. Nir, and J. M. Soares, *Phys. Rev. D* **48**, 3960 (1993).

- [64] A. J. Buras and M. Münz, *Phys. Rev. D* **52**, 186 (1995).
- [65] N. G. Deshpande, J. Trampetic, and K. Panrose, *Phys. Rev. D* **39**, 1461 (1989); C. S. Lim, T. Morozumi, and A. I. Sanda, *Phys. Lett. B* **218**, 343 (1989); Z. Ligeti and M. Wise, *Phys. Rev. D* **53**, 4937 (1996).
- [66] N. G. Deshpande and J. Trampetic, *Phys. Rev. Lett.* **60**, 2583 (1988); B. Grinstein, M. J. Savage, and M. B. Wise, *Nucl. Phys. B* **319**, 271 (1989).
- [67] A. Ali, G. F. Giudice, and T. Mannel, *Z. Phys. C* **67**, 417 (1995); A. Ali, T. Mannel, and T. Morozumi, *Phys. Lett. B* **273**, 505 (1991).
- [68] J. L. Hewett, *Phys. Rev. D* **53**, 4964 (1996).
- [69] T. Goto, Y. Okada, Y. Shimizu, and M. Tanaka, hep-ph/9609512.
- [70] E. Ma and A. Pramudita, *Phys. Rev. D* **24**, 2476 (1981).
- [71] A. Fryberger *et al.* (CLEO Collaboration), *Phys. Rev. Lett.* **76**, 3065 (1996); E. M. Aitala *et al.* (E791 Collaboration), *Phys. Rev. Lett.* **76**, 369 (1996); M. Selen, CLEO Collaboration, presented at *APS Spring Meeting*, Washington D.C., April 1994; T. Alexopoulos *et al.*, E771 Collaboration, Fermilab Report Fermilab-Pub-95-286-E (1995); K. Kodama *et al.* (E653 Collaboration), *Phys. Lett. B* **345**, 85 (1995); M. Adamovich *et al.* (WA92 Collaboration), *Phys. Lett. B* **353**, 563 (1995); A. Weir *et al.* (MARK II Collaboration), *Phys. Rev. D* **41**, 1384 (1990).
- [72] A. Acker and S. Pakvasa, *Mod. Phys. Lett. A* **7**, 1219 (1992).
- [73] S. Kettell (E787 Collaboration), hep-ex/9701003.
- [74] C. Q. Geng, I. J. Hsu, and Y. C. Lin, *Phys. Lett. B* **355**, 569 (1995); S. Fajfer, Helsinki University Report HU-SEFT-R-1996-05, hep-ph/9602322.
- [75] G. Buchalla and A. Buras, *Nucl. Phys. B* **412**, 106 (1994), and *Phys. Rev. D* **54**, 6782 (1996).
- [76] I. Bigi and F. Gabbiani, *Nucl. Phys. B* **367**, 3 (1991).
- [77] J. S. Hagelin and L. S. Littenberg, *Prog. Part. Nucl. Phys.* **23**, 1 (1989).
- [78] S. Weinberg, *Phys. Rev. Lett.* **37**, 657 (1976); P. Krawczyk and S. Pokorski, *Nucl. Phys. B* **364**, 10 (1991); Y. Grossman and Y. Nir, *Phys. Lett. B* **313**, 126 (1993); Y. Grossman, *Nucl. Phys. B* **426**, 355 (1994).
- [79] For recent reviews and original references, see L. Littenberg and G. Valencia, *Ann. Rev. Nucl. Part. Sci.* **43**, 729 (1993); J. L. Ritchie and S. G. Wojcicki, *Rev. Mod. Phys.* **65**, 1149 (1993); R. Battiston *et al.*, *Phys. Rep.* **214**, 293 (1992).
- [80] G. Eilam, J. L. Hewett, and A. Soni, *Phys. Rev. D* **44**, 1473 (1991).
- [81] B. Grzadkowski, J. F. Gunion, and P. Krawczyk, *Phys. Lett. B* **286**, 106 (1991); N. G. Deshpande, B. Margolis, and H. Trottier, *Phys. Rev. D* **45**, 178 (1992); M. Luke and M. Savage, *Phys. Lett. B* **307**, 387 (1993).
- [82] C. S. Li, R. J. Oakes, and J. M. Yang, *Phys. Rev. D* **49**, 293 (1994); G. Cou-ture, C. Hamzaoui, and H. Konig, *Phys. Rev. D* **52**, 1713 (1995).
- [83] T. Han, R. D. Peccei, and X. Zhang, *Nucl. Phys. B* **454**, 527 (1995); T. Han *et al.*, Univ. California Davis Report UCD-96-07, hep-ph/9603247; E. Malkawi and T. Tait, *Phys. Rev. D* **54**, 5758 (1996).
- [84] T. J. LeCompte, CDF Collaboration, presented at the *2nd Rencontres du Vietnam*, Ho Chi Minh City, Vietnam, October 1995, Fermilab-CONF-96/021-E.
- [85] I. I. Bigi *et al.*, *Phys. Lett. B* **181**, 157 (1986); V. Barger and R. J. N. Phillips, *Phys. Rev. D* **41**, 884 (1990), *ibid.* **40**, 2875 (1990), and *Phys. Lett. B* **201**, 553 (1988); C. S. Li and T. C. Yuan, *Phys. Rev. D* **42**, 3088 (1990).
- [86] S. Pakvasa and H. Sugawara, *Phys. Lett. B* **73**, 61 (1978); S. Pakvasa, H. Sugawara, and Y. Yamanaka, *Phys. Rev. D* **25**, 1895 (1982); T. P. Cheng and M. Sher, *Phys. Rev. D* **35**, 3484 (1987); L. J. Hall and S. Weinberg, *Phys. Rev. D* **48**, 979 (1993); A. Antaramian, L. J. Hall, and A. Rasin, *Phys. Rev. Lett.* **69**, 1871 (1992).
- [87] T. P. Cheng and M. Sher, *Phys. Rev. D* **35**, 3483 (1987); B. Mukhopadhyaya and S. Nandi, *Phys. Rev. Lett.* **66**, 285 (1991); T. P. Cheng and L. F. Li, *Phys. Rev. D* **45**, 1708 (1992); W.-S. Hou, *Phys. Lett. B* **296**, 179 (1992); L. J. Hall and S. Weinberg, *Phys. Rev. D* **48**, R979 (1993); W.-S. Hou and H. C. Huang, *Phys. Rev. D* **51**, 5285 (1995).
- [88] K. Hikasa and M. Kobayashi, *Phys. Rev. D* **36**, 724 (1987); H. Baer *et al.*, *Phys. Rev. D* **44**, 725 (1991); J. Sender, hep-ph/9602354.
- [89] K. Agashe and M. Graesser, LBNL Report LBNL-37823 (1995), hep-ph/9510439.
- [90] S. Herrlich and U. Nierste, *Nucl. Phys. B* **419**, 292 (1994); *ibid.* **476**, 27 (1996), and *Phys. Rev. D* **52**, 6506 (1995).
- [91] A. J. Buras, M. Jamin, and P. H. Weisz, *Nucl. Phys. B* **347**, 491 (1990).
- [92] W. A. Bardeen, A. J. Buras, and J. M. Gerard, *Phys. Lett. B* **211**, 343 (1988); J. M. Gerard, *Acta Phys. Pol. B* **21**, 257 (1990); J. Bijnens and J. Prades, *Nucl. Phys. B* **444**, 523 (1995); A. Pich and E. de Rafael, *Phys. Lett. B* **158**, 477 (1985); J. Prades *et al.*, *Z. Phys. C* **51**, 287 (1991); J. F. Donoghue, E. Golowich, and B. R. Holstein, *Phys. Lett. B* **119**, 412 (1993); R. Decker, *Nucl. Phys. B Proc. Suppl. A* **7**, 190 (1989); S. Narrison, *Phys. Lett. B* **351**, 369 (1995); V. Antonelli *et al.*, hep-ph/9610230.
- [93] For a review, see J. M. Gerard, in *Proceedings of the 12th Warsaw Symposium on Elementary Particle Physics*, Kazimierz, Poland, 1989.
- [94] G. Beall, M. Bander, and A. Soni, *Phys. Rev. Lett.* **48**, 848 (1982).
- [95] See, for example, J. Ellis and D. V. Nanopoulos, *Phys. Lett. B* **110**, 44 (1982).
- [96] S. Dimopoulos and J. Ellis, *Nucl. Phys. B* **182**, 505 (1981); S. Dimopoulos, H. Georgi, and S. Raby, *Phys. Lett. B* **127**, 101 (1983); R. S. Chivukula and H. Georgi, *Phys. Lett. B* **188**, 99 (1987); R. S. Chivukula, H. Georgi, and L. Randall, *Nucl. Phys. B* **292**, 93 (1987); L. Randall, *Nucl. Phys. B* **403**, 122 (1993).
- [97] T. E. Browder and S. Pakvasa, *Phys. Rev. D* **52**, 3123 (1995).
- [98] J. C. Anjos *et al.* (FNAL E691 Collaboration), *Phys. Rev. D* **60**, 1239 (1988).
- [99] E. M. Aitala *et al.* (FNAL E791 Collaboration), *Phys. Rev. Lett.* **77**, 2384 (1996); G. Blaylock, A. Seiden, and Y. Nir, *Phys. Lett. B* **355**, 555 (1995).

- [100] A. Datta, *Z. Phys. C* **27**, 515 (1985).
- [101] For further details, see G. Burdman, E. Golowich, J. Hewett, and S. Pakvasa, SLAC-PUB-7136; G. Burdman in *CHARM2000 Workshop*, Fermilab, June 1994; J. Donoghue *et al.*, *Phys. Rev. D* **33**, 179 (1986).
- [102] H. Georgi, *Phys. Lett. B* **297**, 353 (1992); T. Ohl *et al.*, *Nucl. Phys. B* **403**, 605 (1993).
- [103] K. S. Babu *et al.*, *Phys. Lett. B* **205**, 540 (1988); T. G. Rizzo, *Int. J. Mod. Phys. A* **4**, 5401 (1989).
- [104] S. Pakvasa and H. Sugawara, *Phys. Lett. B* **73**, 61 (1978); T. P. Cheng and M. Sher, *Phys. Rev. D* **35**, 3484 (1987); L. Hall and S. Weinberg, *Phys. Rev. D* **48**, 979 (1993).
- [105] C. Jarlskog, *Phys. Rev. Lett.* **55**, 1039 (1985).
- [106] Y. Grossman, Z. Ligeti, and Y. Nir, hep-ph/9701231.
- [107] V. Kuzmin, V. Rubakov, and M. Shaposhnikov, *Phys. Lett. B* **155**, 36 (1985); G. Farrar and M. Shaposhnikov, *Phys. Rev. Lett.* **70**, 2833 (1993), and *Phys. Rev. D* **50**, 774 (1994); P. Huet and E. Sather, *Phys. Rev. D* **51**, 379 (1995); A. Cohen, D. Kaplan, and A. Nelson, *Ann. Rev. Nucl. Part. Sci.* **43**, 27 (1993).
- [108] For reviews, see *CP Violation*, edited by C. Jarlskog (World Scientific, Singapore, 1989); Y. Nir and H. Quinn, *Ann. Rev. Nucl. Part. Sci.* **42**, 211 (1992).
- [109] A. B. Carter and A. I. Sanda, *Phys. Rev. Lett.* **45**, 952 (1980), and *Phys. Rev. D* **23**, 1567 (1981); I. I. Bigi and A. I. Sanda, *Nucl. Phys. B* **193**, 85 (1981), and *ibid.* **B 281**, 41 (1987).
- [110] E. Ma, W. A. Simmons, and S. F. Tuan, *Phys. Rev. D* **20**, 2888 (1979); L.-L. Chau, W.-Y. Keung, and M. D. Tran, *Phys. Rev. D* **27**, 2145 (1983).
- [111] See, for example, L. Wolfenstein, *Comments Nucl. Part. Phys.* **21**, 275 (1994).
- [112] T. T. Wu and C. N. Yang, *Phys. Rev. Lett.* **13**, 380 (1964).
- [113] G. Buchalla, A. J. Buras, and M. K. Harlander, *Nucl. Phys. B* **337**, 313 (1990); A. J. Buras, M. Jamin, M. E. Lautenbacher, and P. H. Weisz, *Nucl. Phys. B* **370**, 69 (1992); addendum, *ibid.*, **B 375**, 501 (1992); A. J. Buras, M. Jamin, and M. E. Lautenbacher, *Nucl. Phys. B* **408**, 209 (1993); M. Ciuchini, E. Franco, G. Martinelli, and L. Reina, *Nucl. Phys. B* **415**, 403 (1994).
- [114] J. M. Flynn and L. Randall, *Phys. Lett. B* **224**, 221 (1989); Erratum, *ibid.*, **B 235**, 412 (1990).
- [115] A. J. Buras, M. Jamin, and M. E. Lautenbacher, hep-ph/9608365.
- [116] E. Gabrielli, A. Masiero, and L. Silvestrini (1995) hep-ph/9509379 and hep-ph/9510215; J. Hagelin, S. Kelley, and T. Tanaka, *Nucl. Phys. B* **415**, 293 (1994), and *Mod. Phys. Lett. A* **8**, 2737 (1993).
- [117] B. Winstein and L. Wolfenstein, *Rev. Mod. Phys.* **65**, 1113 (1993).
- [118] D. Boutigny *et al.*, BABAR Collaboration, SLAC Report SLAC-0443 (1994); M. T. Cheng *et al.*, BELLE Collaboration, KEK Report KEK-94-02 (1994); The CLEO III Detector Proposal, Cornell Report CLNS-94/1277 (1994); The CDF Collaboration, CDF-DOC-ADVISORY-PUBLIC/2436; T. Lohse *et al.*, HERA-B Collaboration, DESY Report DESY-PRC-93-04 (1994); K. Kirsebom *et al.*, LHC-B Collaboration, CERN Report CERN/LHCC 95-5 (1995).
- [119] M. Gronau and D. London, *Phys. Rev. Lett.* **65**, 3381 (1990); Y. Nir and H. Quinn, *Phys. Rev. Lett.* **67**, 541 (1991); N. G. Deshpande and X.-G. He, *Phys. Rev. Lett.* **74**, 26 (1995), Erratum *ibid.*, **74**, 4099 (1995).
- [120] Y. Grossman and Y. Nir, *Phys. Lett. B* **313**, 126 (1993).
- [121] G. C. Branco, G. C. Cho, Y. Kizukuri, and N. Oshimo, *Phys. Lett. B* **337**, 316 (1994), and *Nucl. Phys. B* **449**, 483 (1995); M. Wohar *Phys. Rev. D* **54**, 2198 (1996).
- [122] D. Silverman, *Int. J. Mod. Phys. A* **11**, 2253 (1996).
- [123] T. E. Browder and S. Pakvasa, Univ. of Hawaii Report UH-511-828-95 (1995); L. Wolfenstein, Carnegie Mellon Univ. Report CMU-HEP-95-04 (1995); G. Blaylock, A. Seiden, and Y. Nir, Univ. of Santa Cruz Report SCIPP-95-16 (1995).
- [124] G. Burdman, E. Golowich, J. L. Hewett, and S. Pakvasa, SLAC Report SLAC-PUB-7136.
- [125] F. Buccella *et al.*, *Phys. Lett. B* **302**, 319 (1993); G. Burdman in *Proceedings of the CHARM2000 Workshop*, Fermilab 1994, edited by D. Kaplan.
- [126] P. L. Frabetti *et al.*, *Phys. Rev. D* **50**, 2953 (1994); J. Bartelt *et al.*, CLEO Collaboration, *Phys. Rev. D* **52**, 4860 (1995).
- [127] A. Le Yaouanc *et al.*, *Phys. Lett. B* **292**, 353 (1992); S. Pakvasa, in *Proceedings of CHARM2000 Workshop*, Fermilab, June 1994, edited by D. Kaplan; M. Gronau, and S. Wakaizumi, *Phys. Rev. Lett.* **68**, 1814 (1992).
- [128] I. I. Bigi, F. Gabbiani, and A. Masiero, *Z. Phys. C* **48**, 633 (1990).
- [129] See, for example, G. Eilam, J. L. Hewett, and A. Soni, *Phys. Rev. Lett.* **67**, 1979 (1991), *ibid.*, **68**, 2103 (1992).
- [130] For an overview, see R. Frey, talk presented at the *Future  $e^+e^-$  Collider Physics Study Group Meeting*, Estes Park, Colorado, June 21-23, 1995. See also, G. Kane, G. A. Ladinsky, and C. P. Yuan, *Phys. Rev. D* **45**, 124 (1992); C. P. Yuan, *Phys. Rev. D* **45**, 782 (1992); D. Atwood, A. Aeppli, and A. Soni, *Phys. Rev. Lett.* **69**, 2754 (1992); D. Atwood, A. Kagan, and T. G. Rizzo, *Phys. Rev. D* **52**, 6264 (1995); M. Peskin, in *Proceedings of the Second International Workshop on Physics and Experiments at Linear  $e^+e^-$  Colliders*, Waikoloa, HI, April 1993, edited by F. A. Harris *et al.* (World Scientific, 1994); M. Peskin and C. R. Schmidt, in *Proceedings of the First Workshop on Linear Colliders*, Saariselkä, Finland, September 1991 (World Scientific, 1992); P. Zerwas, *ibid.*; W. Bernreuther *et al.*, in *Proceedings of the Workshop on  $e^+e^-$  Collisions at 500 GeV, The Physics Potential*, (DESY, Hamburg) edited by P. Igo-Kemenes and J. H. Kühn, 1992; A. Djouadi, ENSLAPP-A-365-92 (1992); T. G. Rizzo, *Phys. Rev. D* **50**, 4478 (1994); M. Frigeni

and R. Rattazzi, Phys. Lett. B **269**, 412 (1991); R. D. Peccei, S. Persis, and X. Zhang, Nucl. Phys. B **349**, 305 (1991); D. O. Carlson, E. Malkawi, and C.-P. Yuan, Phys. Lett. B **337**, 145 (1994); T. G. Rizzo, Phys. Rev. D **51**, 3811 (1995), and SLAC-PUB-95-6914, 1995.

- [131] J. F. Donoghue and G. Valencia, Phys. Rev. Lett. **58**, 451 (1987), and **E 60**, 243 (1988); C. A. Nelson, Phys. Rev. D **43**, 1465 (1991); C. R. Schmidt and M. E. Peskin, Phys. Rev. Lett. **69**, 410 (1992); W. Bernreuther *et al.*, Nucl. Phys. B **388**, 53 (1992), and **E B 406**, 516 (1993); A. Brandenburg and J. P. Ma, Phys. Lett. B **298**, 211 (1993), and Z. Phys. C **56**, 97 (1992); B. Grzadkowski, Phys. Lett. B **305**, 384 (1993); B. Grzadkowski and W.-Y. Keung, Phys. Lett. B **319**, 526 (1993), and *ibid.* **B 316**, 137 (1993); D. Atwood *et al.*, Phys. Rev. Lett. **70**, 1364 (1993); T. Arens and L. M. Sehgal, Nucl. Phys. B **393**, 46 (1993), Phys. Lett. B **302**, 501 (1993), and Phys. Rev. D **50**, 4372 (1994); W. Bernreuther and A. Brandenburg, Phys. Lett. B **314**, 104 (1993), and Phys. Rev. D **49**, 4481 (1994); D. Chang, W.-Y. Keung, and I. Phillips, Nucl. Phys. B **408**, 286 (1993), and **B 429**, 255(E) (1994); W. Bernreuther and P. Overmann, PITHA 95/30 (1995).